CONTENTS

ABSTRACT

This work is a petrological research on the partial melting of metapelitic rocks, and includes a petrographic-microstructural study, a bulk- and microchemical characterization, and the thermodynamic modelling of phase equilibria.

The Nordmannwick nappe is a high grade tectonic unit occurring structurally below the Lyngen Ophiolite (Northern Scandinavian Caledonides, Northern Norway). This unit is compositionally heterogeneous (metapelitic schists, metapsammites, carbonatic layers, mafic bodies) but it is clearly characterized by the occurrence of high grade metamorphic imprint with the formation of migmatites.

Two samples of migmatites (LY4f and LY131) belonging to this high grade portion were studied. The metapelitic sample LY4f shows relicts of kyanite porphyroblasts and a peak mineral assemblage constituted by biotite + garnet + plagioclase + quartz + sillimanite + former melt. The mineral assemblage formed after the retrogression is biotite + white mica + garnet + plagioclase + quartz + sillimanite. The metapsammitic sample LY131 is characterized by the presence of partially replaced kyanite crystals and by a peak mineral assemblage constituted by biotite + garnet + K-feldspar + plagioclase + quartz + sillimanite + former melt, whereas the mineral assemblage formed after the retrogression is biotite + white mica + garnet + plagioclase + quartz + sillimanite.

A sequence of three main metamorphic events is detected by means of microstructural observations and electron microprobe analyses for both samples. The first one is a high pressure event, followed by a high temperature melt-bearing event. The last metamorphic event occurs during retrogression. Phase equilibria modelling, performed with Perple_X in the MnO – Na_2O – CaO – K_2O – FeO – MgO – Al_2O_3 – SiO_2 – H_2O – TiO_2 (MnNCaKFMASHT) system, was applied to sample LY4f and LY131. The temperature and the pressure estimated for sample LY4f at the peak conditions are $800 \pm 30°$ and 0.85 ± 0.07 GPa, whereas after the retrogression are $650 \pm 30°$ and 0.77 ± 1.8 GPa. The temperature estimated

for sample LY131 at the peak conditions is 790±10°, whereas the pressure could not be constrained. The temperature and the pressure estimated after the retrogression are 670±10° and 0.75±0.07 GPa.

This work allows a satisfactory modelling of the anatectic history of these rocks in the low-, medium-P conditions, and also of their retrograde cooling history.

Conversely, the high-P event leading to the widespread crystallization of kyanite predating sillimanite could not be constrained.

RIASSUNTO ESTESO

Questo lavoro rappresenta una ricerca petrologica sul processo di fusione parziale delle metapeliti. Esso comprende uno studio petrografico-microstrutturale, una caratterizzazione della composizione totale e microchimica dei campioni analizzati e la modellizzazione termodinamica degli equilibri di fase.

Il metamorfismo di alta temperatura è spesso associato a una crosta ispessita in un contesto di collisione crostale. Il processo di fusione parziale della crosta è un problema di rilevanza non solo petrologica, poichè i processi deformativi diventano più efficaci quando la temperatura del solidus viene oltrepassata.

La Nordmannwick nappe è un'unità tettonica di alto grado, situata al contatto inferiore delle ofioliti di Lyngen (Caledonidi norvegesi settentrionali, Norvegia settentrionale). Tale unità è composizionalmente eterogenea (scisti metapelitici, metapsammti, livelli carbonatici, corpi mafici) ma in particolare si osserva la presenza di relitti di rocce metamorfiche di alto grado.

Lo scopo principale di questo lavoro è analizzare nel dettaglio il metamorfismo di alto grado delle migmatiti appartenenti alla Nordmannwick nappe e fornire una ricostruzione dei principali eventi metamorfici. In letteratura non sono presenti studi a proposito del metamorfismo di questa zona.

Sono stati studiati due campioni di migmatiti (LY4f e LY131) appartenenti alla porzione di alto grado metamorfico. Il campione metapelitico LY4f mostra la presenza di relitti di porfiroblasti di cianite e un'associazione mineralogica di picco costituita da biotite + granato + plagioclasio + quarzo + sillimanite + segregazioni leucocratiche. L'associazione mineralogica prodotta dal metamorfismo retrogrado è biotite + mica bianca + granato + plagioclasio + quarzo + sillimanite. Il campione metapsammitico LY131 è caratterizzato dalla presenza di cristalli di cianite parzialmente sostituiti e un'associazione mineralogica di picco costituita da biotite + granato + K-feldspato + plagioclasio + quarzo + sillimanite + segregazioni leucocratiche, mentre l'associazione mineralogica prodotta dal metamorfismo retrogrado è biotite + mica bianca + granato + plagioclasio + quarzo + sillimanite.

In entrambi i campioni sono state individuate tre generazioni del polimorfo Al_2SiO_5. La cianite rappresenta una fase relitta, che ha cristallizzato prima della sillimanite inclusa nei porfiroblasti di granato. La terza generazione è rappresentata da una seconda generazione di sillimanite cristallizzata lungo la foliazione durante il percorso retrogrado.

Le analisi microchimiche effettuate con la microsonda elettronica (EMP) e il microscopio elettronico a scansione (SEM) hanno permesso di distinguere tre generazioni di cristalli di biotite. La prima generazione è rappresentata da inclusioni di biotite all'interno del granato, la seconda è rappresentata da cristalli di biotite all'interno della matrice, mentre la terza è rappresentata da cristalli di biotite a grana fine sempre all'interno della matrice. I due diversi tipi di cristalli di granato, distinti sulle basi delle osservazioni microstrutturali, appartengono alla stessa generazione, dal momento che hanno profili di zonatura chimica simili e lo stesso valore assoluto di concentrazione degli elementi.

Una sequenza caratterizzata da tre eventi metamorfici principali è stata determinata attraverso le osservazioni microstrutturali e le analisi chimiche con la microsonda elettronica. Il primo è un evento di alta pressione, al quale segue un evento di alta temperatura, caratterizzato dalla produzione di fuso anatettico. L'evento metamorfico finale coincide con il metamorfismo retrogrado.

Sono stati applicati ai campioni LY4f e LY131 modelli termodinamici calcolati con Perple_X nel sistema $MnO - Na_2O - CaO - K_2O - FeO - MgO - Al_2O_3 - SiO_2 - H_2O - TiO_2$ (MnNCaKFMASHT). E' stato considerato nel calcolo dei modelli anche il MnO perché condiziona il campo di stabilità del granato a basse pressioni e temperature. Anche la presenza del TiO_2 è significativa dal momento che influenza la stabilità della bioitite a temperature elevate. La modellizzazione termodinamica ha permesso di vincolare in modo soddisfacente le condizioni di pressione e temperatura, alle quali si è equilibrata l'associazione di picco metamorfico nel campo di stabilità della sillimanite, e il successivo percorso retrogrado durante il raffreddamento e la cristallizzazione del fuso anatettico.

Per ottenere stime precise sulla pressione e temperatura di riequilibrazione delle fasi al picco metamorfico e durante il processo retrogrado, sono state plottate le

isoplete sui diagrammi (pseudosezioni) P-T. In questo modo è possibile osservare la variazione di composizione delle soluzioni solide all'interno dell'intervallo di pressione e temperatura considerato. Per vincolare la temperatura sono stati considerati i parametri chimici sensibili a variazioni di temperatura, ovvero il valore di X_{Mg} del granato e della biotite e il contenuto di titanio della biotite. Allo stesso modo, per vincolare la pressione sono stati considerati i parametri chimici sensibili a variazioni di pressione, ovvero il contenuto di grossularia del granato e il contenuto di anortite nel plagioclasio. La temperatura e la pressione stimate per il campione LY4f alle condizioni di picco metamorfico sono $800\pm30°$ and 0.85 ± 0.07 GPa, mentre la temperatura e la pressione stimate per il metamorfismo retrogrado sono $650\pm30°$ and 0.77 ± 1.8 GPa. La temperatura stimata per il campione LY131 alle condizioni di picco metamorfico è $790\pm10°$, mentre la pressione non è stata ottenuta, a causa del completo riequilibrazione del granato. La temperatura e la pressione stimate per il metamorfismo retrogrado sono $670\pm10°$ and 0.75 ± 0.07 GPa.

Attraverso i dati ottenuti dalla modellizzazione termodinamica è possibile affermare che entrambi i campioni studiati sono accomunati da un evento di picco metamorfico e un processo retrogrado, caratterizzati da circa le stesse condizioni di temperatura e pressione. Essi sono dunque caratterizzati da un percorso P-T simile.

INTRODUCTION

The present study is focused on the high temperature metamorphic rocks from the Nordmannwick nappe. The Nordmannwick nappe is high grade tectonic unit, belonging to the Northern Scandinavian Caledonides (Northern Norway). The studied rock samples crop out over a restricted area, located along a section of the eastern coast of the Lyngen Peninsula (Nord-Troms).

The main purpose of this work is to analyze in detail the high-grade metamorphisms of the migmatites from the Nordmannwick nappe and to provide a reconstruction of the metamorphic events, in order to evaluate the temperature and the pressure of these latter. Extensive investigations about the Nordmannwick nappe are still lacking, since there are no studies about the metamorphism of this area in the literature. The only works available are the Master Thesis of Livia Nardini and Thomas Hibelot (2013), students at the University of Tromsø.

A consistent part of this Thesis was carried out at the University of Tromsø, during my stay in Norway, thanks to the Erasmus program. The project was carried out under the co-supervision of Holger Stunitz, professor at the University of Tromsø, who is studying the metamorphic and deformational processes of the tectonic units close to the Nordmannwick nappe.

The Master thesis project was articulated in the following stages:

- petrographic and petrological study of the samples collected;
- X-ray fluorescence analyses in order to obtain the bulk rock composition
- microchemical investigation of the minerals (in particular solid solutions) carried out with the Scanning Electron Microscope (SEM) at the University of Tromsø and with the Electron Microprobe at the University of Padova;
- thermodynamic modelling of two of the selected samples performed with the Perple_X software package;
- thermo-barometry applied to the pseudosections in order to constrain the main metamorphic stages.

The Thesis is constituted by five chapters. The first chapter is an introduction to

the main features of the high temperature metamorphism of metapelites. The second and the third chapter provide respectively a description of the geological setting of the studied area and a description of the petrological characteristics and microstructures of the samples collected. Chapter 4 reports the description of the chemical analyses carried out on the two rock samples selected for the thermodynamic modelling. Chapter 5 reports the thermodynamic models and the relative thermo-barometric evaluations. The Thesis ends with the concluding

CHAPTER 1

HIGH TEMPERATURE METAMORPHISM AND ANATEXIS OF METAPELITES

1.1 PARTIAL MELTING OF METAPELITES

High temperature metamorphism is often associated with a thickened crust in continent collisional settings. Partial melting affects the structure of the continental crust, since the deformational process is more effective when the temperature rise above the solidus and melt starts to be present in the rock (Rosenberg & Handy, 2005). Therefore, partial melting cannot be considered only a matter of petrological interest, because the effects of this process are crustal-scale. The product of partial melting is a migmatite, a rock often constituted by crystallized melt (leucosome) and the residual solid material (melanosome).

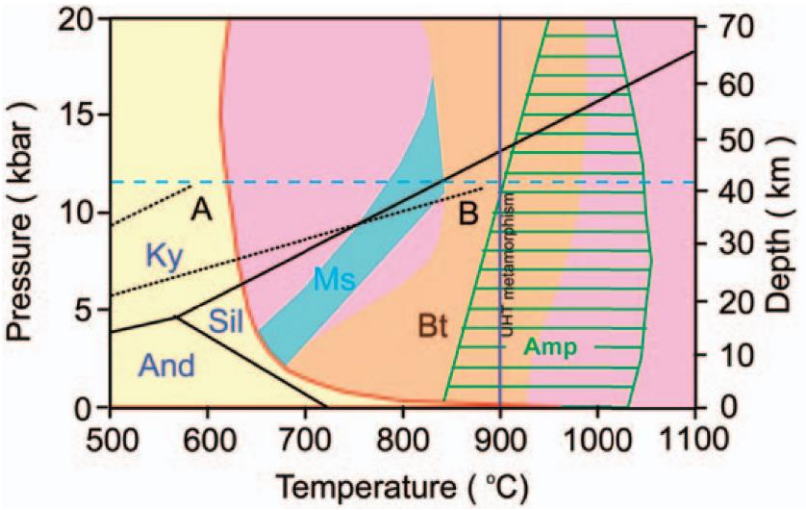

Figure 1.1 P-T section illustrating the types of melting for the continental crust. The red line is the water saturated solidus. The partial melting region is the pink field. The purple line marks the start of ultra-high temperature metamorphism (900°). (Sawyer et al. 2011)

A significant part of the upper continental crust is constituted by pelitic and quartzo-feldspathic rocks. Also the lower crust is constituted by significant amount of peraluminous sediments since more than 27% of samples collected from granulitic terrains are pelitic metasediments (Hacker et al. 2011). Given the

importance of the pelitic sediments I will focus my attention in this work on this type of rocks.

Metapelites and metagreywackes may start to melt at relatively low temperature (650°) under water saturated conditions and they produce a liquid of granitic composition. White mica and biotite breakdown reactions control the melting process in the metapelitic system. The temperature interval of white mica (Ms) and biotite (Bt) incongruent melting reactions are highlighted respectively in blue and orange in figure 1.1. Figure 1.1 shows also the incongruent melting reaction of amphibole (green field). Partial melting of mafic rocks occurs at higher temperatures and the melt produced is tonalitic.

Figure 1.2 shows that partial melting primarily takes place in the lower part of the crust and migmatites forms when the temperature rises above the solidus. The melt produced commonly migrates away from the source rock along focused pathways. It can end in the middle crust to form dike complexes or it can collect at the transition between the middle crust and the brittle crust to form plutons.

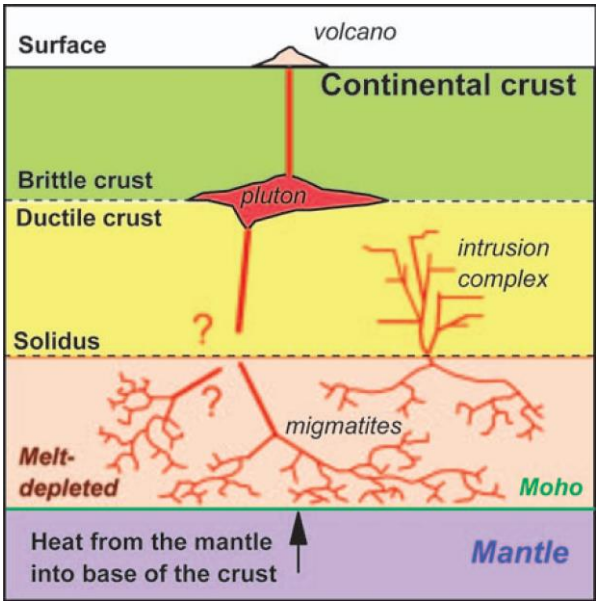

Figure 1.2 Schematic representation of the reworking of the continental crust due to partial melting (Sawyer and Cesare, 2011).

Partial melting has been studied from both theoretical and experimental points of view for many decades. Such studies have provided an estimation of the melt

fertility of the rocks and they have also constrained the reactions that govern the melting process. In the last thirty years software like Thermocalc and Perplex allowed the development of quantitative thermodynamic models. Thermodynamic models of the melting process in general and of specific rock compositions via pseudosections has become common ever since (White et al, 2011).

In the following part of the chapter, I provide some examples of phase diagrams (P-T and T-X pseudosections) calculated by the thermodynamic modelling approach, to introduce the main characteristics of partial melting of metapelites.

1.2 EXAMPLES OF CALCULATED PHASE DIAGRAMS

In order to describe an example of the behavior of metapelites which undergo partial melting, I have calculated the pseudosection in the NCaKFMASH system reported in figure 1.3. I have used the average shale composition reported in Gromet et al. (1984). Silica is assumed to be in excess and I have added an amount of water enough to saturate the mineral assemblage immediately below the solidus at moderate pressures (0.5 GPa, see also figure 1.4). I have used an approach similar to that outlined by White et al. (2001).

No univariant lines appear and the divariant fields take up a small portion of the diagram. As temperature rises, the variance increase because the melting process becomes more advanced. At very high temperature, cordierite and garnet melt out and the variance reaches the value of 7, the assemblage being made of garnet or cordierite and melt alone.

Chlorite and staurolite should be present in the low temperature part of the diagram. However, they are not considered in the calculation, in order to focus the attention on the melting reactions.

Along the medium P/T metamorphic field gradient, namely at pressure above than point 1, melt first appears as a result of the reaction

White mica + plagioclase + quartz + H_2O = melt + sillimanite

Given that a little amount of water is available for the reaction, very little melt is produced. Continuous reactions involving white mica, garnet, sillimanite, quartz

and biotite produces further melt, nevertheless at this point the melt volume does not exceed a few units percent.
The first major melting reaction (green in fig. 1.3) is

White mica + plagioclase + quartz = sillimanite + K-feldspar + melt

This reaction involves the breakdown of white mica and the likely appearance of leucocratic segregations in the rock. The consequence of this process is the formation of a migmatite, a rock characterized by small patches or lenses of granitic melt intermixed with the gneissic part. The amount of melt produced depends on the amount of the reactants (white mica in particular). Spear et al. (1999) calculated that the amount of melt generated corresponds to 70% of the volume of the white mica consumed. In this case white mica constitutes the 30% of the rock, thus the volume of melt generated is 20%.
Further melt is produced because of dehydration melting of biotite, which is due to several reactions depending on the pressure. At moderate pressure (0.5 GPa) the biotite breakdown reaction is

Biotite + sillimanite + plagioclase + quartz = garnet + cordierite + K-feldspar + melt

Whereas at slightly lower pressure biotite is consumed by the reaction

Biotite + garnet + plagioclase + quartz = cordierite + orthopyroxene + K-feldspar + melt

At higher pressures (about 0.8-1 GPa) cordierite and orthopyroxene are not involved and biotite breaks down as a result of the reaction

Biotite + sillimanite + plagioclase + quartz = garnet + K-feldspar + melt

At this point the amount of melt produced is relevant and up to 40-50% of the rock is molten. The solid residue contains K-feldspar, garnet, plagioclase and sillimanite and all the hydrous phases have reacted out. The remaining phases are gradually melted as temperature rises. For instance, K-feldspar is consumed at ~ 800 °C at low pressure, whereas at high pressure is stable up to 900-950 °C. Plagioclase melts out at the same temperature of K-feldspar at low and moderate

pressures, whereas at high pressure it is consumed at lower temperature (~ 850 °C).

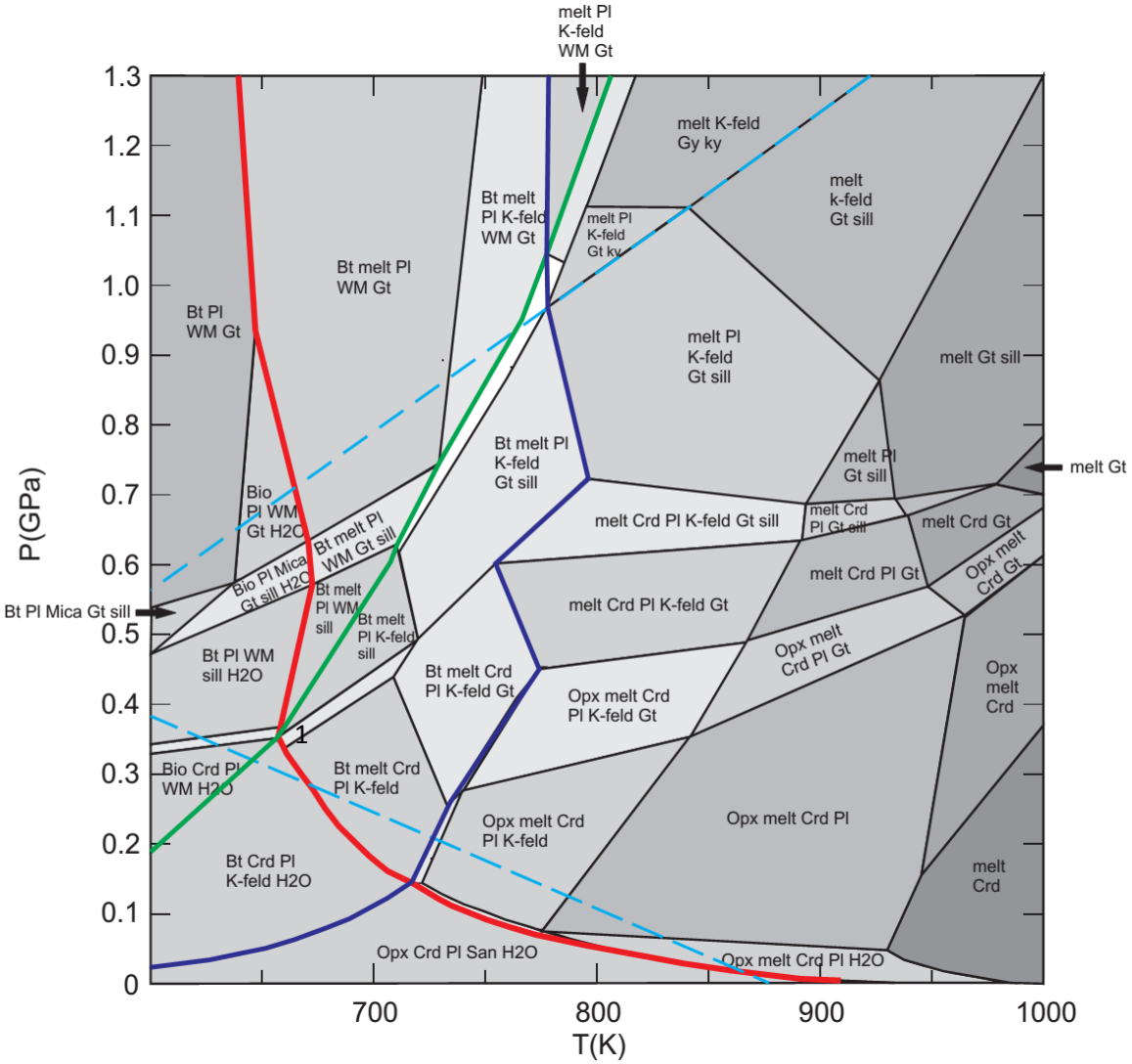

Figure 1.3 P-T pseudosection in the NCaKFMASH system for the average shale composition of Gromet et al. (1984) mol% Na_2O = 2.89 MgO =11.34 Al_2O_3=32.12 CaO = 4.10 K_2O = 8.52 FeO = 18.74. Quartz is assumed to be in excess and H_2O is added in sufficient quantity to saturate the solidus at 0.5 GPa. The solidus is highlighted with the red line, whereas white mica and biotite breakdown reactions are highlighted respectively with the green and blue line. The extensions of Al_2SiO_5 polymorph reactions are shown with the dashed line for clarity.

The temperature of granite-wet solidus rises as pressure drops, so that at pressures below the point of intersection of the solidus curve and the muscovite out curve, muscovite and biotite breakdown reactions take place before melting. At very low pressure, in contact metamorphism conditions, cordierite and orthopyroxene occur

before the rock has crossed the solidus.

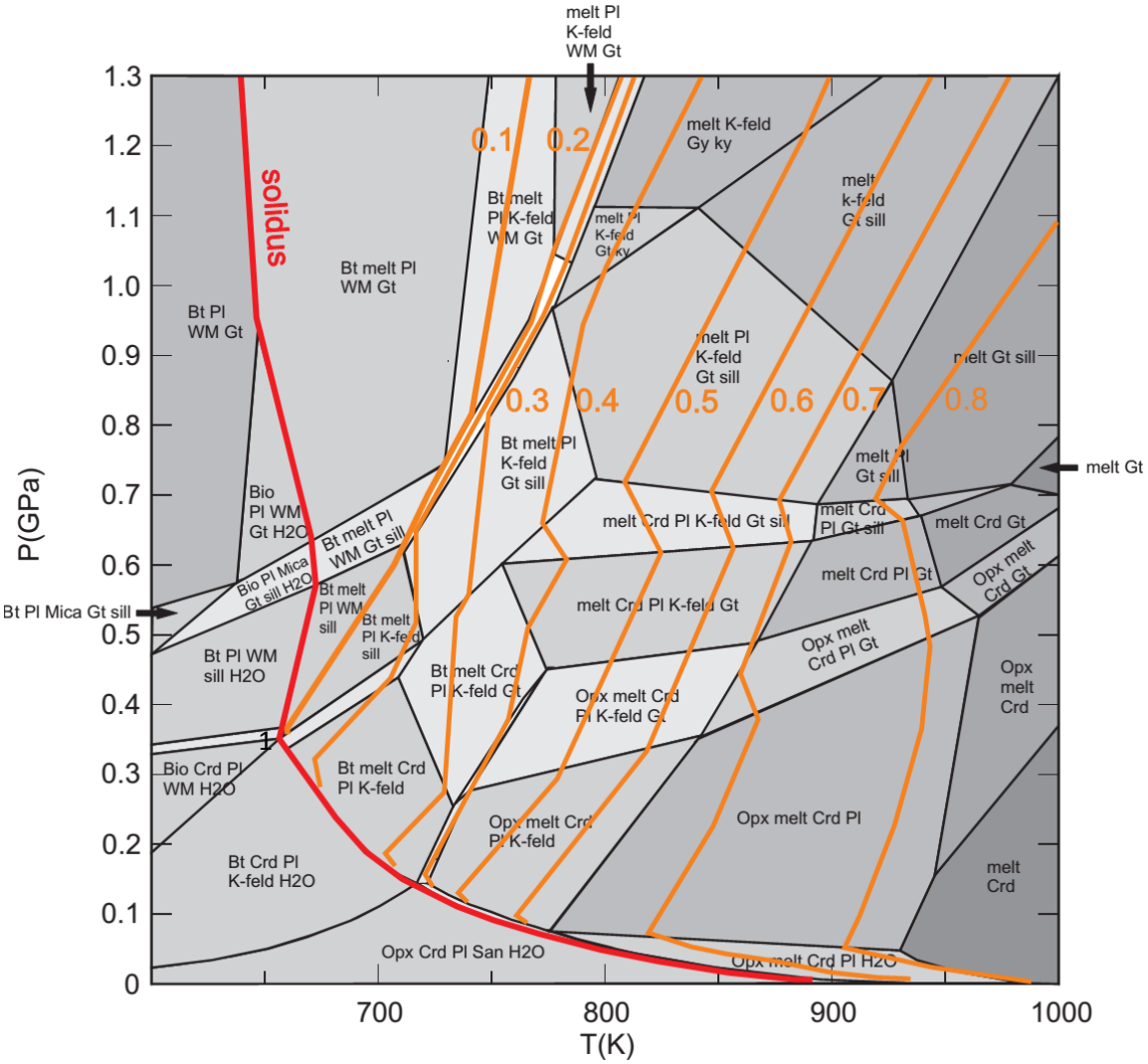

Figure 1.4 Pseudosection showing the melt mode contours (volume fraction)

Melt mode contours are shown in figure 1.4. Melt mode contours are generally very steep and have a positive slope. They tend to occur inside the mineral assemblage fields, supporting the fact that the melt production is caused by continuous reactions.

Note that very little melt is produced near the solidus and that the melt volume fraction does not exceed 0.1 (10%) until white mica breaks down. White et al. (2001) called this reaction the effective solidus, because before this point the melt amount is very low and it would be very difficult to recognize it in the rock.

1.3 DEPENDENCE OF THE EQUIIBRIA ON WATER CONTENT AND X_{Mg} CHANGES

An important aspect to be evaluated during partial melting is the amount of water present in the system. The pseudosection in figure 1.5 shows the dependence of the mineral assemblages on the H_2O content of the system. The water content is 0 at 0 and enough to saturate the subsolidus assemblage at x =1. The water saturated mineral assemblages are contoured with the red dashed line.

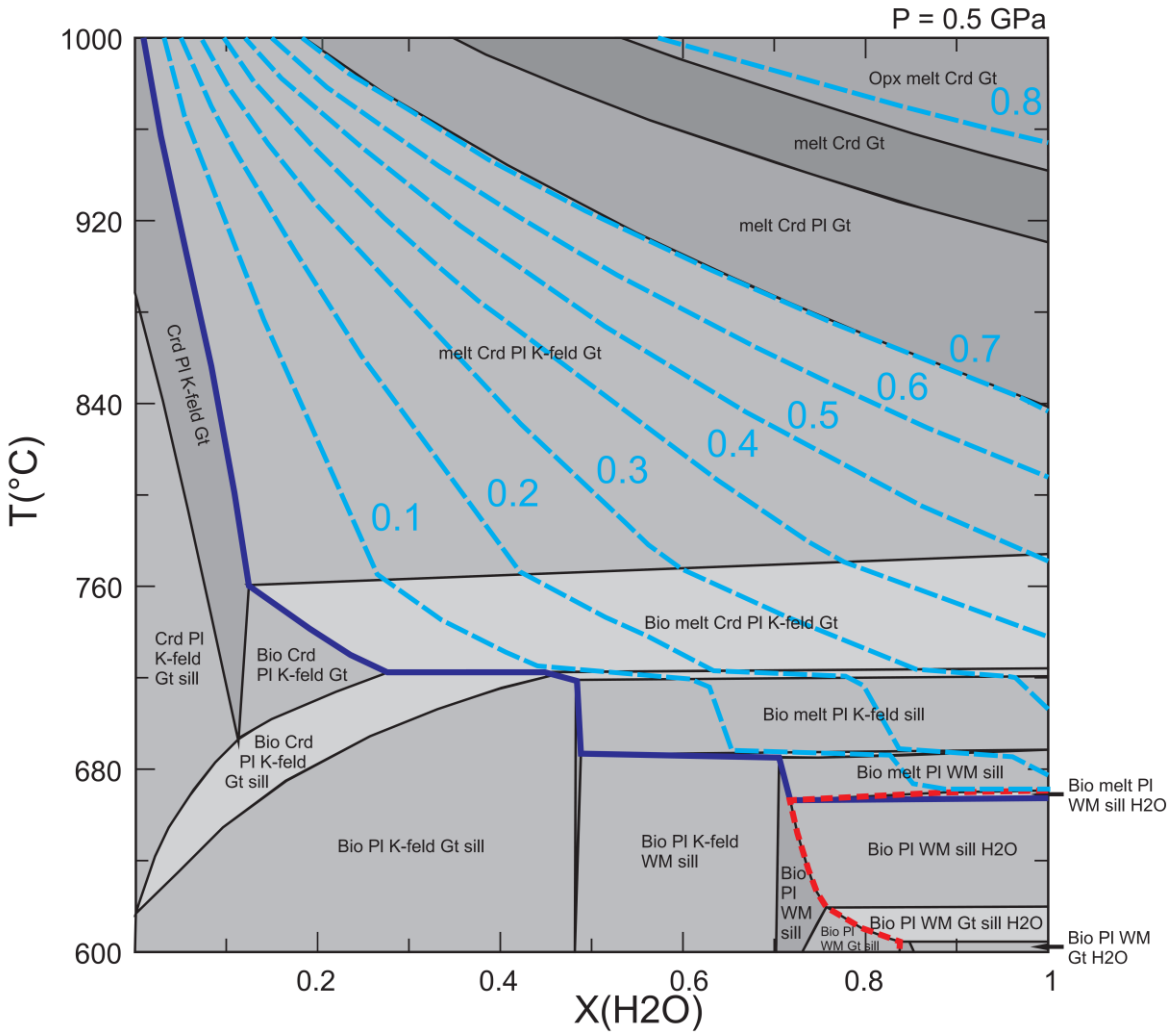

Figure 1.5 T-X_{H2O} pseudosection at 5 GPa in the NCaKFMASH system for the bulk composition used in figure 1.1. The x axis varies from H_2O = 0 (x = 0) to H_2O = 25 (x = 1). Quartz is assumed to be in excess.

The melt mode contours are shown as well. The amount of melt produced is a function of the amount of water present, because the larger the water amount

present in the system is, the greater is the melt volume produced. Also the temperature of the solidus is sensitive to the water content, since the rock starts to melt several hundred degrees earlier under water saturated conditions.

Observing the melt mode contours trend, it is clear that water plays a fundamental role, because the water amount affects also the proportions of hydrous minerals. The main increase in the amount of melt produced occurs where the hydrous phases, such as biotite and white mica, are being consumed. Note how the melt contours are flatter inside the narrow fields where the hydrous phases are progressively consumed and how they get steeper inside the fields where the hydrous phases are not consumed. In the high temperature part of the diagram the melt production is more sluggish (melt volume percent remains close to 70% for 120 °C before reaching 80%), even with advanced degrees of partial melting, since the hydrous phases are totally consumed and the solid assemblage has become very refractory.

Another important aspect is the variation of Fe and Mg of the bulk composition, because the majority of the reactions involve Fe-Mg solid solution-phases. Variations of X_{Mg} (X_{Mg} = Mg/(Mg+Fe)) affect the topology of the divariant fields and shift the location of the metamorphic reactions of several degrees or kilobars (Vielzeuf and Holloway, 1988).

The minerals affected by X_{Mg} changes of the bulk composition are biotite, garnet, cordierite, orthopyroxene and spinel (fig. 1.6).

Garnet in metapelites is usually almandine rich. For $X_{Mg} > 0.60$ it disappears from the diagram. Considering other T-X_{Mg} pseudosections calculated at progressively higher pressure, it is possible to notice that as X_{Mg} increases, the lower boundary of garnet stability field shifts to higher pressures.

On the contrary, orthopyroxene is not stable at low X_{Mg} values. As X_{Mg} increases orthopyroxene is stable at higher pressures.

Biotite is stable over the entire compositional range, but at low X_{Mg} the breakdown reaction occurs at lower temperature than at high X_{Mg} values.

Spinel is a hercynite-rich solid solution, therefore is stable only at very low X_{Mg} values.

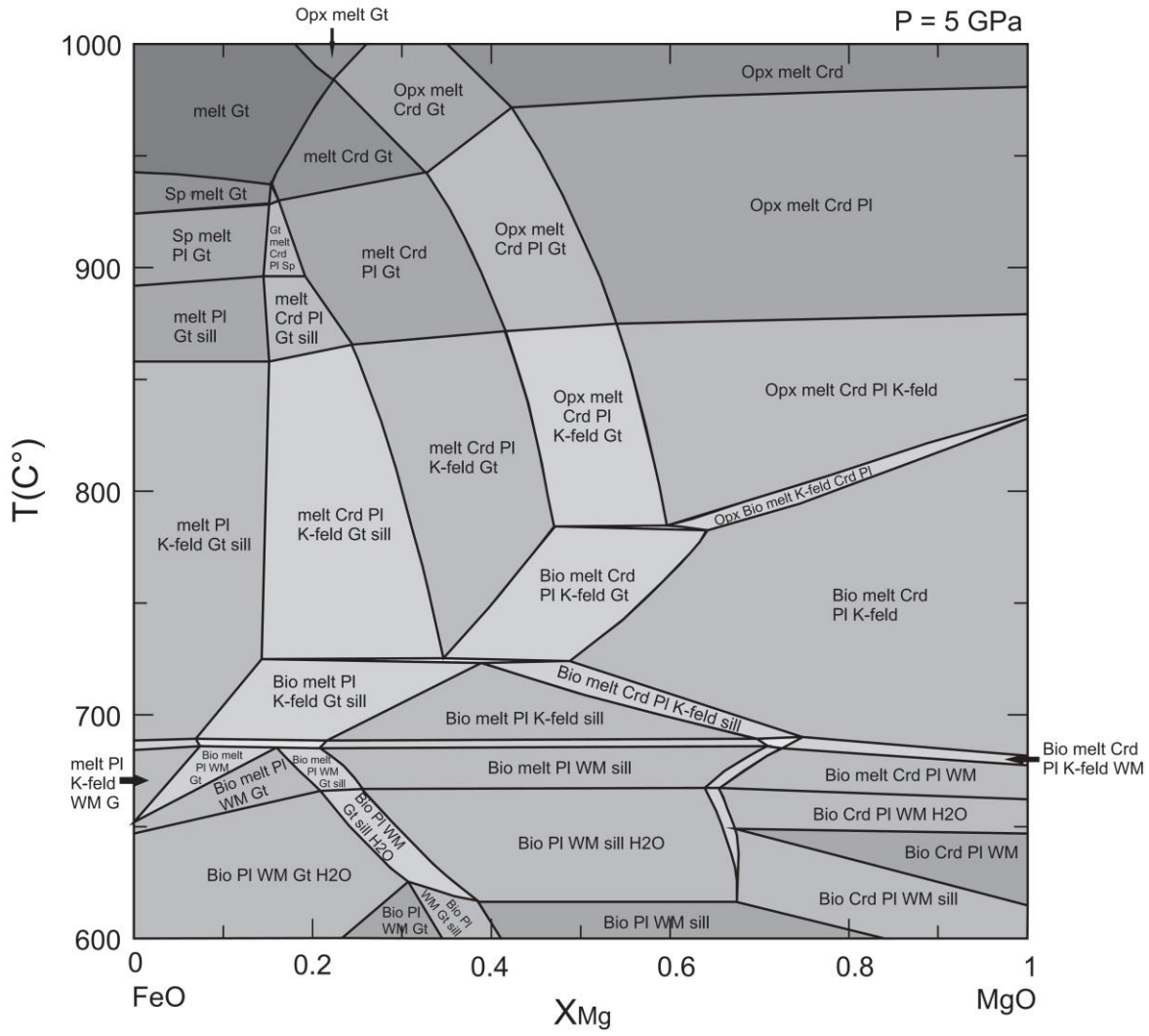

Figure 1.6 T-XMg pseudosection at 0.5 GPa for the bulk composition used in figure 1.1. The axis varies from FeO = 30.08 and MgO = 0 (x = 0) to FeO = 0 and MgO = 30.08 (x = 1).

1.4 BIOTITE BREAKDOWN REACTION AT HIGH PRESSURE

Phase equilibria modelling can have several applications. One is the calculation of T - X_{Mg} diagrams, which can be useful to illustrate phase relationships where Fe – Mg solid solutions are involved.

In order to illustrate properly the reaction

Biotite + sillimanite (+ quartz + plagioclase) = garnet + K-feldspar + liquid

I have calculated the pseudosection reported below (figure 1.7).

This diagram provides a schematic isobaric T - X_{Mg} representation. In order to

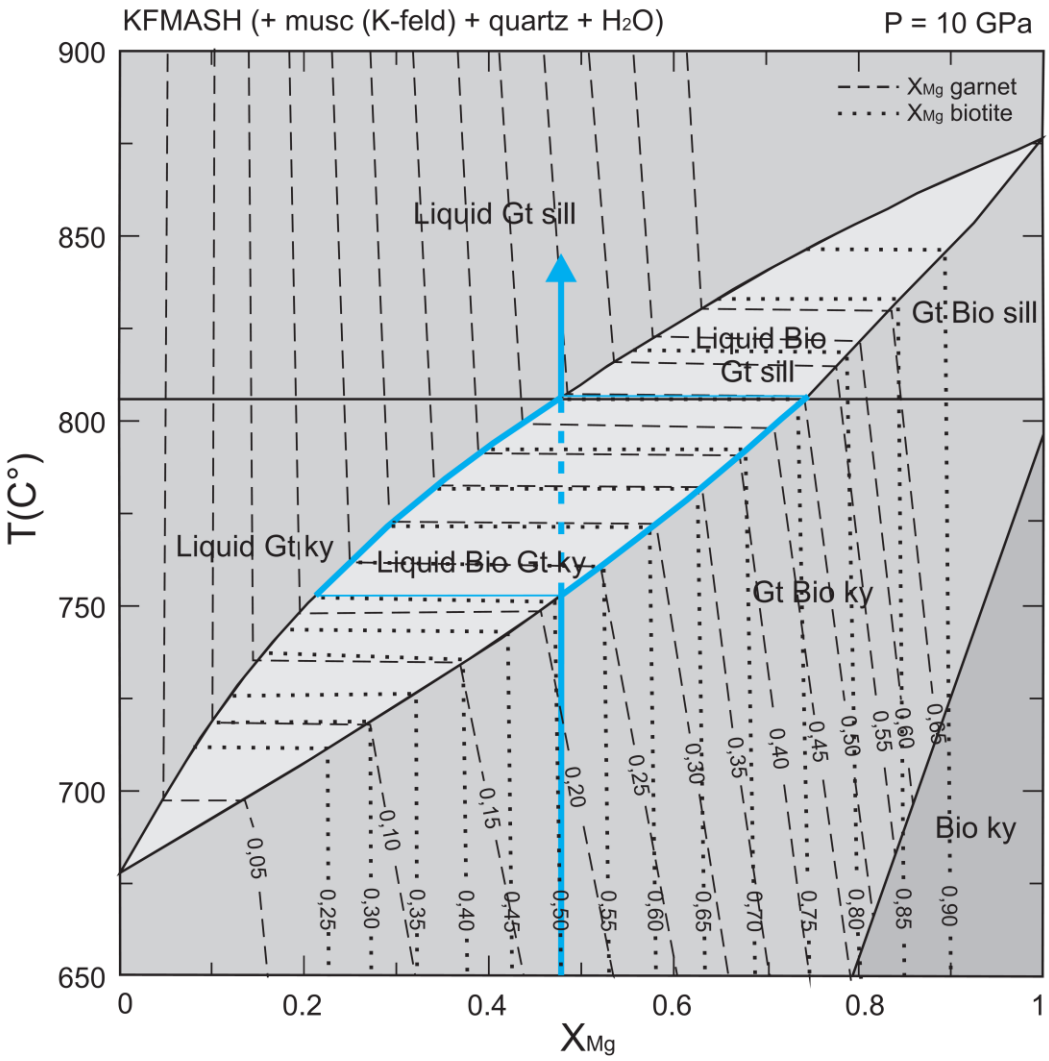

Fig. 1.7 T-X_{Mg} pseudosection at 1 GPa calculated in the KFMASH system. The x axis varies in mol% from FeO = 37.13 and MgO = 0 (X_{Mg} = 0) to FeO = 0 and MgO = 37.13 (X_{Mg} = 1). Al_2O_3 and K_2O are set respectively to 31.74 and 6.76 mol%, whereas SiO_2 and H_2O are assumed to be in excess.

represent the reaction in a simplified two component system, muscovite (K-feldspar), quartz and water are assumed to be in excess. The reaction is discontinuous if we consider the pure Fe or Mg system, because it occurs at a single temperature, whereas in the mixed Fe-Mg system the reaction becomes continuous. As typical of most Fe – Mg equilibria, the reaction in the KFASH system occurs at lower temperature than the reaction in the KMASH system. During the temperature interval over which biotite, garnet and sillimanite coexist together, the solid solution phases increase their Mg content. The proportions

between the minerals involved vary as well, because the amount of the reactants will progressively decrease until one of the reactants will be completely consumed. Because biotite is more magnesian than the associated garnet, while biotite breaks down it releases Fe and Mg. The amount of Mg released from biotite is enough to cause the formation of new biotite and garnet crystals richer in Mg than they were previously.

The temperature at which the first drop of melt is generated, depends on the X_{Mg} of the bulk composition. For instance, if we heat a rock characterized by an X_{Mg} equal to 0.2, biotite starts to break down at about 700°C, whereas if we heat a rock characterized by an X_{Mg} equal to 0.7, biotite starts to melt at about 800°C. The temperature at which the reaction begins varies by 100°C considering these two examples.

Let's consider now the case in which a rock is characterized by the X_{Mg} ratio of 0.50, a composition which characterizes the rocks studied in the following chapters. According to this model, the rock is heated isobarically at a pressure of 1 GPa. Almost nothing happens until the blue line meets the light shaded field. At this point biotite and sillimanite start to be consumed, in order to produce garnet plus liquid. The rock is now constituted by garnet, sillimanite, biotite, liquid and, of course, by K-feldspar, quartz and water are assumed to be in excess. Because of continuous isobaric heating, the continuous reaction

Biotite + Sillimanite (+ quartz) = garnet (+ K-feldspar) + liquid

involves the progressive garnet growth in the presence of anatectic melt and the consumption of biotite and sillimanite. The reaction begins at 750°C but it is not completed until 810°C, when biotite is totally consumed and the X_{Mg} of garnet has become equal to the X_{Mg} bulk composition. This reaction involves also a continuous change of biotite and garnet composition, since these minerals will be characterized by increasing X_{Mg} (Mg/(Fe+Mg)) values. Garnet, in particular, will show an increasing pyrope content towards the rim (Spear et al.1999).

The trend of biotite and garnet X_{Mg} isopleths is relevant, since they are characterized by a steep slope before and after the occurrence of the reaction, so that the composition of the solid solution is not affected in these parts of the

diagram. On the contrary, they are rather flat in the light shaded field, where the composition of garnet and biotite changes as the temperature rises.

This process can be described with a sequence of AFM diagrams as well.

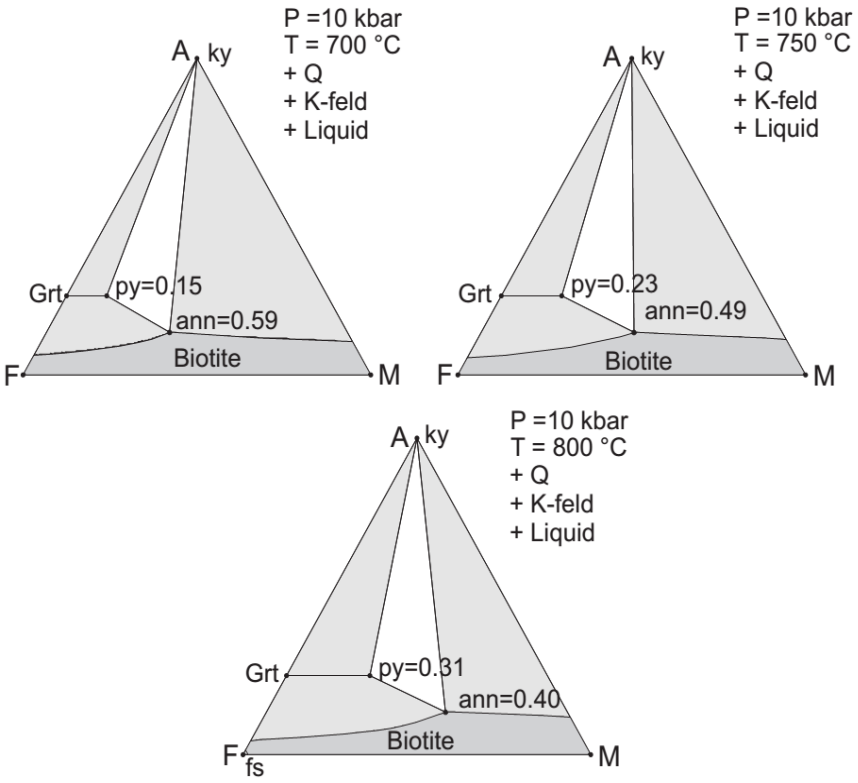

Figure 1.8 A series of AFM compatibility diagrams above the muscovite-out isograd (granulite facies) illustrating the migration of Kyanite - Biotite – Garnet subtriangle toward Mg richer compositions.

Figure 1.8 illustrates that the continuous reaction involves the shift of the kyanite – biotite - garnet subtriangle towards Mg richer composition as temperature rises.

1.5 ANATEXIS OF GRAPHITIC METAPELITES

The rocks that I have studied are graphitic, therefore it is useful to consider the implications of the presence of graphite on the metamorphic equilibria and the melting equilibria.

At high temperature and pressure, the fluid phase is in a supercritical state, because the system is characterized by pressure and temperature conditions above the critical point of CO_2 and H_2O mixtures. At these conditions there is no distinction between the vapor phase and fluid phase. Because of the significant presence of CO_2 and CH_4 in the in the volatile species in graphitic metamorphic

fluids, the diagram in figure 1.9 will be useful to describe the C-O-H fluid system (Connolly, 1995).

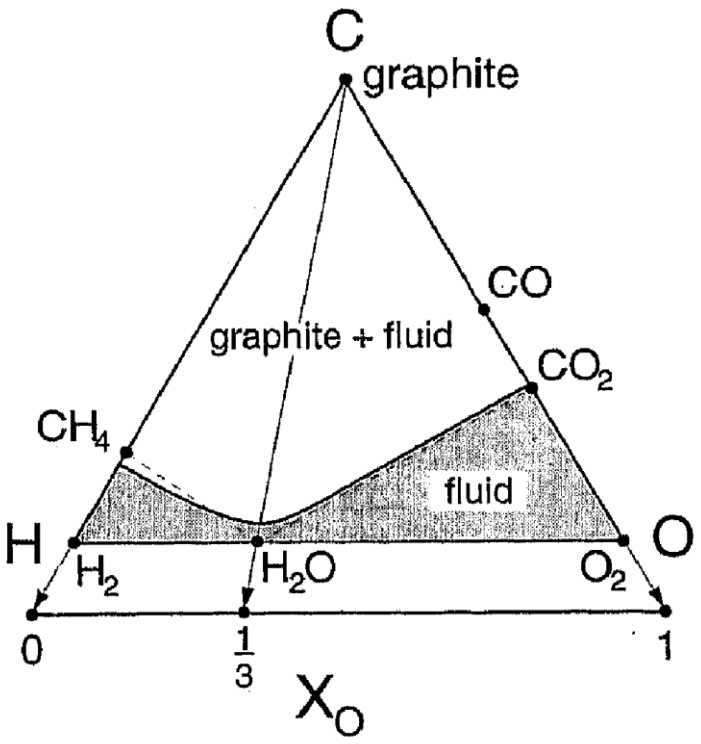

Figure 1.9 Isobaric-isothermal phase diagram for the C-O-H system showing the relation between X_O and GCOH fluid composition (Connolly, 1995)

Fluids characterized by a composition that lies inside the H_2O, CO_2 andO_2 triangle are relatively oxidized and are composed by a H_2O-CO_2-O_2 mixture. On the contrary, fluids inside the H_2O-CH_4-H_2 triangle are more reduced. At fixed temperature and pressure the system is divariant because it is characterized by three components and one phase (F = 3 – 1 + 0 = 2).

The presence of graphite in the rock indicates that the metamorphic process is characterized by the presence of a graphite-saturated fluid in the C-O-H system.

Graphite is stabilized by increasing carbon concentration. The precipitation of graphite substantially prevents the fluid to become C-richer and it also limits the compositional variation of the fluid, because the fluid composition must lie along the graphite saturation surface.

Connolly and Cesare (1993) argued that during dehydration the composition of C-O-H fluid is buffered toward the maximum activity of H_2O. This condition

implies that the atomic ratio H/O of the fluid composition is constrained at 2:1, because in a dehydration reaction the only source of hydrogen and oxygen are the hydroxyl-bearing phases. The only degree of freedom of a fluid with a constant H/O is removed considering that it lies on the graphite saturation surface. Therefore, the presence of a GCOH fluid does not affect the thermodynamic variance of the dehydration equilibria.

The presence of graphite implies that the activity of water is lower than 1. Therefore, the dehydration melting reactions will be displaced toward higher temperature (Johannes and Holtz, 1996), whereas subsolidus dehydrations will occur at lower temperatures. However, as long as the COH fluid is generated by dehydration reactions (H/O = 2) this effect is negligible except at high temperature and low pressure.

Another important effect of the presence of graphite occurs during the initial stages of anatexis. If a fluid is present in the system, not only the melting reactions will be displaced toward higher temperatures for a few tens degrees, but also partitioning of water in the liquid will cause the precipitation of graphite because of the reaction (Cesare, 1995):

$CO_2 + CH_4 = 2H_2O + 2C$

The graphite saturation line is not fixed, but varies as a function of pressure and temperature. At low temperature and pressure it corresponds to the dashes line and it essentially reflects binary H_2O-CO_2 composition or binary H_2O-CH_4 composition. At low metamorphic grades the fluid is characterized by a mixture of H_2O-CO_2 or by a mixture of H_2O-CH_4. When pressure and especially temperature rise significantly, the fluid departs from the dashed line and assumes the bold-highlighted black line configuration. The displacement of the graphite saturation line allows the fluid composition to accommodate a little bit of H_2 or of CO considering respectively the left or right side of the triangle.

CHAPTER 2
GEOLOGICAL SETTING

2.1 GEOLOGICAL SETTING OF NORTHERN NORWAY

The field area is located in Northern Norway and geologically belongs to the Scandinavian Caledonides (figure 2.1).

The nappe complex that characterize the Scandinavian Caledonides of Northern Norway are divided into four main tectonic units. These four main units are named in ascending order Lower Allochthon, Middle Allochthon, Upper Allochthon and Uppermost allochthon (figure 2.2). This group of nappes is characterized by flat-lying thrustsheets that are emplaced upon the Baltoscandian margin.

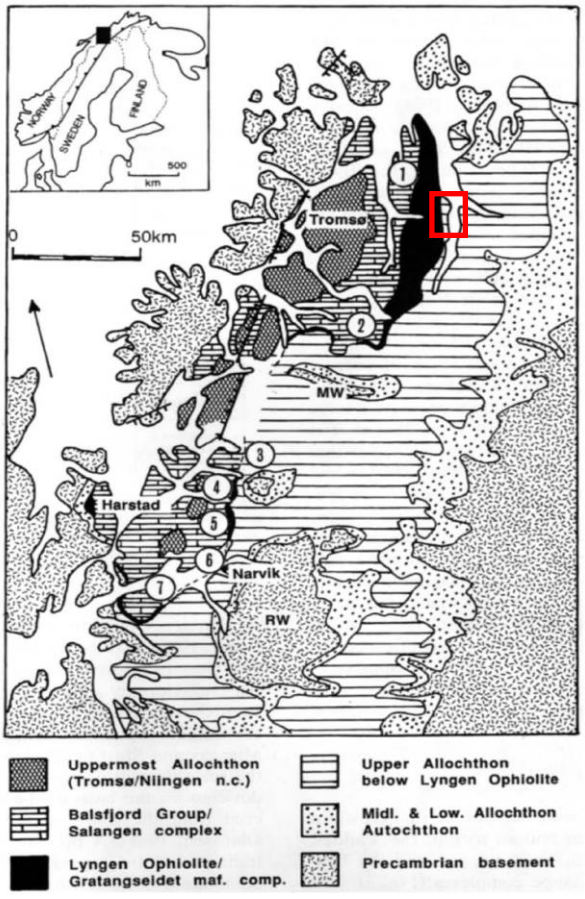

Figure 2.1 Tectonic map illustrating the main lithotectonic units, which characterize the Scandinavian Caledonides of Northern Norway (Andersen and Stelltepohl, 1994). The fieldwork area is highlighted with the red rectangle.

Considering the Lower and the Middle Allochthons, it stands out that the highest thrustsheet has covered the longest distance and the lowermost thrustsheet the shortest distance. The highest thrustsheet of the Middle Allochthon covered a distance of 200-300 Km (Andersen, 1988).

The Upper Allochthon and the Uppermost Allochthon are constituted by exotic terrains that have travelled several hundred kilometers and that were also emplaced on the Baltoscandian platform.

The Lower Allochthon, the Middle Allochthon, the Upper Allochthon and the Uppermost Allochthon are thrustsheet units that lie upon the autochthon sedimentary sequence that covers late Precambrian basement. The late Precambrian metasediments are characterized by a series of flat-lying nappes, which thin towards the north-west.

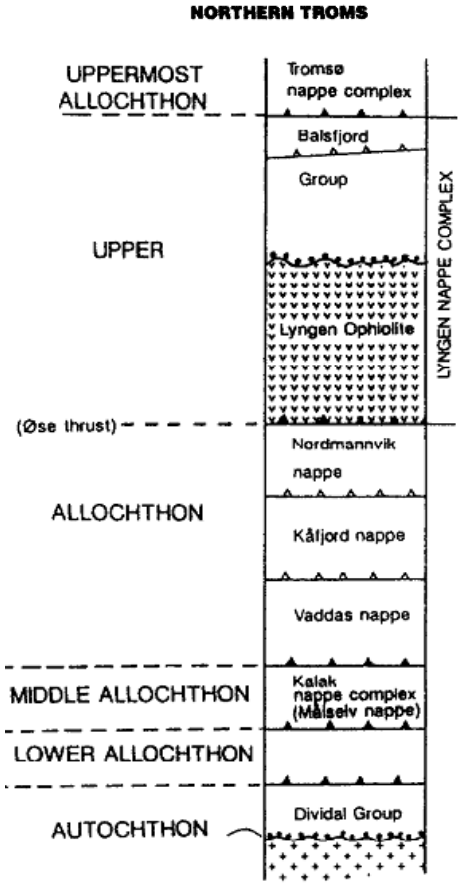

Figure 2.2 Schematic tectonostratigraphic section of the Troms nappe stack proposed by Andersen and Stelltepohl (1994)

2.1.1 PRECAMBRIAN BASEMENT

The rocks that form the Precambrian basement crop out in three different geological settings. They are exposed as undisturbed crystalline basement in the eastern part of the orogen, as tectonic windows in the middle of the orogen and as Precambrian basement rocks showing variable degrees of superimposed Caledonian structures. The basement rocks range in age from Archean to Mid Proterozoic (Andersen, 1988).

2.1.2 AUTOCHTHONOUS AND PARA-AUTOCHTHONOUS DOMAIN

The Autochthonous and Para-autochthonous sequence are exposed in the eastern margin of the Orogen. The Autochthon domain is constituted by three groups named Vadso Group, Tanafjord Group and Vestertana group. They are characterized by variable depositional environment. The Vadso Group is formed by fluviatile sandstone and it is separated by the shallow marine sediments of the Tanafjord Group by an unconformity. Another angular unconformity separates the Tanafjord Group from the Vestertana Group. The Vestertana Group is formed by alternating beds of sandstones, siltstones and conglomerates. This succession of different types of beds suggests alternating depositional environment varying from continental to deep water conditions. The Autochthon domain is considered to be of Precambrian to early Cambrian age.

2.1.3 LOWER ALLOCHTHON

The Lower Allochthon consists of a nappe stack composed by a sedimentary sequence deposited on the outermost part of the passive continental margin of the Baltica plate. It is characterized by a folded and thrusted sedimentary sequence, which underwent a low-grade metamorphism. Mafic dikes, which intrude the sedimentary sequence, are observed locally.

2.1.4 MIDDLE ALLOCHTHON

The Middle Allochthon is considered to be of Baltoscandian origin. The Middle

Allochthon is made up by two principal domains, namely the Laksfjord Nappe and the Kalak Nappe Complex.

The Laksfjord Nappe is a metasedimentary sequence formed by metasandstones, schists and phillytes above a basal conglomerate and covered by a dolomitic domain. The Laksfjord Group is characterized also by the presence of dolerite dykes.

The Kalak Nappe Complex is composed by 8 different thrust sheets. The Kalak Nappe Complex differs considerably from the Laksfjord Group because it is characterized by a higher metamorphic grade and a more intense deformation. Furthermore, it shows larger portions of basement rocks and a larger number of intrusive mafic dykes. It is possible to notice a general increase in the metamorphic grade westward. The sedimentary cover consists of different compositional domains (metapelites, metagreywack, marbles, metapsammite). The Seiland Igneus Province, which is an alkaline plutonic complex, also belongs to the Kalak Nappe Complex. It is considered to have intruded during the early phase of deformation of the Kalak Nappe Complex.

The Upper and the Uppermost Allochthon are considered to be formed by a nappe stack of exotic origin with respect to the Baltica continent, which was emplaced on the outer margin of Baltica.

2.1.5 UPPER ALLOCHTHON

The Upper Allochthon is exposed in two distinct tectonic settings. In Troms it forms a sequence of flat-lying nappes, which lie on top of the Kalak Nappe Complex, whereas in Finnmark it is represented by the Barents Sea Terrane, which constitutes the Northeastern half of the Varanger Peninsula.

The Barents Sea Terrane is a thick pile of sediments (15000 m) divided in two main groups, namely the Barents Sea Group and the Lovikfjell Group. The Barents Sea Group is separated from the Kalak Nappe Complex by a thrust contact.

The flat-lying nappes which form the Upper Allochthon are divided into four main lithotectonic units: Vaddas Nappe, Kafjord Nappe, Nordmannwick Nappe

and Lyngen Nappe.

The Vaddas Nappe is a succession of metasediments and metavolcanic rocks. It is composed at the base by interlayered marbles and schist overlain by a quartzite unit. The metamorphic grade of the Vaddas Nappe ranges from upper greenschist facies to lower amphibolite facies and it is possible to recognize a single tectonothermal event.

The Vaddas Nappe is separated from the Kafjord Nappe by a thrust contact. The lower part of the Kajord Nappe is formed by marbles, meta-psammites and garnet mica-schists, whereas the upper part is dominated by amphibolite layers and granite bodies wrapped up by mylonitic gneisses. The metamorphic grade is hard to establish because of the intense mylonitization and the high strain that this lithotectonic unit underwent. Bergen and Andersen (1995) identified three different deformational events which are also recognized in the overlying lithotectonic unit, namely the Nordmannwick Nappe.

The Nordmannwick nappe is a high grade tectonic unit sandwiched between the Kafjord Nappe and the Lyngen Nappe. It is a very heterogeneous unit, dominated by mylonitic micaschists, which includes amphibolite, marble, dolomitic marble, calc-silicate and ultramafic lenses. The metamorphic grade ranges from middle to upper amphibolite facies, although relict portions of rocks metamorphosed in the granulite facies are present.

The Lyngen Nappe is constituted by three main lithotectonic units, namely the Koppangen formation, the Lyngen Ophiolite and the Balsfjord Group. The Koppangen formation is composed by greenschist facies metapelites with thin metaconglomerate and metasandstone layers and is separated from the underlying Nordmannwick Nappe by a thrust.

The Lyngen Ophiolite is formed at the base by an intensively deformed dolerite dyke swarm followed by a deformed metagabbro. The gabbro, which constitutes most of the Lyngen Peninsula, becomes less deformed departing from the lower limit. The Lyngen Gabbro is a thick layered gabbro unit and it accounts for the largest ophiolitic complex of the Scandinavian Caledonides. It is considered to be the relict oceanic floor of the Iapetus Ocean.

The Balsfjord Group is made up by schists, quarzites, conglomerate and several types of carbonate deposits. The Balsfjord Group represents the upper boundary of the Upper Allochthon.

2.1.6 UPPERMOST ALLOCHTHON

The Uppermost Allochthon is characterized by a clear Laurentian affinity, since it is located on top of the Lyngen Ophiolite. Most of the Uppermost Allochthon is represented by the Tromsø Nappe Complex, whose lowermost part is formed by garnet micaschists and quartzo-felspatic gneisses, intruded by various felsic plutons. The quartzo-feldspatic gneisses are followed by amphibole gneisses and deformed amphibolites (Skattøra Gneiss), which are crosscut by anorthositic dikes. On top of the Skattøra Gneiss lies the Tromsdalstind sequence, which is a heterogeneous unit formed by garnet amphibolites, calc-silicate rocks, marbles, amphibole gneisses, kyanite and sillimanite-bearing garnet schists and gneisses. In the lower part of the Tromsdalstind sequence partly retrogressed eclogites and high-pressure granulites occur as boudins and lenses within marbles. The Tromsdalstind Sequence is characterized by a complex geological history, since several generations of equilibrium mineral assemblages occur. The presence of high pressure rocks suggests that metamorphism and deformation took place in a subduction zone environment.

2.2 CALEDONIAN OROGENY

The Scandinavian Caledonides formed as a result of the collision between Baltica and Laurentia during the closure of the Iapetus Ocean. Nowadays, the Caledonian Orogen is exposed in Western Scandinavia, Svalbard archipelago, Greenland, North America and Great Britain. Its scattered geographical distribution is a consequence of the breaking up process, which led to the opening of the Northern Atlantic Ocean in Cenozoic times.

The Caledonian orogenic history is characterized by an early stage of rifting with formation of passive margins and production of oceanic crust, followed by a compressional stage where the oceanic crust is progressively consumed. The final

stage involves the collision of Baltica and Laurentia continents and the resulting subduction of one plate beneath the other.

Passive margins played an important role during the collisional process. The extensional faults were reactivated and controlled the geometry of the nappes during the emplacement of the exotic terranes (Andreasson, 1994).

The nappes underwent regional metamorphism and multiple deformation processes. The westward increase of the metamorphic grade and the absence of magmatic intrusion in the pre-Cambrian Baltic basement indicate a west-directed subduction, characterized by the underthrusting of Baltica beneath the Laurentian craton during the final collisional phase.

Structural and stratigraphic observations document considerable transport distances, in the order of 500 km. The subduction of the Baltic continental lithosphere is proved by the presence of coesite-bearing eclogites collected in the basement rock of south-western Norway (Andresen and Steltenpohl 1994).

The Scandinavian Caledonides extend for a length of ~2000 km and are characterized by an east-vergent thrust system.

2.3 CALEDONIAN TECTONOMETAMORPHIC EVENTS

According to Roberts (2003), four major tectonothermal events are recognized within the Caledonian Orogen, followed by another important late episode of extensional collapse. They are the Finnmarkian event, the Trondheim event, the Taconian event and the Scandian event.

2.3.1 FINNMARKIAN EVENT

During the Finnmarkian phase the collision of the outermost part of the Baltoscandian margin with an inferred magmatic arc, located in the northeastern Iapetus Ocean (*Ægir* Sea), took place. This tectonic event is characterized by a sea-ward facing subduction zone. The influence of the subduction process decreases progressively moving south along the Baltoscandian margin. The Finnmarkian event accounts for the mid-Cambrian to early Ordovician deformation and metamorphism of the Baltoscandian margin (Andreasson 1994).

The effects of the Finnmarkian event can be detected only in parts of the middle allochthon and at the base of the upper allochthon. In particular, the Kalak Nappe Complex and the lower nappes are extensively deformed and the synorogenic magmatism of the Seiland Igneus Province takes place. The Finnmarkian event is limited in the northern part of the Scandinavian Caledonides and it took place at ~ 520-500 Ma (figure 2.3).

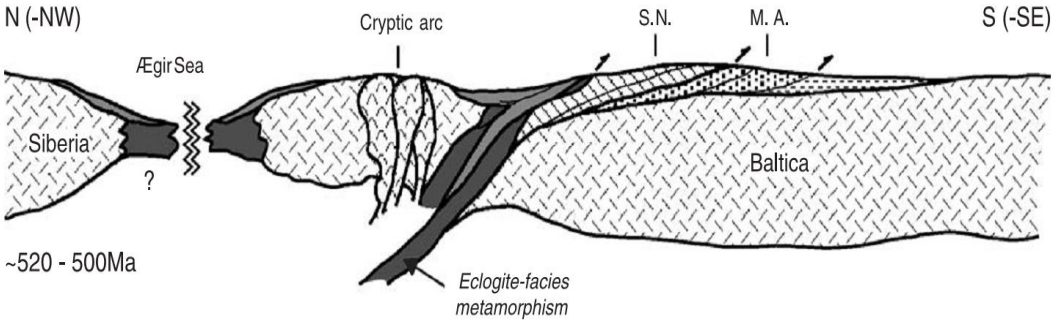

Figure 2.3 Schematic profile showing the Finnmarkian event. The profile is characterized by the ocean-ward subduction and the emplacement of the Finnmarkian nappes onto the Baltoscandian margin. During the subduction process, eclogite facies conditions are reached (Roberts, 2003).

2.3.2 TRONDHEIM EVENT

The Trondheim event is recognized in some parts of the Upper allochthon in the central-western Norway and it involves different paleogeographic scenarios compared to the Finnmarkian event.

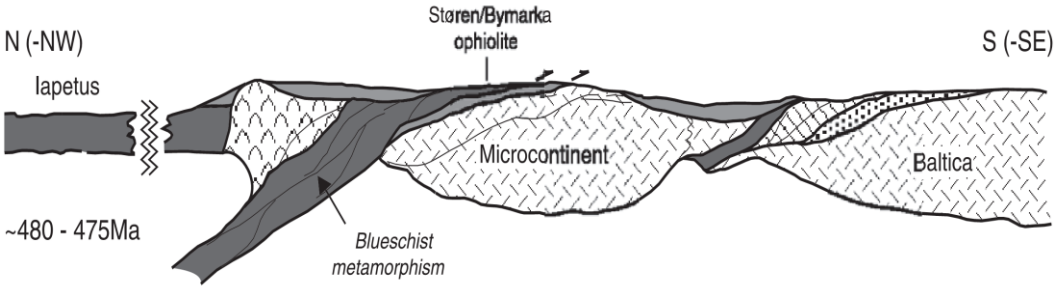

Figure 2.4 Schematic profile of the Trondheim event illustrating ocean-ward subduction and ophiolite obduction. The subduction is characterized by at least blueschists facies depths (Roberts, 2003).

The Trondheim event took place at 470-450 Ma. The Baltica plate rotates slowly

towards the Laurentian plate, away from the Siberia one. The Iapetus Ocean, located between Baltica and Laurentia, starts to be gradually contracted. According to Roberts (2003), this event accounts for a phase of metamorphism and deformation. Blueschists have been found in the ophiolite obducted fragments (figure 2.4).

2.3.3 TACONIAN EVENT

The Taconian event occurs after the Trondheim event. The evidence of the Taconian event is found in the uppermost allochthon. This phase is characterized by an ocean-ward subduction which led to the formation of an accretionary wedge along the Laurentian margin. The shelf and the adjacent slope succession of the Laurentian margin were incorporated in the accretionary wedge and they were later detached from Laurentia and thrust above the Scandinavian Caledonides. According to Roberts (2003), accretion on the continental margin of Laurentia took place at ~ 470-465 Ma (figure 2.5).

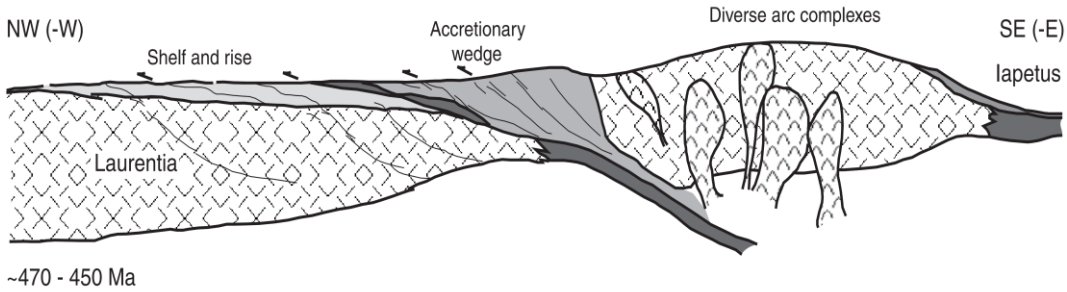

Figure 2.5 Schematic profile illustrating the Taconian event. In this particular case, subduction, accretion and ophiolite obduction involve the continental margin of Laurentia (Roberts, 2003).

2.3.4 SCANDIAN EVENT

The Scandian event is the principal tectono-metamorphic event that is responsible for the characteristic distribution of the allochthon of the Scandinavian Caledonides.

The orogenesis is the consequence of the subduction of Baltica beneath Laurentia, which occurred in late Silurian to early Devonian time. The subduction, which reached depths of 125 km, and the following exhumation were extremely rapid, because they were confined to a time period of 10 Ma. The Scandian orogenesis

affected all the allochthons involved in the previous Finnmarkian, Trondheim and Taconian events. The uppermost allochthon that is characterized by Laurentian affinity and was formed during the Taconian event, during this phase is detached from the Laurentian root and dragged upon the ophiolites of the Upper Allochthon. The Scandian event took place at 420-400 Ma (figure 2.6).

Elvevold and Gilotti (2000) and Gilotti and Ravna (2002) described the presence of high pressure and ultrahigh pressure eclogites in Northeast Greenland. They proposed that the Scandian collision involved also crustal-thrust imbrication and consequent thickening.

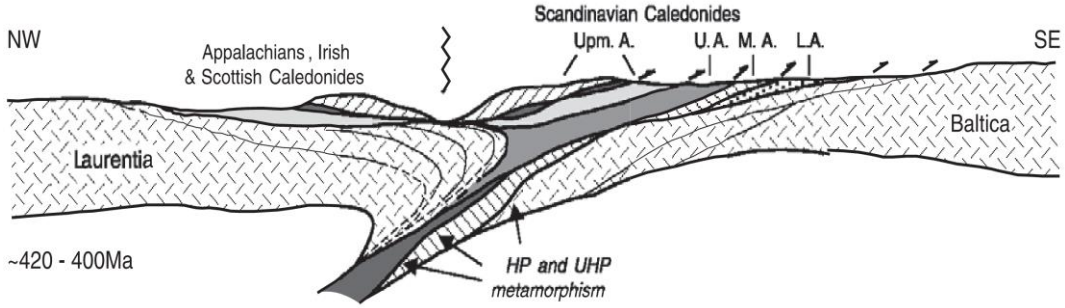

Figure 2.6 Schematic profile illustrating the Scandian event. The profile shows the Baltica-Laurentia collision. Some terrains with Laurentian affinity were detached and later emplaced onto the higher levels of the orogenic wedge (Roberts, 2003)

2.3.5 LATE TO POST SCANDIAN EVENT

A late-stage of extensional deformation characterizes the final phase of the Scandian orogenesis. This phase takes place shortly after the peak of the Scandian event. The extensional event involved the same structures which were involved during the compressional phase of the Scandian event. The same surfaces that allowed thrusting during the compressional phase, during the extensional phase acted as extensional surfaces. The transport direction does not change but the movement direction is the opposite. The main cause of this extensional process is the gravitational collapse of the orogen.

2.4 FIELDWORK AREA

The fieldwork area (figure 2.7) is located in the northern part of the Scandinavian

Caledonides, in the North-eastern portion of Troms County. It is comprised between the town of Lyngseidet and the small community of Koppangen. The outcrops are situated alongside the eastern coast of the Lyngen Peninsula. The fieldwork was carried out alongside the road section, because of the logistic impossibility that characterizes the inland. The rock samples that are analyzed in this work belong to the lithologic unit named Nordmannwik nappe.

The Nordmannwik is a thrust sheet unit imbricated above the Baltoscandian shield during the collisional phase that led to the formation of the Caledonian Orogen.

Fourteen rock samples were collected by Carly Faber (Phd student at the University of Tromsø) during the summer of 2013 and have been studied in this work.

The Nordmannwik nappe is a high grade tectonic unit. It differs markedly from the underlying and the overlying units since it is delimited by tectonic surfaces which represent marked jumps in metamorphic conditions.

The lower contact, which separates the Nordmannwik Nappe from the Balsfjord group, is defined by a jump from greenschists/lower amphibolite facies conditions to upper amphibolite/granulite facies conditions.

The upper contact is characterized by a jump from the high metamorphic grade of the Nordmannwik Nappe to the greenschists facies of the Lyngen Nappe Complex.

According to Bergh et al (1985), the Nordmannwik Nappe underwent two main deformational events. The first deformational event accounts for a strong mylonitization, with isoclinal folding highlighted by the parallel orientation of micaceous layers. In biotite and white mica gneisses, K-feldspar, garnet and kyanite porphyroblasts shows an elongate shape, oriented along the main foliation.

The second deformational event accounts for a weak folding of the mylonitic layers. It occurred as a result of the nappe transport during the formation of the accretionary wedge.

The Nordmannwick nappe is composed by five main types of lithologies:

- phyllites

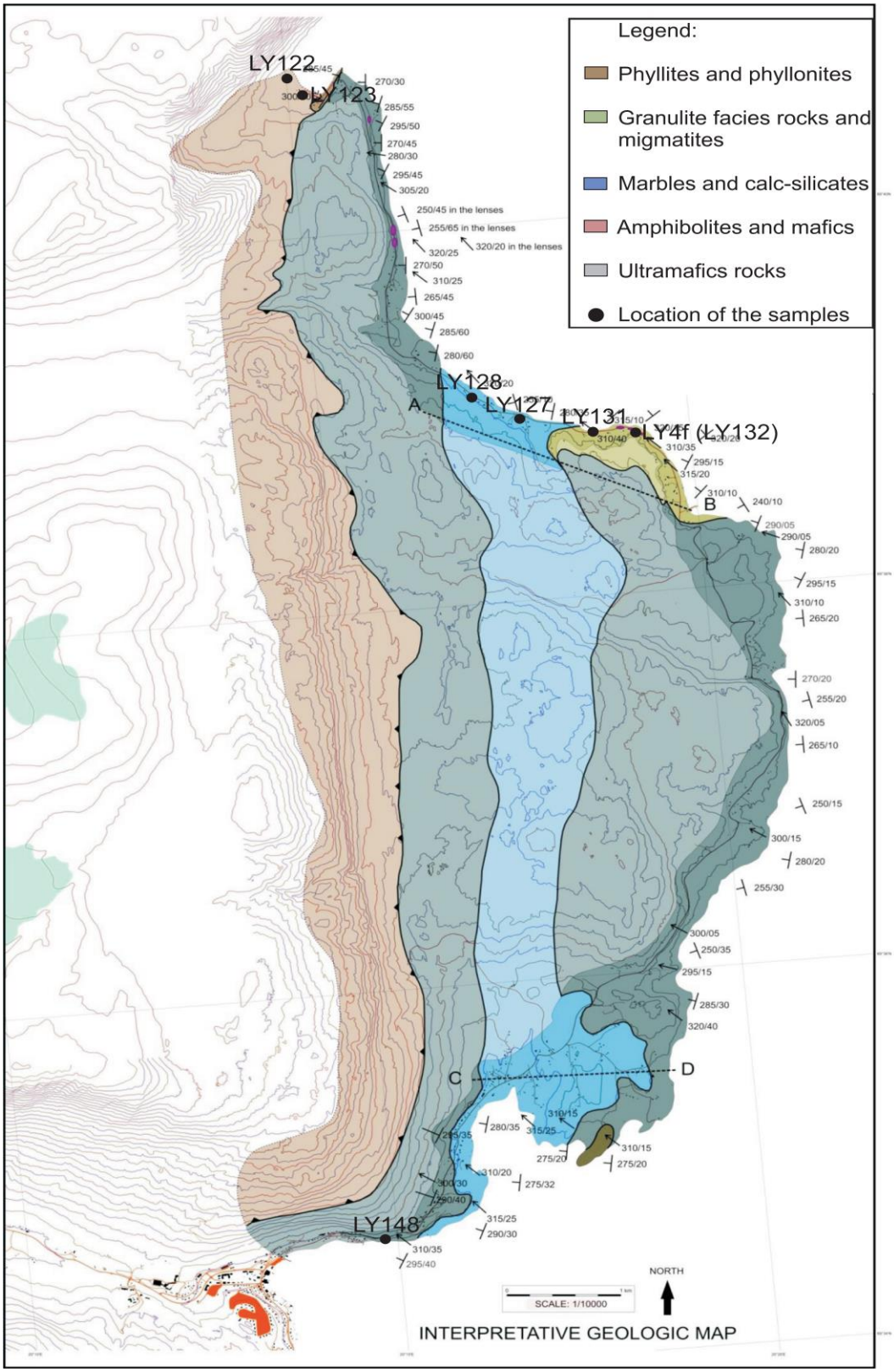

Figure 2.7 Geologic map of the studied area taken from Nardini (2013) and Hibelot (2013)

- garnet-bearing micaschists
- relict granulite facies rocks
- mafic lenses and layers
- carbonatic layers and marbles lenses

Phyllites constitute an out-of-sequence unit at the contact with the Lyngen Nappe. They are characterized by the presence of very fine white mica, biotite and chlorite layers alternated with quartz veins.

The garnet-bearing micaschist represent the most abundant lithology and they are characterized by a strong mylonitic structure. They show a significant variability, since both pelitic and psammitic layers are observed. The typical lithologies are coarse-grained augen gneisses, characterized by alternating quartz-feldspar and biotite-rich layers, and strongly schistose bands of micaceous gneisses.

A large body of granulite facies rocks is also found. The migmatitic gneisses are easily recognizable, since they show the typical migmatitic structure characterized by the association of leucosome and melanosome. Sometimes, leucosome and melanosome are difficult to distinguish, because of the deformational process that the rock underwent.

It is possible to notice the presence of undeformed mafic bodies metamorphosed in the amphibolite facies, embedded in garnet-bearing micaschists and in granulite facies rocks and migmatites.

The carbonatic domain often occurs as marble lenses and layers, characterized by variable thickness and wrapped up by garnet-bearing micaschists. Sometimes, calc-silicate layers are involved in the general gneissic structure.

2.5 DISCUSSION ABOUT THE PREVOUS WORKS

The Nordmannwik nappe has not been studied in the literature from a petrological point of view. The only works available are the master thesis of Nardini and Hibelot (2013).

Considering the distinctive features of the rocks which belong to the Nordmannwik nappe, the above works inferred a sequence of metamorphic events. First, we can see a pre-Caledonian high-temperature metamorphic event,

testified by the presence of fibrolite inclusions inside large and extensively replaced garnet porphyroblasts.

Afterwards, during the Caledonian thrusting, the rocks underwent a high temperature and high pressure metamorphic event, with the occurrence of partial melting. The metamorphic peak assemblage is constituted by garnet, kyanite and K-feldspar porphyroblasts, biotite flakes and leucocratic segregations.

Finally, the continuing nappe thrusting produced a retrograde overprint, with the crystallization of a second generation of sillimanite as a later product. This later stage of the metamorphic path is characterized by the growth of extremely fine-grained biotite, together with fibrolite along the cleavage. It accounts also for the development of the strong anisotropy that now is observable in the rock.

The above assumptions are tested in this thesis by a petrological, microchemical and phase equilibria approach. Using the precise chemical composition of the solid solution phases, we can understand if the different types of the same mineral, distinguished on the basis of the observation of the thin sections, actually belong to different stages of the metamorphic path.

CHAPTER 3
DESCRIPTION OF THE ROCK SAMPLES

The samples collected during the fieldwork were observed under the microscope. Here follows the description of the mineral phases and the microstructures which characterize such samples

3.1 MIGMATITE LY 4f

The rock shows a migmatitic structure; it is possible to notice that the leucosome, formed by quartz and plagioclase crystals, is surrounded by the residual part, namely the melanosome. The migmatitic structure underwent a deformational process, which led to the development of a new anisotropy.

The leucosome is characterized by a texture similar to that of the igneus rocks, which in essence is what these patches and lenses in migmatites were. The minerals which crystallize first are characterized by a euhedral shape and show growth faces. The later-formed minerals fill in the gaps left between the early-formed crystals (Holness et al. 2011).

The melanosome is constituted mainly by biotite, which is often associated with kyanite. It is possible to notice the presence of garnet porphyroblasts, which reach at most a diameter of 9 mm.

The foliation is mainly determined by the presence of crystals of biotite and to a lesser extent by crystals of white mica and sillimanite.

The main minerals are garnet, biotite, white mica, kyanite, sillimanite, plagioclase quartz, whereas tourmaline, zircon and graphite are present as accessory phases.

Sillimanite: there are two different types of crystals of sillimanite, which are found in different location inside the thin section. The first type of sillimanite appears in the form of fibrolite inclusions inside garnet porphyroblasts (figure 3.1) and plagioclase. The second type of sillimanite occurs in small elongated crystals, located along the cleavage. Together with biotite, the second type determines the anisotropy of the rock. The sillimanite that belongs to the second phase, occurs in

the form of fibrolite as well and is sometimes observed inside the leucosome, typically located between quartz and plagioclase grains (figure 3.2).

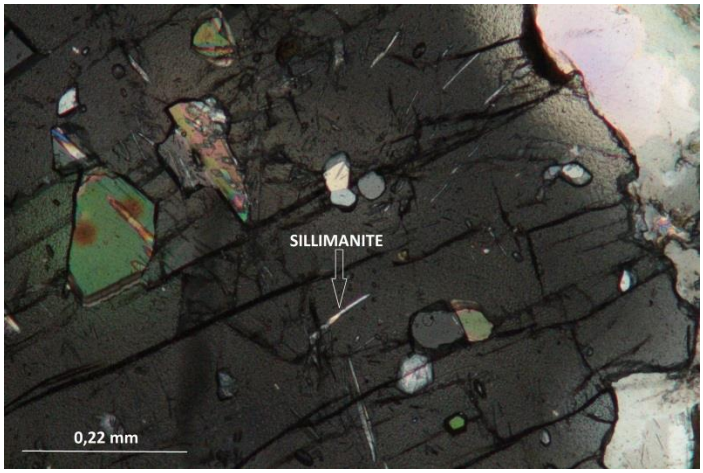

Figure 3.1 Sillimanite inclusions inside garnet

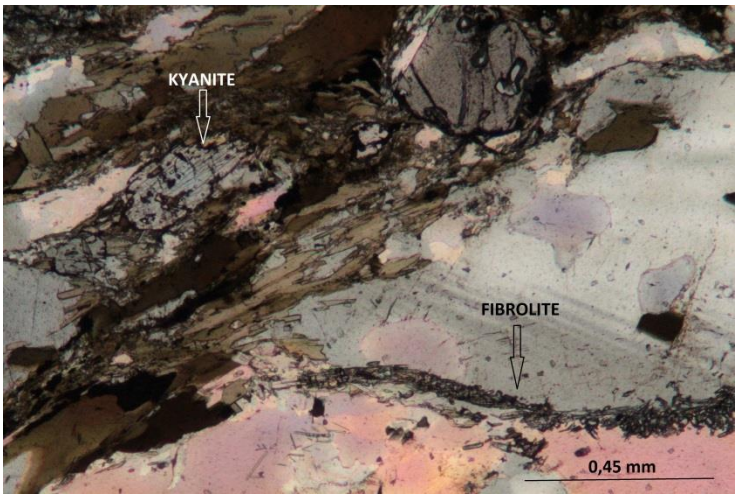

Figure 3.2 Fibrolite in contact with quartz and plagioclase

Kyanite: kyanite is present as a metastable phase. Kyanite crystals, sometimes twinned, are oriented according to the anisotropy of the rock. Kyanite is altered and fractured, and it can be found in association with crystals of fibrolite, muscovite and biotite (figure 3.4). In particular, kyanite seems to be replaced by large flakes of biotite. Biotite inclusions are also found in the kyanite crystals.

It is important to highlight the presence of kyanite inside the leucosome; this means that the partial melting process took place in the stability field of kyanite

(figure 3.3).

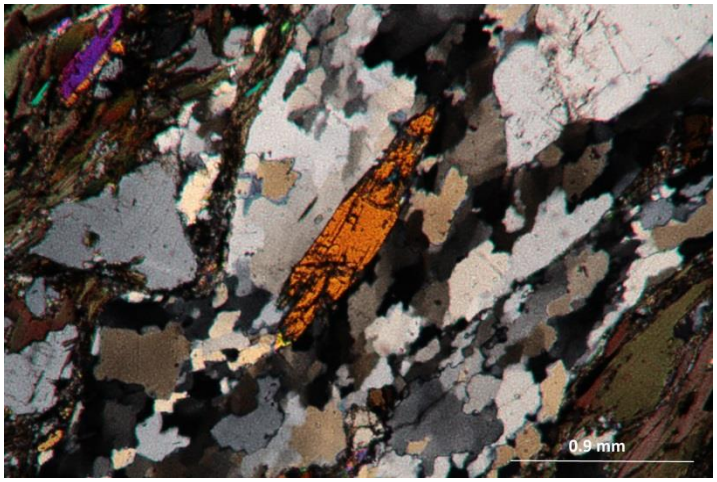

Figure 3.3 Kyanite inside the leucosome

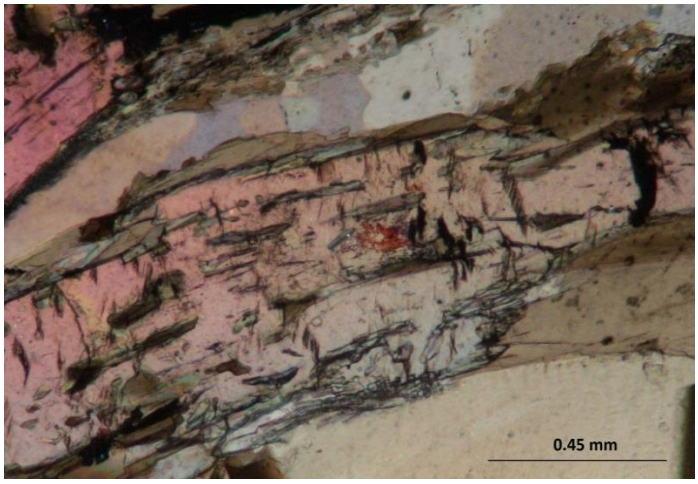

Figure 3.4 Kyanite partially replaced by fibrolite and in association with biotite

Quartz: quartz and plagioclase form the leucosome. Quartz crystals are often characterized by ameboidal and irregular boundaries, indicative of a high temperature recrystallization process such as grain boundary migration.

Plagioclase: plagioclase appears in crystals of variable size and it shows the characteristic twins, namely albite and pericline. It is possible to find plagioclase associated with quartz, inside the leucosome, and in isolated crystals, associated with biotite (figure 3.5). Sillimanite inclusions occur in plagioclase crystals.

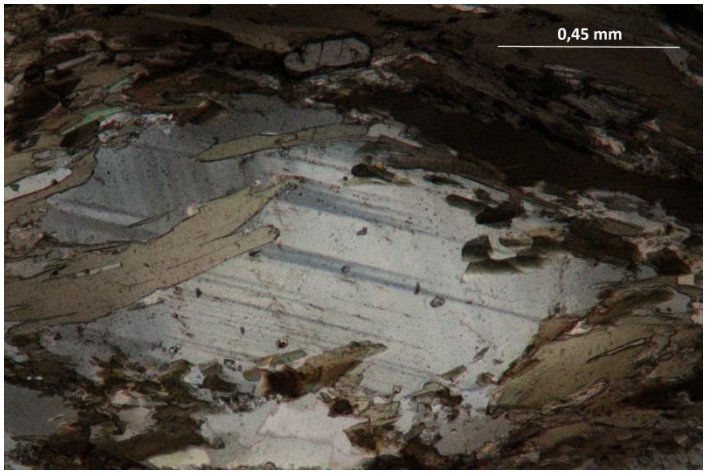

Figure 3.5 Plagioclase in association with biotite

Biotite: biotite occurs in crystals of variable grain-size and it shows a grey-brown color under parallel polars. Two types of biotite can be distinguished: the first type of biotite is characterized by large crystals (3 mm length); such crystals are metastable and replaced by second generation biotite. The second type of biotite appears in extremely fine grained crystals; It sorrounds the lenses of leucosome and it is associated with garnet, plagioclase and kyanite. It is possible to notice the presence of zircon inclusions inside the biotite, characterized by the typical pleochroic halos.

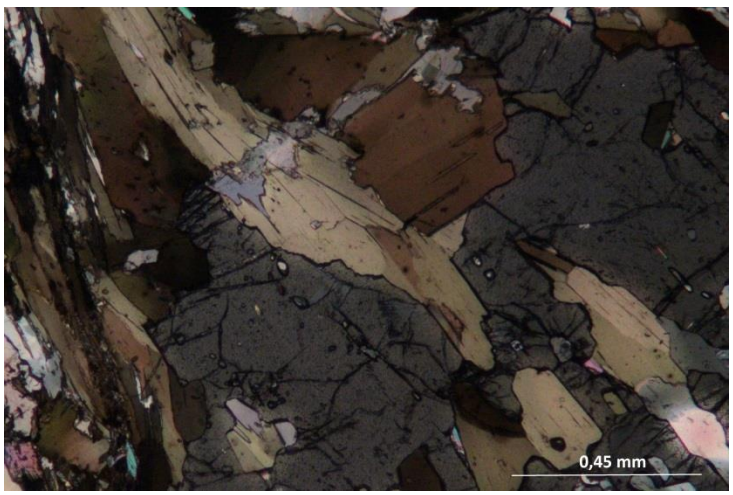

Figure 3.6 Garnet porphyroblast (first generation) partially replaced by biotite

Garnet: two generations of garnet can be distinguished, characterized by different

dimensions. The first type of garnet appears in large crystals (about 1 cm of diameter), characterized by inclusions of fibrolite, biotite and quartz (figure 3.6). The second type of garnet appears in smaller crystals. This latter does not appear to be altered like the crystals of the first generation and it does not show fibrolite inclusions (figure 3.7). Both types of garnet appear to be replaced by biotite.

Figure 3.7 Garnet porphyroblasts (second generation) without sillimanite inclusions partially replaced by biotite

White mica: white mica occurs in platy crystals, oriented along the foliation and associated with both coarse grained and fine grained biotite. Big white mica flakes appear only partially replaced, therefore the white-mica breakdown reaction didn't go to completion.

Graphite: graphite is found inside the matrix as opaque crystal and as fine-grained black dispersions.

Zircon: zircon is characterized by high relief. It often occurs as inclusions in biotite crystals, showing the dark halo, resulting from its radioactive decay.

Tourmaline: the sections of tourmaline are pleochroic and show a dark green color. The basal sections are not pleochroic and appear always in estinction under crossed polars.

Calcite: calcite is characterized by low relief and high birefringence. It is a very rare mineral inside the section.

3.2 MIGMATITE LY 131

The rock shows a gneissic structure, characterized by the presence of K-feldspar and garnet porphyroblasts. The leucosome lenses, formed by quartz and k-feldspar crystals, are wrapped by fine-grained biotite crystals and fibrolite. K-feldspar porphyroblasts are often surrounded by myrmekites, formed by plagioclase and quartz.

The foliation is determined mainly by fine-grained biotite, fibrolite and in lesser extent by white mica, which is also present along the cleavage.Most of the sample is constituted by leucocratic lenses, formed entirely by quartz and oriented according to the foliation direction. These lenses are wrapped by fine-grained biotite and fibrolite. The rock underwent a deformational process, which is responsible for a strong mylonitization. It is possible to distinguish an S-C structure and the presence of mica-fish-shaped porphyroclasts formed by large biotite flakes.

The main minerals are represented by quartz, K-feldspar, biotite, garnet, sillimanite, white mica, and plagioclase-forming myrmekites. Zircon is present as an accessory phase.

K-feldspar: the rock is characterized by the presence of K-feldspar porphyroblasts. Some crystals shows tartan twin, distinctive of microcline. K-feldspar is often surrounded by myrmekites.

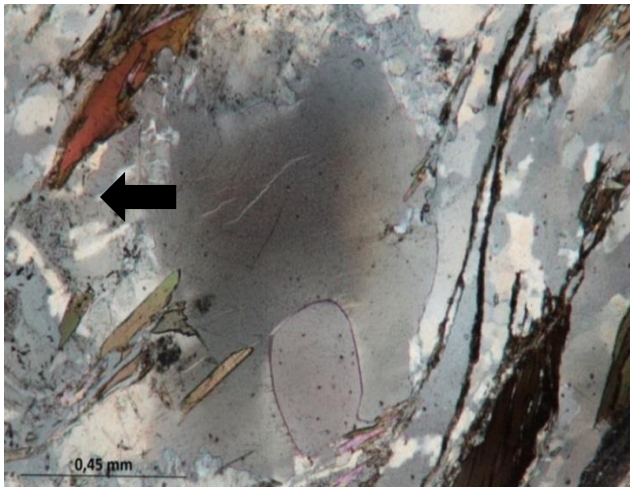

Figure 3.8 Perthite in contact with myirmekite (black arrow) surrounding k- feldspar

The presence of perthitic exsolution inside k-feldspar crystals testifies that a phase of re-equilibration occurred after the peak metamorphic event. Perthites consist of exolution lamellae of Na-rich feldspar inside K-feldspar. The lamellae are commonly characterized by lenticular shape and they are arranged sub-parallel to each other inside the host crystal (figure 3.8).

Myrmekites: myrmekites are typically associated with K-feldspar porphyroblasts and they are formed by vermicular intergrowth of Na-plagioclase and quartz. Myrmekites show lobate shapes in contact with k-feldspar grains.

Garnet: garnet porphyroblasts are present in the section. The average size of the grains is 1 mm of diameter. It is possible to notice that only one garnet crystal differs from the average, since it is characterized by a diameter of 2 mm; this particular crystal shows fibrolite inclusions. Some garnet porphyroblasts are partially replaced by biotite (figure 3.9).

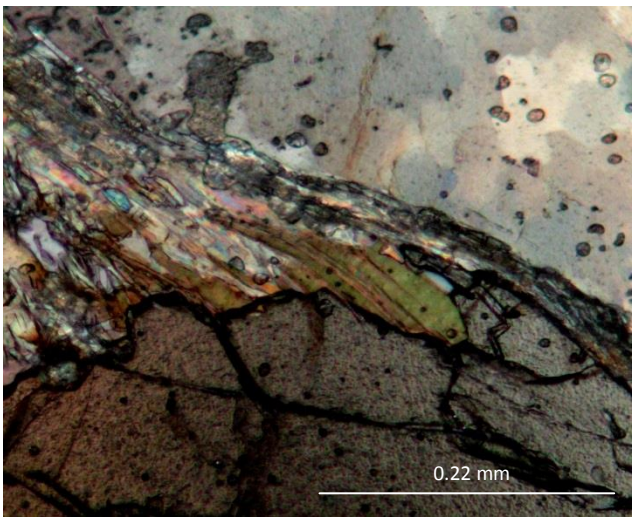

Figure 5.14 Garnet partially resorbed by biotite and fibrolite.

Biotite: biotite is characterized by a reddish-brown color under plane-polarized light. Fine-grained biotite surrounds the leucosome lenses and garnet porphyroblasts. A second type of biotite is present in the rock, characterized by larger crystals, often associated with fine grained biotite and sillimanite (figure 3.10).

Quartz: Quartz is the most abundant mineral in the rock. It appears in leucocratic

lenses, oriented according to the main foliation and surrounded by crystals of fine

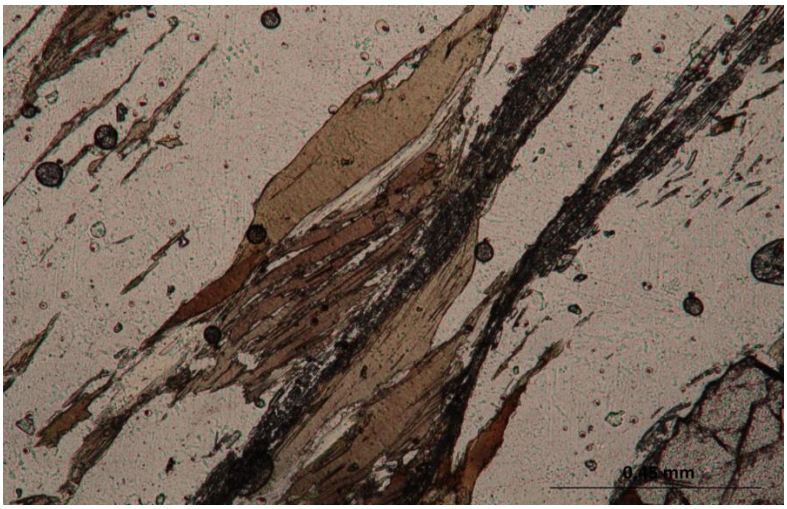

Figure 3.10 Biotite partially replaced by fibrolite

grained biotite. The aspect of the quartz grains is characteristic of grain boundary migration process. Some crystals show a square subgrain structure, known as chessboard extinction. The process causing this structure is due to the slip of both basal and prismatic planes, and it is indicative of temperatures higher than 700°C (Passchier, 2005).

Sillimanite: sillimanite appears in the form of fibrolite and forms aggregates of tiny crystals oriented in the direction of the main foliation. These aggregates surround the leucocratic lenses and they are often associated with biotite crystals. Sillimanite pervasively replaces the coarse grained biotite.

Fibrolite is also present in the section in the form of tiny inclusions inside the garnet porphyroblasts as well.

White mica: white mica is an abundant mineralogical phase in this sample. It is found mainly along foliation planes and is associated with biotite. White mica appears in large crystals (0.9 mm length). White mica large flakes appear to be only partially replaced, therefore, as in sample LY4f, this implies that the white mica breakdown reaction didn't go to completion.

Plagioclase: plagioclase is present in very little amount. It occurs in small crystals inside the matrix.

Zircon: zircon often appears as inclusions in biotite crystals. Such inclusions show the characteristic radioactive halo.

Graphite: graphite is present in the section as black powder dispersed in the matrix.

3.3 GARNET AND BIOTITE MICASCHIST LY1

The rock shows a schistose structure. It is characterized by well-developed leucocratic lenses, oriented according to the foliation direction, constituted mainly by quartz and to a lesser extent by plagioclase. The most abundant mineral in the section is quartz, which constitutes about 50% of the sample. Biotite and white mica are present along the cleavage and they determine the foliation of the rock. It is also possible to notice the presence of garnet porphyroblasts.

Amphibole and epidote are also present in the thin section; the presence of such Ca-bearing minerals means that the protolith was not characterized by a pure pelite composition.

The main minerals in the section are quartz, garnet, plagioclase, biotite, white mica, sillimanite and kyanite. Epidote, rutile and amphibole are present in very amounts, while tourmaline and zircon are present as accessory phases.

Quartz: quartz is the most abundant mineral in the section and it appears in crystals of variable grain-size. It is possible to notice that, inside the leucochratic lenses, quartz crystals show a characteristic shape of grain boundary migration process.

Plagioclase: plagioclase is an abundant mineral in the rock and it can be distinguished because of the characteristics twins pericline and albite. It is often associated with crystals of biotite and white mica, inside the matrix. Plagioclase is rarely associated with quartz inside the leucocratic lenses.

Garnet: garnet porphyroblasts show no sign of alteration. The crystals are euhedral and inclusions-rich; such inclusions are constituted mainly by quartz and tiny crystals of fibrolite (figure 3.11).

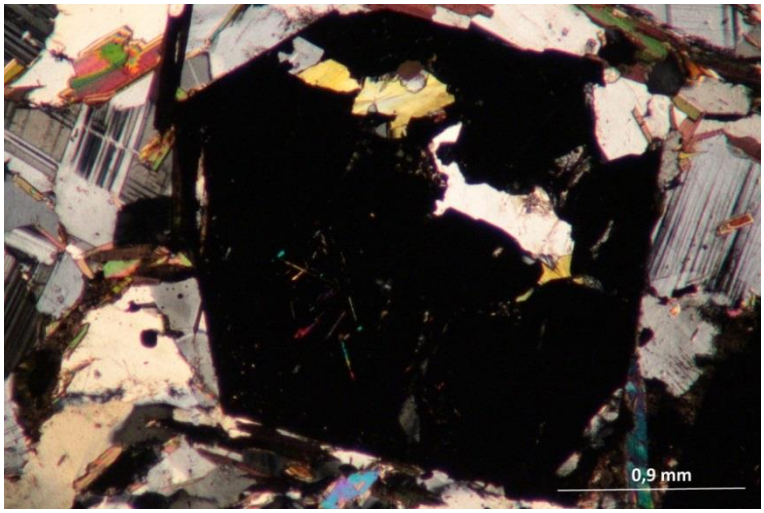

Figure 3.11 Garnet with inclusions of fibrolite

Biotite: biotite determines the foliation of the rock and it is often associated with white mica. Biotite surrounds the leucocratic lenses.

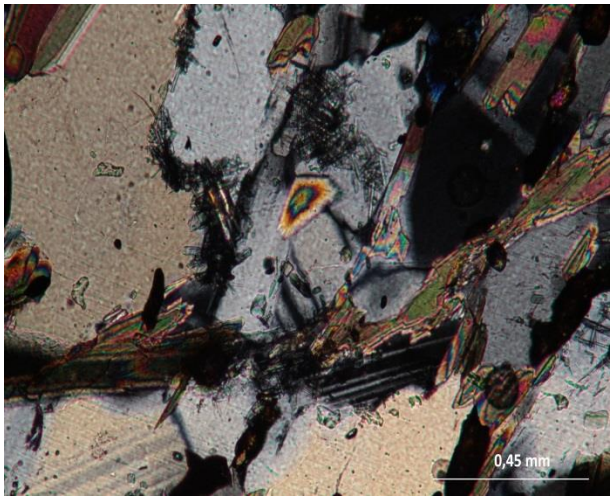

Figure 3.12 Fibrolite in contact with plagioclase and biotite

Sillimanite: two types of sillimanite are present inside the section. Sillimanite inclusions inside garnet porphyroblasts represent the first type. A second type of sillimanite is represented by fibrolite crystals present inside the matrix. This type of sillimanite is mainly found between quartz and feldspar grains and in contact with biotite (figure 3.12). It is possible to notice that, sometimes, fibrolite forms aggregates of tiny crystals, associated with biotite and oriented according to the

foliation.

Kyanite: kyanite crystals are rare and they appear t altered and partially replaced by white mica (figure 3.13).

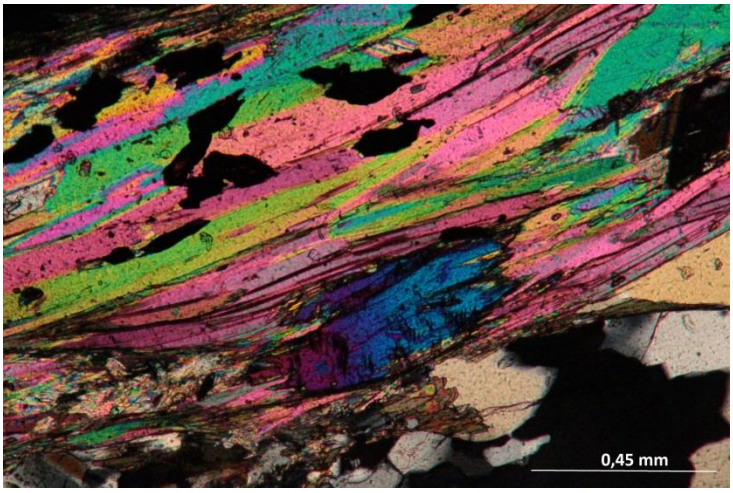

Figure 3.13 Kyanite partially replaced by white mica

Epidote: crystals of epidote are rare and they are replaced by biotite (figure 3.14).

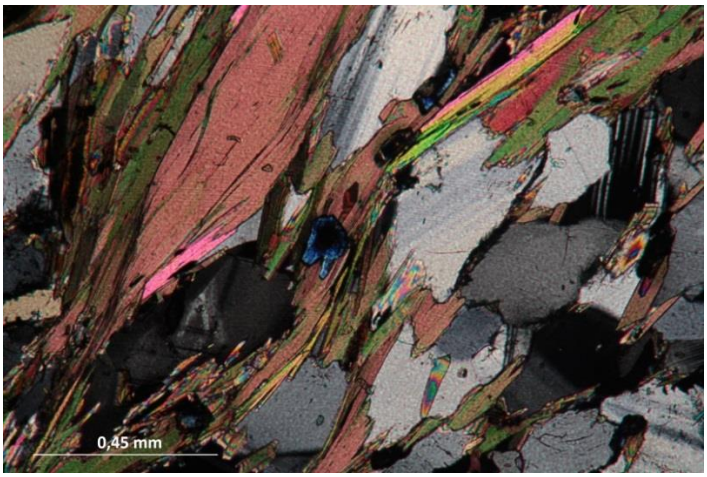

Figure 3.14 Epidote and plagioclase in association with biotite and white mica

White mica: white mica is associated with biotite and it appears in crystals oriented along foliation planes. It is possible to notice that white mica is replaced by fibrolite. Large white mica crystals (1 mm length) are rarely observed in the section and they are characterized by tourmaline inclusions (figure 3.15).

White mica is in textural equilibrium with quartz, indicating the "second sillimanite reaction" (e.g. White mica + plagioclase + quartz = Al_2SiO_5 + K-feldspar + melt (Spear 1989)) has not occurred.

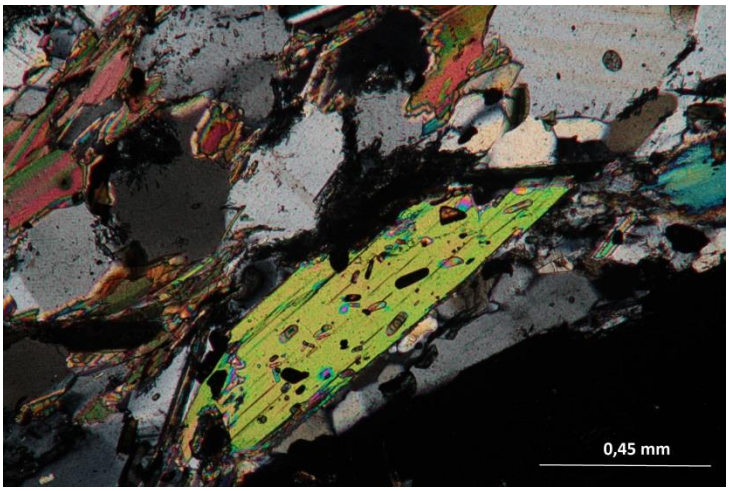

Figure 3.15 White mica in contact with fibrolite

Rutile: rutile is characterized by a light brown color under plane-polarized light and a very high relief.

Amphibole: crystals of amphibole are rarely observed in the section. They are present inside thin levels surrounded by leucocratic lenses often associated with biotite. They are characterized by a strong pleocroism and a green color under parallel nicols.

3.4 GARNET MICASCHIST LY127a

The rock shows a schistose structure. It is characterized by the presence of leucocratic lenses, elongated according to the schistosity; they are constituted mainly of quartz and in lesser amount by plagioclase. The foliation is determined by the presence of biotite and white mica along the cleavage. It is possible to notice the presence of inclusions-rich garnet porphyroblasts.

The main minerals are garnet, plagioclase, quartz, biotite, white mica, epidote and amphibole. Tourmaline and zircon are present as accessory phases.

Plagioclase: two types of plagioclase crystals are present in the rock. The first

type of plagioclase is associated with quartz and forms the leucocratic lenses. The second appears in isolated crystals, in association with biotite and muscovite (figure 3.16).

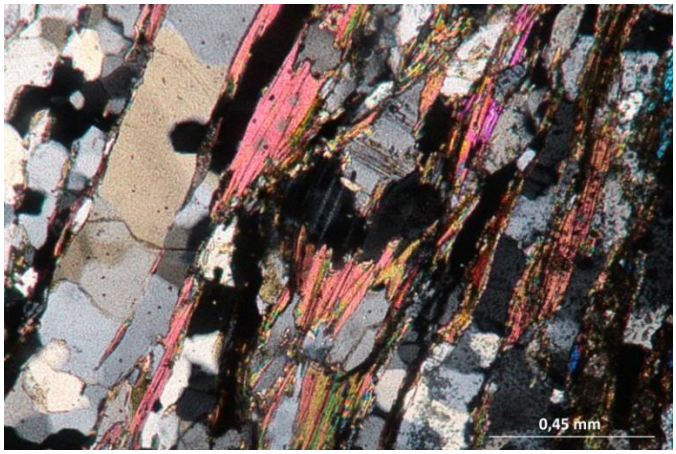

Figure 3.16 Plagioclase in association with biotite

Garnet: garnet porphyroblasts appear in textural equilibrium with the matrix, since crystals show a sharp rim when in contact with sheet silicates, quartz and plagioclase. Garnet appears in large crystals (0.9 mm of diameter at most) characterized by inclusions of quartz, plagioclase and biotite (figure 3.17).

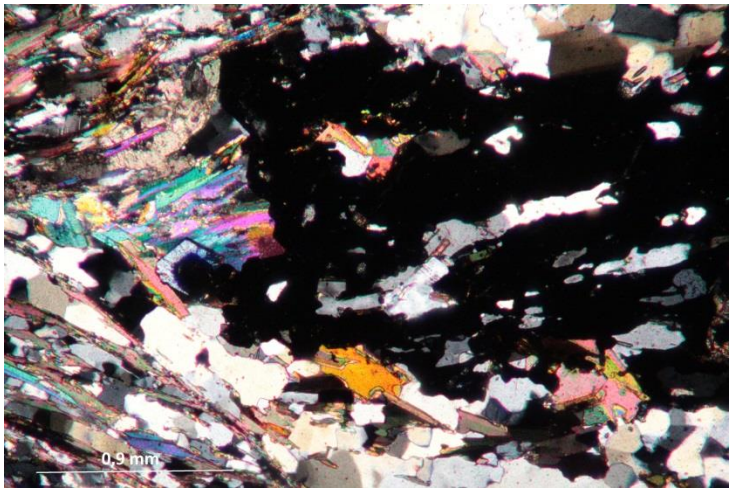

Figure 3.17 Garnet in contact with muscovite, biotite and quartz

Quartz: quartz forms leucocratic lenses, oriented according to the foliation planes. Quartz is present also in isolated crystals. In this case it is associated with

plagioclase, biotite and muscovite.

Biotite: biotite determines the foliation of the rock and it grows in association with muscovite.

White mica: white mica is the most widespread sheet silicate in the section. It appears in elongated crystals, sometimes of large size (1 mm length), elongated in the foliation direction.

Epidote: Epidote appears in crystals elongated in the direction of foliation and it is partially in association biotite and muscovite. It is possible to notice allanite inclusions inside crystals of epidote (figure 3.18).

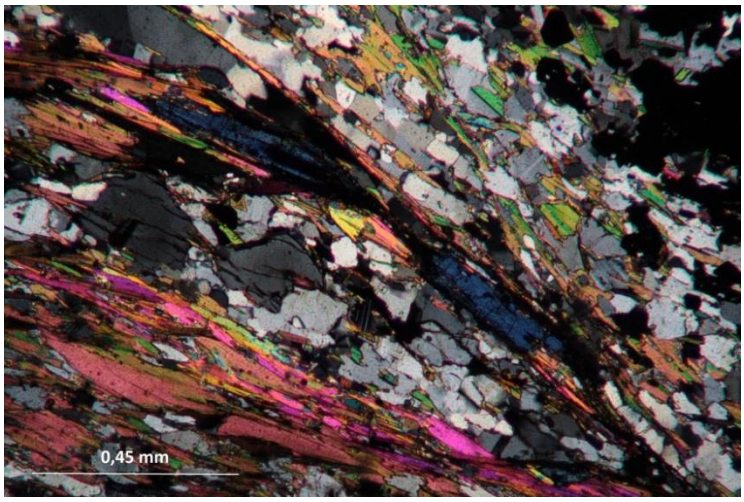

Figure 3.18 Epidote in association with muscovite

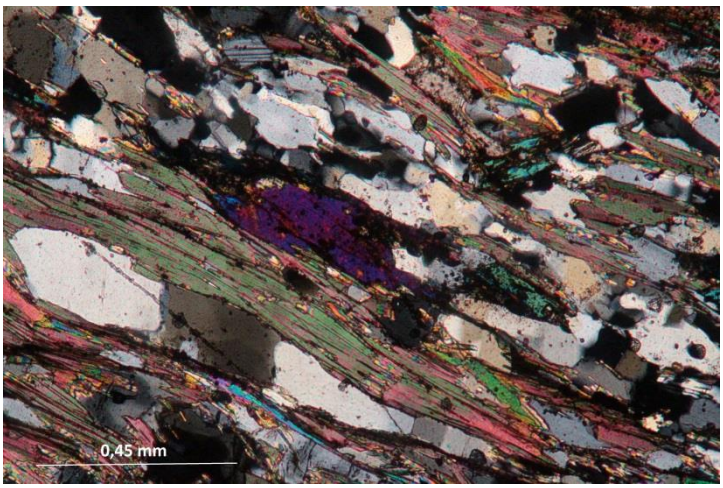

Figure 3.19 Amphibole in contact with quartz and biotite

Amphibole: amphibole crystals show a marked pleochroism and it is characterized by green colors. Amphibole appears often in association with quartz and biotite (figure 3.19).

3.5 GARNET MICASCHIST LY127b

The rock shows a schistose structure. The sample is formed for the most part by sheet silicates, which account for about 50% of the thin section. White mica is the most abundant sheet silicate and it appears in platy crystals, associated with biotite. White mica and biotite determine the foliation of the rock. The rest of the sample is mainly constituted by leucocratic minerals such as quartz and plagioclase, and calcium-bearing silicates, like epidote and amphibole.

The main minerals are biotite, white mica, quartz, plagioclase, epidote, amphibole, garnet and scapolite. Zircon is present as an accessory phase.

Quartz: quartz is an abundant mineral in the section and it forms typically thin leucocratic lenses. Quartz crystals show obvious consequences of dynamic recrystallization process; in particular, they have a characteristic shape of grain boundary migration process.

Plagioclase: plagioclase forms, in lesser extent with respect to quartz, the leucocratic lenses. Plagioclase is present in the matrix in isolated crystals, associated with sheet silicates. In this case it is typically present in association with biotite and white mica.

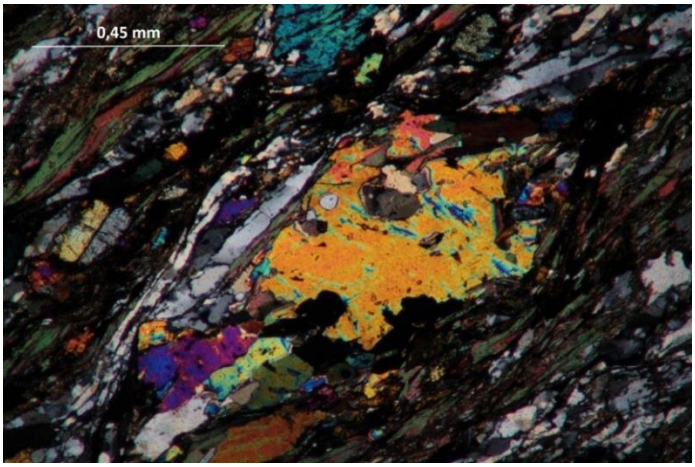

Figure 3.20 Scapolite

White mica: white mica is the most abundant sheet silicate in the section. It appears in elongated crystals, sometimes of large size (1 mm average length), elongated in the foliation direction.

Scapolite: scapolite is a rare mineral inside the section and it is characterized by low relief (figure 3.20). It may represent the relict evidence of a high grade metamorphic event; scapolite is an index mineral of the granulite facies in calc-silicate rocks (Bucher and Grapes, 2011).

Biotite: biotite appears in two different types of crystals, probably formed in two different stages of the metamorphic path. The first type of biotite is characterized by large crystals, which are in association with white mica and is rimmed by a second generation biotite. Second generation biotite is extremely fine-grained and is located along the foliation planes.

Epidote: epidote is an abundant phase in the thin section and it appears in elongated crystals, oriented along the foliation (figure 3.21).

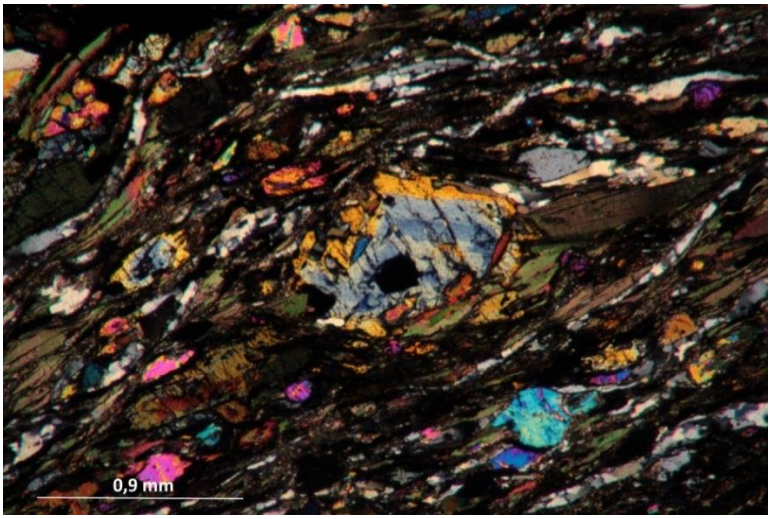

Figure 3.21 Epidote in contact with biotite

Amphibole: amphibole is characterized by a marked pleochroism and green colors under parallel nicols. It appears in altered crystals, oriented in the foliation direction. Amphibole is often replaced by fine-grained biotite.

Garnet: garnet porphyroblasts are rare in the rock and occur as altered crystals, replaced by biotite.

3.6 AMPHIBOLITE LY132

The sample shows a granofelsic structure. It is not possible to recognize any kind of anisotropy at the scale of the thin section, therefore the specimen does not show evidence of a deformational event. The amphibole constitutes the most part of the rock, about 60% of the volume. Plagioclase is the second most abundant phase and it accounts for the 30% of the total volume. Biotite and sphene appear in lesser amount.

Amphibole: amphibole is the most abundant mineral and it is characterized by a strong pleochroism, which varies between pale green and green-brown colors. It appears in variable-sized crystals. Sometimes, the crystals of amphibole are rich in quartz inclusions. These inclusions suggest the replacement of clinopiroxene by amphibole, which is characterized by an excess of silica, which formed the quartz inclusions inside the amphibole (figure 3.22).

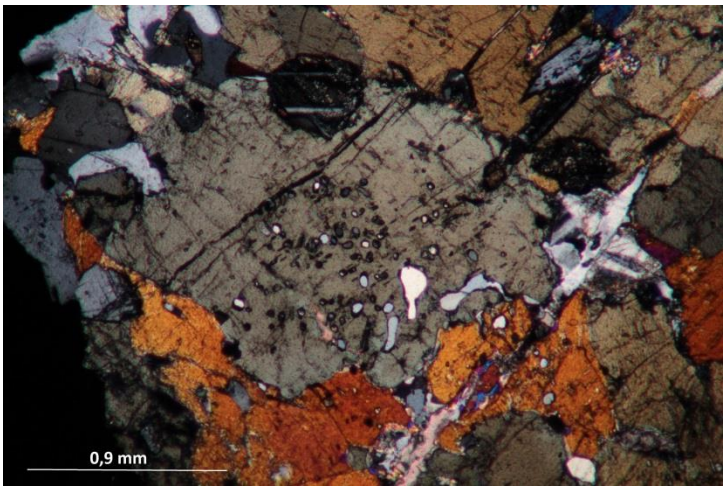

Figure 3.22 Quartz inclusions in amphibole

Plagioclase: plagioclase shows albite and pericline twins. The average grain size of plagioclase crystals is much smaller than the crystals of amphibole.

Biotite: biotite is rare in the rock. It is often associated with amphibole and it grows at the crystal boundary of the latter.

Quartz: quartz forms aggregates of coarse-grained crystals or small inclusions in amphibole. The rims of the quartz crystals show the evidence of the grain

boundary migration process.

Simplectites: it is possible to notice simplectites of epidote and an unknown opaque mineral in contact with amphibole and plagioclase (figure 3.23).

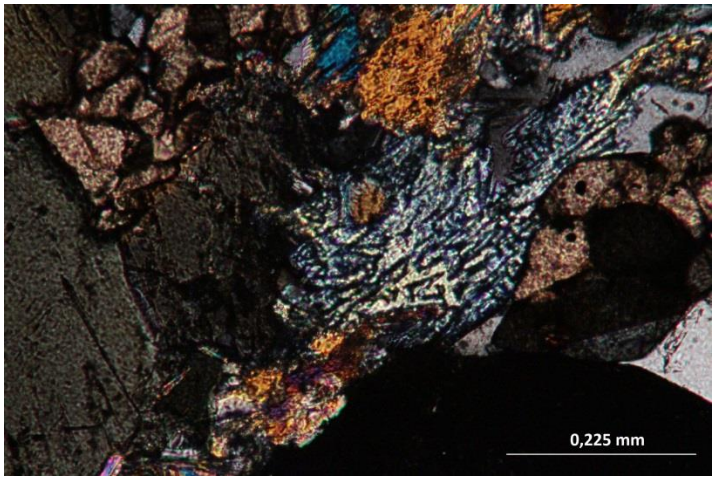

Figure 3.24 Epidote simplectite

White mica: small crystals of white mica are present in the thin section. It probably belongs to the retrograde metamorphism.

Sphene: titanite is present as accessory phase. It is characterized by a weak pleochroism of pale brown color and under crossed polars shows high interference colors.

Apatite: apatite is present as accessory mineral. Basal sections are hexagonal-shaped and always in extinction under crossed polars.

3.7 MILONITE LY4b

The sample is formed by two distinct domains, characterized by different mineral assemblages. The first part represents a strongly mylonitized rock. The foliation is determined mainly by biotite and to a lesser extent by white mica. It is possible to notice the presence of elongated quartz lenses, oriented according to the foliation and surrounded by crystals of biotite and muscovite. This part is characterized by the presence of inclusions-rich garnet porphyroblasts. The main minerals, which characterize this part of the rock, are biotite, white mica, quartz, plagioclase, epidote and kyanite. Zircon is often present as inclusions inside biotite.

The second domain of the rock is mainly formed by quartz. Inside this leucocratic domain, crystals of amphibole, pyroxene and calcite also can be found.

3.7.1 FIRST DOMAIN

Biotite: biotite appears in two different types of crystals, which can be distinguished on the base of the size. The first type biotite is characterized by large meta-stable crystals, which are in association with white mica and second-type biotite. The second type of biotite is extremely fine-grained and it often wraps the leucocratic lenses.

White mica: white mica is present in lesser amounts than the biotite. White mica is replaced by fine-grained biotite and fibrolite (figure 3.27).

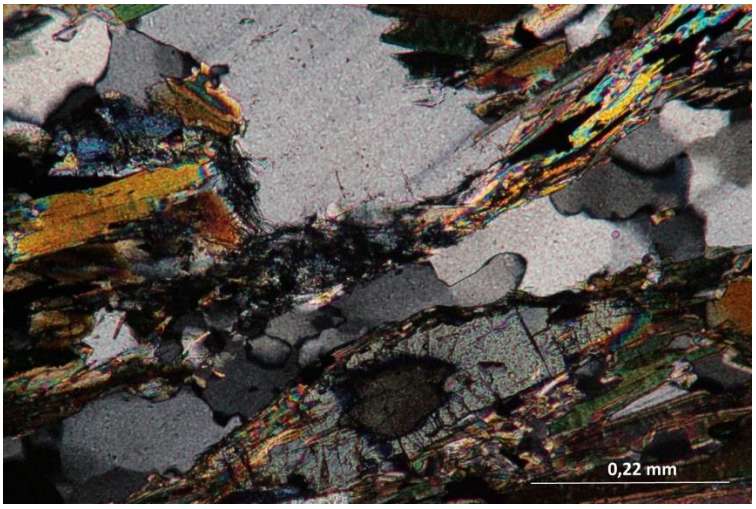

Figure 3.25 Fibrolite in contact with white mica and plagioclase

Quartz: quartz is widespread in the section and forms the leucocratic lenses. The leucocratic lenses account for the most part of the rock. The shape of the crystals of quartz is indicative of grain boundary migration process, which means a dynamic recrystallization process occurred at high temperature. Some grains show the chessboard structure, which testifies to high grade metamorphic conditions.

Plagioclase: plagioclase shows typically albite twins. It appears to be replaced by biotite, white mica and fibrolite. Sometimes, plagioclase is associated with quartz within the leucocratic lenses.

Epidote: the epidote appears in elongated crystals, oriented according to the

foliation. Epidote is often in association with biotite (figure 3.26).

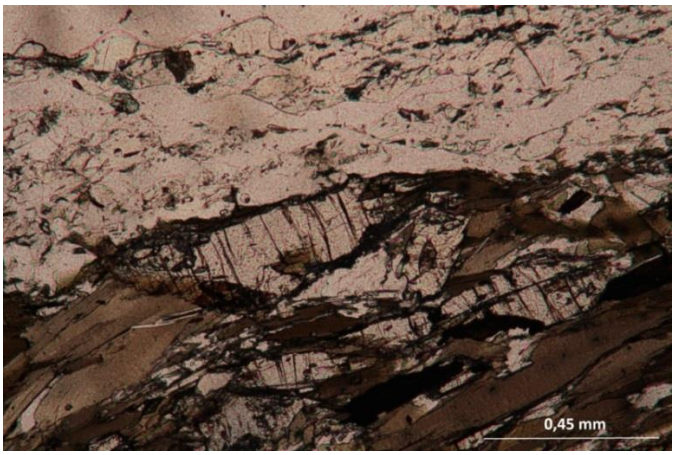

Figure 3.26 Epidote in contact with biotite and quartz

Kyanite: kyanite appears in altered crystals, elongated in the foliation direction. Kyanite is replaced by biotite and it often contains inclusions of biotite. Kyanite crystals are clearly deformed, therefore they crystallized before the deformational event (figure 3.27).

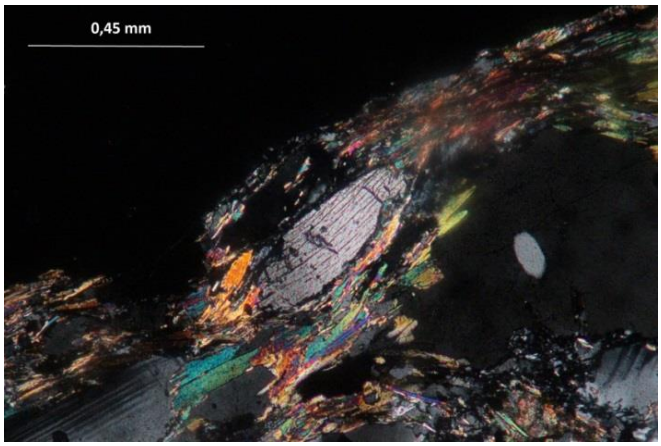

Figure 3.27 Kyanite in association with white mica

Sillimanite: sillimanite is present in the form of fibrolite. It is associated with crystals of muscovite, biotite and plagioclase.

3.7.2 SECOND DOMAIN

Clinopyroxene: clinopiroxene shows high relief and a light pleochroism of pale

green under parallel nicols. It is present exclusively inside the leucocratic lenses. Clinopiroxene is associated with amphibole and it appears to be replaced by this latter.

Amphibole: amphibole is intimately associated with clinopiroxene inside the leucosome lenses.

Calcite: calcite is found in contact with amphibole and clinopiroxene (figure 3.28).

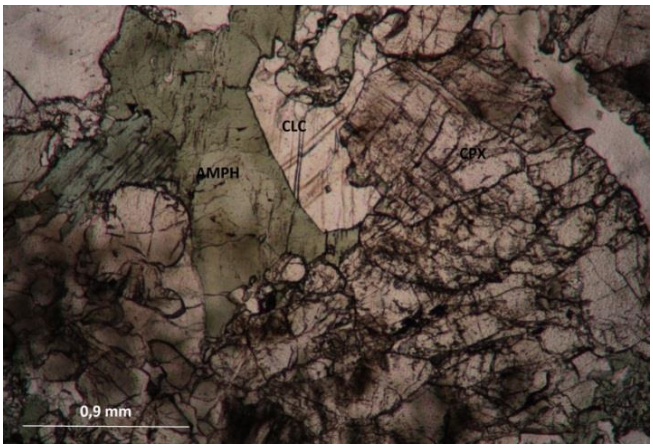

Figure 3.28 Clinopiroxene in contact with amphibole

Scapolite: small crystals of scapolite are present in the thin section. It is typically associated with quartz and plagioclase.

3.8 PHYLLITE LY123

The rock shows a schistose structure, characterized by the presence of muscovite biotite and chlorite along the foliation planes. The presence of garnet porphyroblasts and leucocratic lenses, oriented according to the schistosity, is a characteristic structural feature of the rock.

The main minerals in the section are quartz, plagioclase, biotite, white mica, chlorite and garnet. Epidote and amphibole are present as secondary phases, while zircon and tourmaline are present as accessory phases.

Quartz: quartz is the most abundant mineral in the rock and it forms leucocratic lenses, surrounded typically by muscovite, biotite and chlorite. The quartz crystals

shape is characteristic of grain boundary migration process.

Plagioclase: plagioclase is scarce in the thin section. It can be found in association with quartz inside the leucocratiche lenses. Sometimes, it is possible to notice isolated crystals of plagioclase, in association with biotite.

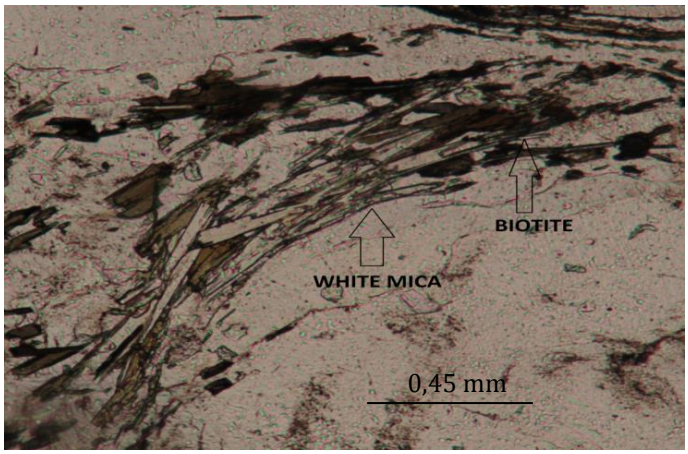

Figure 3.29 Biotite in contact with white mica

Biotite: the biotite occurs in crystals of variable grain-size. Biotite shows textural equilibrium with chlorite, muscovite and garnet (figure 3.29).

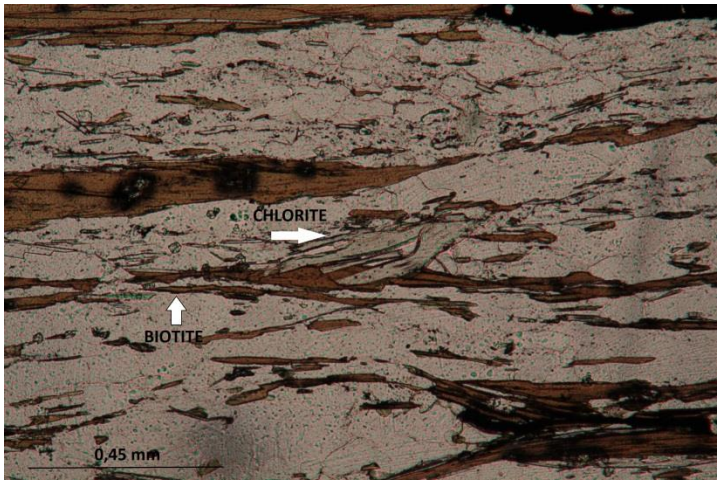

Figure 3.30 Biotite in association with chlorite

White mica: white mica appears in elongated crystals located along the cleavage. It appears to be coeval with chlorite and it replaces biotite like the latter.

Chlorite: chlorite appears in lamellae, oriented along the cleavage. It shows a

pale green color and a slight pleochroism under parallel nicols; it displays anomalous birefringence colors under crossed nicols. This type of chlorite, characterized by a light grey birefringence colour, is rich in magnesium, therefore it can be stable at relatively high temperatures, together with biotite. Chlorite grows in association with white mica and biotite (figure 3.30). With this latter, it forms a sharp contact.

Garnet: the rock is characterized by the presence of garnet porphyroblasts, which seem to grow in textural equilibrium with the matrix. In particular, where garnet is in contact with sheet silicates, it shows a euhedral shape.

Epidote: epidote occurs in elongated crystals, according to the direction of foliation. Epidote crystals are often in association biotite.

Amphibole: amphibole appears in rare isolated crystals oriented according to the foliation. It is characterized by a strong pleochroism and a green color; it is typically associated with quartz and biotite.

3.9 PHYLLITE LY122

The rock shows a schistose structure, characterized by the presence of biotite, muscovite and chlorite along the foliation planes. As a distinctive structural feature, it is possible to notice the presence of large garnet porphyroblast and leucocratic lenses, formed mainly by quartz and elongated in the foliation direction. Sample LY122 is similar to sample LY123, since both specimens show a similar structure and a similar mineralogy; however, some differences are present, because chlorite is more widespread and epidote, amphibole and plagioclase are totally absent in the sample LY122.

The main minerals in the section are garnet, quartz, biotite, white mica and chlorite. Zircon represents an accessory phase.

Garnet: garnet porphyroblasts are present in the rock and they are in textural equilibrium with the matrix. Garnet crystals are characterized by abundant quartz inclusions.

Quartz: quartz is the major component of the rock, it forms leucocratic lenses elongated in the foliation direction. The aspect of the crystal boundaries appears

to be typical of grain boundary migration process

Biotite: biotite is located along the cleavage and it grows in association with white mica and chlorite.

White mica: white mica is the most plentiful sheet silicate in the section. It seems to be coeval with chlorite.

Chlorite: chlorite is pale green and shows anomalous interference colors. It is associated with white mica and biotite. Like in sample LY123 chlorite is characterized by a light-grey birefringence colour, indicative of a high magnesium content.

3.10 MYLONITE LY128

The specimen LY128 represents a strongly mylonitized rock with a gneissic structure, characterized by the presence of K-feldspar and plagioclase porphyroclasts. As a structural characteristic of the rock, it is possible to notice the presence of leucocratic lenses, formed by quartz and elongated in the foliation direction. The foliation is determined by thin layers of fine-grained biotite and white mica.

The main minerals in the section are K-feldspar, plagioclase, quartz, biotite and white mica. Zircon is also present as accessory phase.

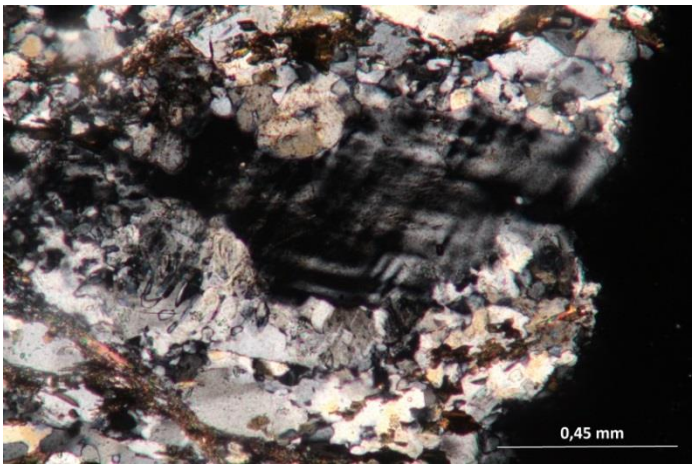

Figure 3.31 K-feldspar porphyroblast in contact with myrmekites

K-feldspar: K-feldspar porphyroclasts show, sometimes, tartan twin,

characteristic of microcline. They are in most cases associated with myrmekites, formed by quartz and Na-plagioclase (figure 3.31). K-feldspar porphyroblasts are often wrapped by fine-grained biotite.

Quartz: leucocratic lenses, formed by quartz, are very abundant in the thin section. The aspect of the quartz crystals boundaries is indicative of grain boundary migration, a recrystallization mechanism occurring at high grade metamorphic conditions. It is possible to notice the presence of quartz inclusions inside plagioclase.

Plagioclase: plagioclase porphyroblasts are less abundant than K-feldspar porphyroblasts and they show typically albite and albite-Carlsbad twins. Like K-feldspar, plagioclase is often surrounded by sheet silicates (figure 3.32).

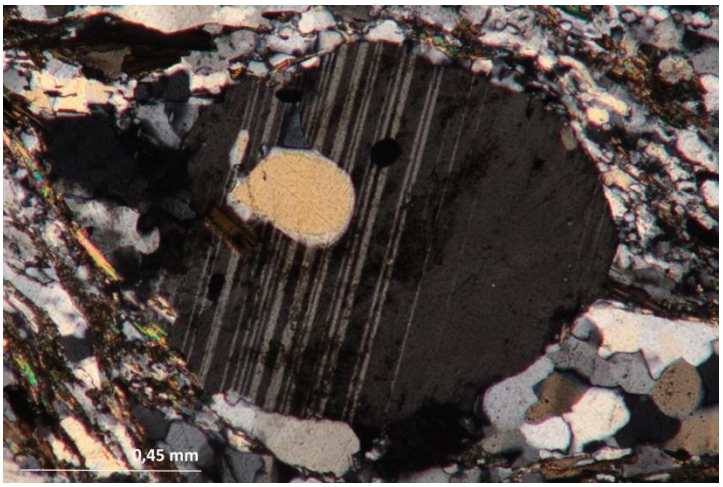

Figure 3.32 Plagioclase porphyroclast

Biotite: biotite is the most abundant sheet silicate in the section. Extremely fine-grained biotite defines the foliation of the rock and wraps plagioclase and K-feldspar porphyroclasts and the leucocratic lenses. Biotite flakes are also found in the thin section; such crystals are often found in association with muscovite and fine-grained biotite.

White mica: fine grained white mica is often associated with biotite along the cleavage. White mica appears to be retrograde, since it doesn't show well-developed crystals and it is much less abundant then biotite.

Zircon: zircon is characterized by high relief. It often occurs as inclusions in

biotite crystals, showing the dark halo resulting from its radioactive decay.

3.11 GARNET MICASCHIST LY148

The rock shows a schistose structure, determined by the presence of white mica and biotite along the cleavage. A distinctive feature of the rock is the presence of large garnet porphyroblasts (5 mm of diameter) and leucocratic lenses, formed by quartz and oriented along the foliation direction. The foliation is defined mainly by white mica crystals, which wrap the garnet porphyroblasts and the leucocratic lenses.

The main minerals are quartz, plagioclase, garnet, white mica, biotite, sillimanite. Tourmaline and zircon are present as accessory phases.

Quartz: quartz is very abundant in the section. The aspect of the grain boundary is typical of grain boundary migration process, supporting high grade recrystallization mechanism conditions.

Garnet: garnet porphyroblasts are fractured and partially replaced by biotite and white mica

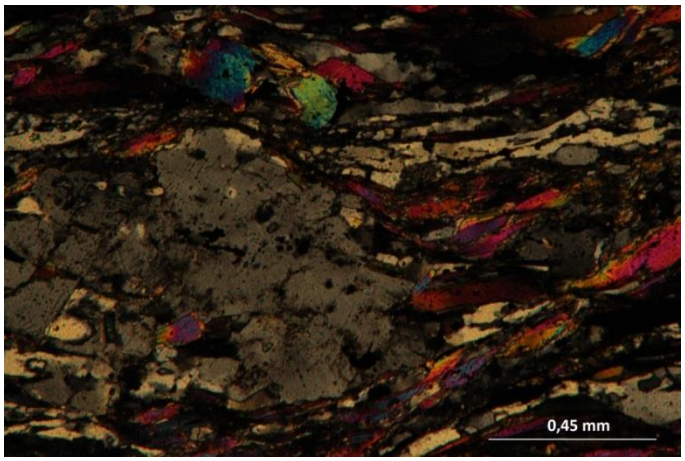

Figure 3.33 Plagioclase in association with white mica and biotite

Plagioclase: plagioclase appears in the matrix, in association with sheet silicates and fibrolite (figure 3.33). Sometimes, it is associated with quartz and forms the leucocratic lenses. It is often characterized by albite twins and some grains show undulose extinction.

White mica: white mica is the most abundant sheet silicate in the section and it appears in variable grain size. White mica is replaced by fine-grained biotite.

Biotite: biotite appears in two different types of crystals, probably formed in two different stages of the metamorphic path. The first type of biotite is characterized by large crystals (1mm length), which are replaced by white mica and by second generation biotite. Second type biotite is extremely fine-grained and seems to replace muscovite; sometimes, it is associated with sillimanite.

Sillimanite: fibrolite is often located between quartz grains and, sometimes, it nucleates at the expense of biotite.

3.12 DISCUSSION OF PETROGRAPHIC OBSERVATIONS

On the base of the observations carried out on the analyses of the thin sections, it's useful to highlight some key points.

The thin sections LY4f and LY131 are the most representative samples and they contain some important hints, which allow us to infer the main events that are recorded in these particular rocks.

Considering sample LY4f, it is possible to notice the presence of two micrastructural types of sillimanite, since we observe crystals of fibrolite inside garnet porphyroblasts, inside plagioclase crystals and inside the matrix. There is a third aluminum silicate, namely kyanite, which might be temporarily located before or between the two generations of sillimanite. It is important to highlight that kyanite is to be found inside the leucosome, therefore the melting-bearing event occurred in the stability field of this phase.

Furthermore, two types of garnet can be distinguished. The garnet porphyroblasts characterized by inclusions of sillimanite appear to be altered and they are pervasively replaced by biotite. The second type of garnet porphyroblasts distinguishes itself from the first type because of the smaller grain-size and because of the absence of sillimanite inclusions. However, both types of garnet appear to be partly replaced by biotite.

Two types of biotite are also present in the rock. Large flakes of biotite seems to be coeval with kyanite, since we observe biotite inclusions in kyanite and both

minerals show sharp rims when they are in contact with each other. Extremely fine-grained biotite is located along the cleavage and it highlights the anisotropy of the rock.

Considering the samples described earlier, we can state that the Nordmawick nappe is a very heterogeneous tectonic unit.

In order to undertake the thermodynamical modelling we need to choose the rocks that are more suitable to evaluate the pressure and temperature conditions.

We have chosen the sample LY4f first of all because it is a pure metapelite, and furthermore because it is characterized by the presence of leucosome lenses and kyanite porphyroblasts indicating that the melting process took place in the stability field of kyanite.

We have chosen also the sample LY131 for the same reasons. It is a meta-psammite and it contains leucocratic patches of crystals that are the product of partial melting. Kyanite is very rare because this rock was strongly deformed in the stability field of sillimanite and therefore kyanite was easily replaced than in sample LY4f.

The other samples were not considered in the thermodynamic modelling since they are more difficult to treat because they are not representative of model chemical systems.

CHAPTER 4

CHEMICAL ANALYSES

4.1 BULK ROCK COMPOSITION ANALYSES

X-ray fluorescence analyses have been carried out for samples LY4f and LY131 and are reported in Table 4.1

	LY4f	LY131
SiO_2	57,28	76,00
Al_2O_3	18,65	11,13
TiO_2	0,99	0,80
FeO	8,83	5,45
MnO	0,09	0,06
MgO	4,17	2,13
CaO	2,06	0,21
Na_2O	1,57	0,37
K_2O	3,71	2,18
P_2O_5	0,19	0,03
L.O.I.	2,47	1,64
Total	100,00	100,00

Table 4.1: bulk rock composition of samples LY4f and LY131

It's useful to compare the composition of these samples with the average composition of rocks reported in the literature.

Let us consider the metapelite sample LY4f first.

Gromet et al (1984) have studied the composition of the North American shale composite and they have compared it with the average shale composition.

I have used the same approach, so I have built a diagram with the data taken from Gromet et al (1984), which belong to the average shale composition of samples coming from all over the world (Gromet et al 1984; Clark, 1924; Ronov and

Migdisov, 1971; Cameron and Garrels, 1980).

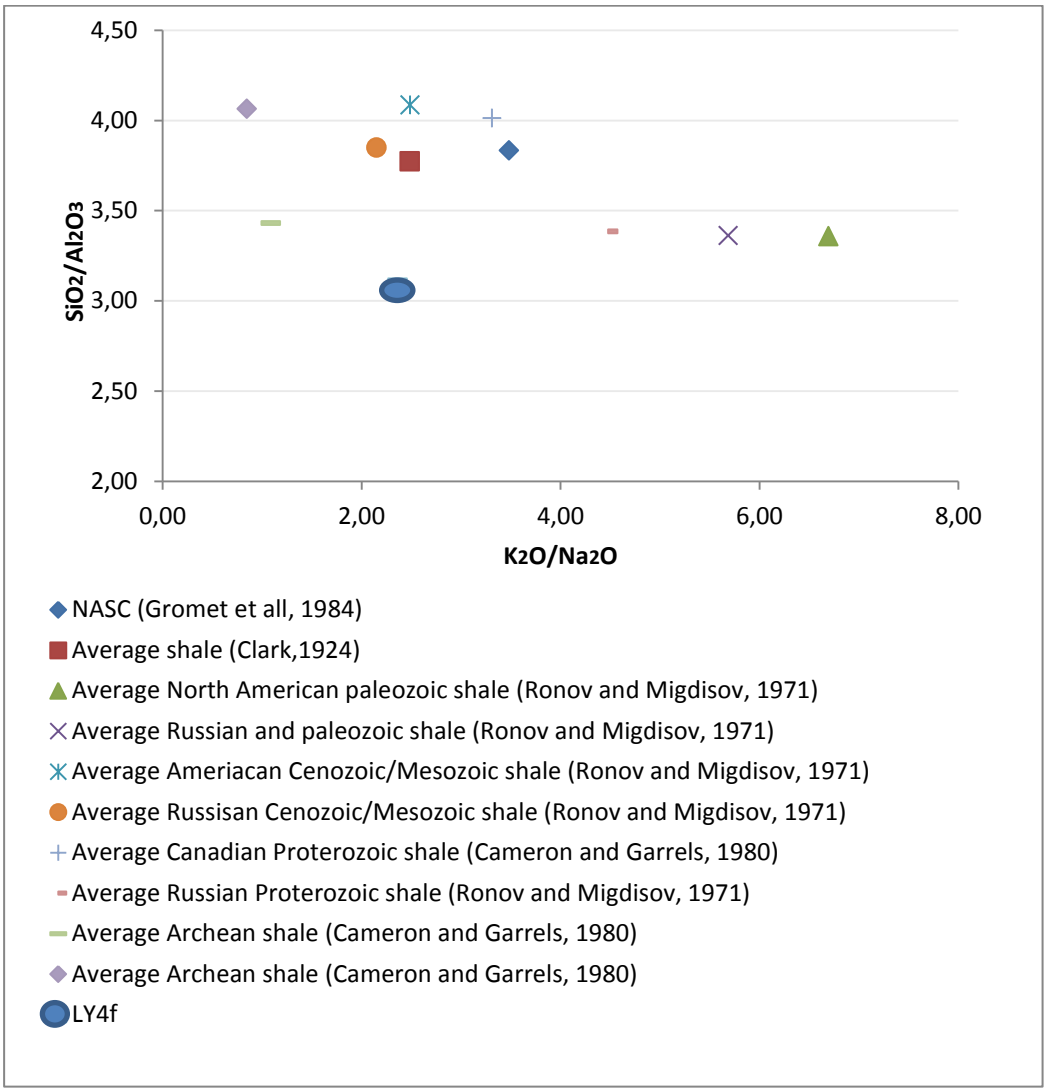

Figure 4.1: SiO_2/Al_2O_3 vs K_2O/Na_2O diagram based on the data from Gromet et al., 1984; the diagram shows a major elements comparison of the average shale composition

This diagram shows the relationship between SiO_2/Al_2O_3 weight ratio plotted versus K_2O/Na_2O weight ratio. The first thing that stands out is that there is a significant variation of the chemical parameters expressed in the diagram, especially for the K_2O/Na_2O ratio, when we consider different average shale composition.

The SiO_2/Al_2O_3 weight ratio of sample LY4f is the lowest, since the SiO_2 content is low (57.28%) and the Al_2O_3 content is relatively high (18.65%). Extraction of

melt during an anatectic process may explain such low SIO_2/Al_2O_3 weight ratio value. The liquid that forms the leucocratic part of the migmatite is characterized by high silica content (SiO_2~72%) and lower aluminum content (Al_2O_3~11%) (Le Breton and Thompson,1988). Therefore, melt extraction involves a decrease of the SiO_2/Al_2O_3 weight ratio. The K_2O/Na_2O weight ratio does not differ from that average shale composition.

Sample LY131 is a quartzo-feldspathic meta-psammite, which is less aluminous than normal pelites (Al_2O_3 = 11.25%). The silica content is very high (76.00 %). The alkali content is very low (Na_2O+K_2O = 2.55%), especially if we consider Na_2O (0.37%). This value is consistent with the microstructural observation, because plagioclase is present in the rock only in myrmekites, surrounding K-feldspar.

Although the Al_2O_3 value matches quite well with the Al_2O_3 value of the average wacke composition given by in Hacker et al. 2011 the other major element contents are significantly different. In particular the alkali content is lower and the silica content higher. The higher silica content is higher probably related to the presence of quartz-rich parts in the sample collected from the outcrop during the field work.

4.2 MINERAL CHEMISTRY

This chapter describes the chemical analyses of minerals carried out on the samples LY4f and LY131.

The main purpose of this research is to characterize the chemical composition of the solid-solution minerals that are playing an important role during the formation of these rocks.

There are basically two reasons why we are interested in these analyses.

These analyses are useful to figure out if the different types of the same mineral, more precisely garnet and biotite, distinguished according to the microstructural observations, effectively display also different composition and therefore may belong to different metamorphic stages.

Furthermore, the chemical composition of the solid-solution phases are necessary to constrain more in detail the field of the peak metamorphic event on the P-T diagram, because the chemical composition of garnet, biotite and plagioclase are sensitive to temperature and pressure changes.

The chemical analyses have been carried out both on Scanning Electron Microscope with the energy dispersive spectroscopy (EDS) detector and on Electron Microprobe, which uses a wavelength dispersive spectroscopy (WDS).

The EDS analyses were carried out at the University of Tromsø (Norway), using a ZEISS MERLIN Compact VP SEM. The SEM is equipped with detectors BSD, WDS, EDS, EBSD, CLD.

The Electron Microprobe analyses were carried out using the Cameca SX50 microprobe of the Consiglio Nazionale delle Ricerche-Istituto di Geosceinze e Georisorse at the University of Padova (Italy).

The normalization parameters used to recalculate the chemical formulae of minerals are the following:

- Garnet: 12 oxygens, Fe^{2+}
- Biotite and white mica: 20 oxygens, Fe^{2+}
- Feldspars: 8 oxygens.

All analyses are reported in the APPENDIX.

4.2.1 SAMPLE LY4f

The minerals analyzed in this sample are garnet, biotite, white mica and plagioclase. Table 4.2 shows representative analyses of these minerals.

GARNET

We have carried out this analysis considering two types of garnet. The first type is characterized by the presence of sillimanite inclusions whereas the second type of garnet is characterized by the absence of sillimanite inclusions.

It stands out, from a general point of view, that the garnet present in this rock is an almandine-rich solid solution (mole fraction of Almandine ~ 0.65, see table 4.2). This is typical of garnet in metapelites.

We have analyzed three crystals of garnet that belong to the first type (garnet 1, garnet 2, garnet 3).

Garnet 1 (figure 4.2) shows a homogeneous core. The composition of the core is $Alm_{0.64}Pyp_{0.24\text{-}0.25}Grs_{0.6\text{-}0.7}Sps_{0.5\text{-}0.6}$. Garnet is zoned in the most external part. Pyrope content increases towards the rim and almandine, obviously, shows the opposite behavior. Also grossular content increases getting closer to the rim. Spessartine remains constant throughout the whole crystal.

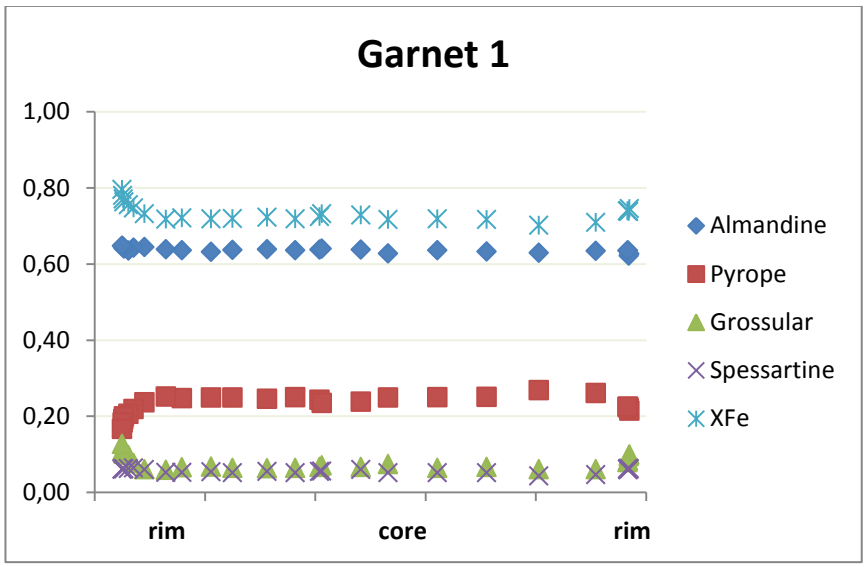

Figure 4.2 The diameter of garnet 1 is 9 mm

The zoning is more pronounced where garnet is in contact with biotite. In fact, it

is possible to notice, that the variation of pyrope, grossular, and X_{Fe} is more evident on the left side of the diagram ($Alm_{0.64}Pyp_{0.17}Grs_{0.13}Sps_{0.6}$), where garnet is in contact with biotite, compared to the right part, where garnet is in contact with quartz ($Alm_{0.63}Pyp_{0.21}Grs_{0.10}Sps_{0.6}$).

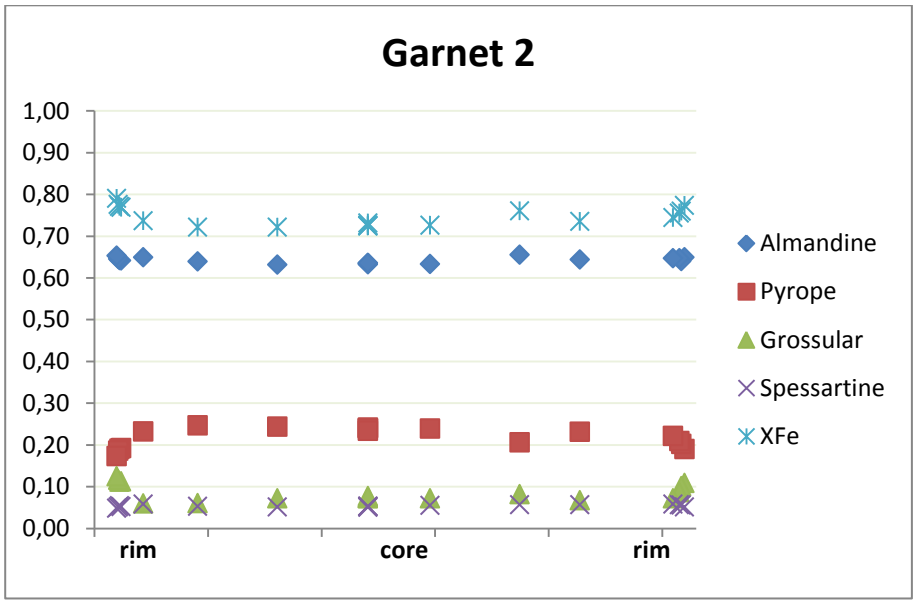

Figure 4.3 The diameter of garnet 2 is 3 mm

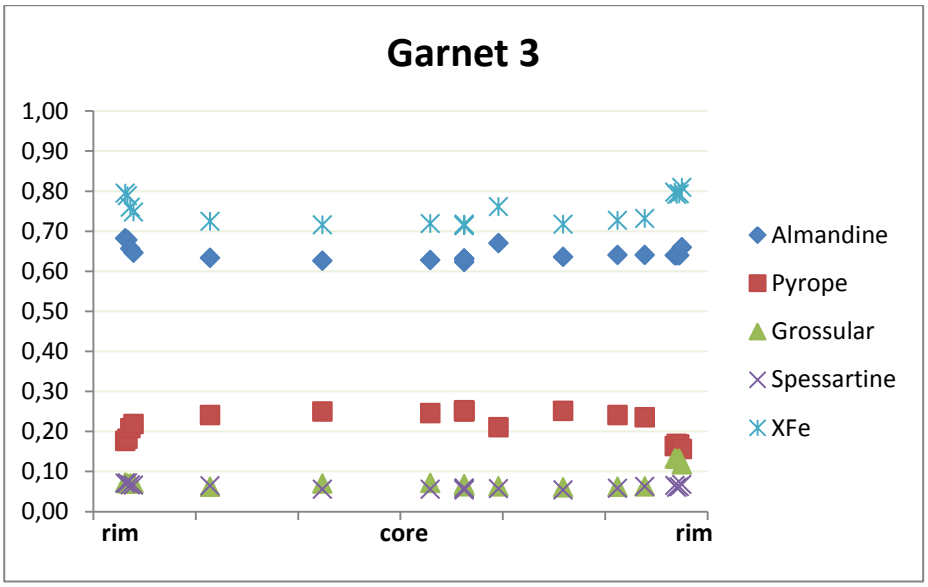

Figure 4.4 The diameter of garnet 3 is 3 mm

Figure 4.3 and Figure 4.4 show that garnet 2 and garnet 3 have the same composition of garnet 1. The zoning is slightly different because these two

crystals are in contact with biotite on both sides, therefore the zoning trends appear more symmetric.According to these compositional trends, we can state that these three garnet crystals belong to the same generation also from a chemical point of view.

The second type of garnet is characterized by a homogeneous core ($Alm_{0.64}Pyp_{0.23}Grs_{0.6\text{-}0.7}Sps_{0.6\text{-}0.7}$). and by a slight zoning towards the rim. Pyrope decreases towards the rim, whereas grossular and almandine increase. Spessartine is constant throughout the crystal. The composition of the rim of the crystal of the second type of garnet is $Alm_{0.66}Pyr_{0.19\text{-}0.21}Grs_{0.7\text{-}0.9}Sps_{0.6\text{-}0.7}$.

BIOTITE

We have analyzed three different types of biotite, according to the microstructural observations. We have considered:

- biotite located along the cleavage, which appears in large flakes;
- biotite located along the cleavage, which shows extremely fine grained crystals;
- biotite inclusions inside garnet porphyroblasts;
- biotite inclusions inside kyanite porphyroblasts, which should represent the composition of biotite at the peak metamorphic conditions while kyanite porphyroblasts were growing.

Biotite flakes located along the cleavage show fairly constant chemical composition throughout the rock. X_{Mg} ranges between 0.52 and 0.57. Titanium content ranges from 0.26 to 0.30 atoms per unit formula (a.p.f.u.).

The composition of fine grained biotite differs from the composition of coarse grained biotite. The main difference concerns the tetrahedral site, because the silica content is higher. X_{Mg} is almost the same and Ti content is slightly lower (Ti = 0.24 a.p.f.u.).

The composition of biotite inclusions inside garnet is different compared to the composition of biotite in the matrix. X_{Mg} is higher (X_{Mg} = 0.62) and the titanium content is lower (Ti = 0.12-0.14 a.p.f.u.).

Biotite inclusions in kyanite porphyroblasts are characterized by the same composition of the biotite large flakes in the matrix. X_{Mg} ranges between 0.55

and 0.56 and Ti content is 0.25-0.28

PLAGIOCLASE

Plagioclase shows constant composition throughout the rock, and the anorthite content does not change if we consider the crystals present in the matrix or inside the leucocratic lenses. More precisely, plagioclase can be classified as andesine, since X_{An} ranges from 0.39 to 0.41.

WHITE MICA

The chemical composition of white mica is constant throughout the sample. White mica is a muscovite-rich term with a low phengitic component, namely the presence of Mg and Fe inside the octahedral site and excess Si in the tetrahedral site. Al^{VI} ranges between 1.67 and 1.69 a.p.f.u.. Fe content is high (Fe^{2+} = 0.20-0.22 a.p.f.u. but Si ranges between 3.08 and 3.10 a.p.f.u.. Titanium content ranges between 0.02 and 0.05 a.p.f.u..

Paragonite content is very low (Na = 0.06-0.08 a.p.f.u.).

4.2.3 SAMPLE LY131

The minerals analyzed for sample LY131 are garnet, biotite, white mica and K-feldspar.

The representative analyses of sample LY131 are reported in table 4.3

GARNET

In order to analyze garnet, we have used the same approach used for sample LY4f, although the features highlighted in LY131 are not as evident as in the previous sample.

Figure 5 shows the chemical profile along a garnet crystal with sillimanite inclusions (garnet 1).

Garnet 1 shows a modest zoning, with .a flat wide core and variations at the rims. The core composition is $Alm_{0.71}Pyp_{0.22}Grs_{0.5}Sps_{0.2}$. The zoning at the rim is more

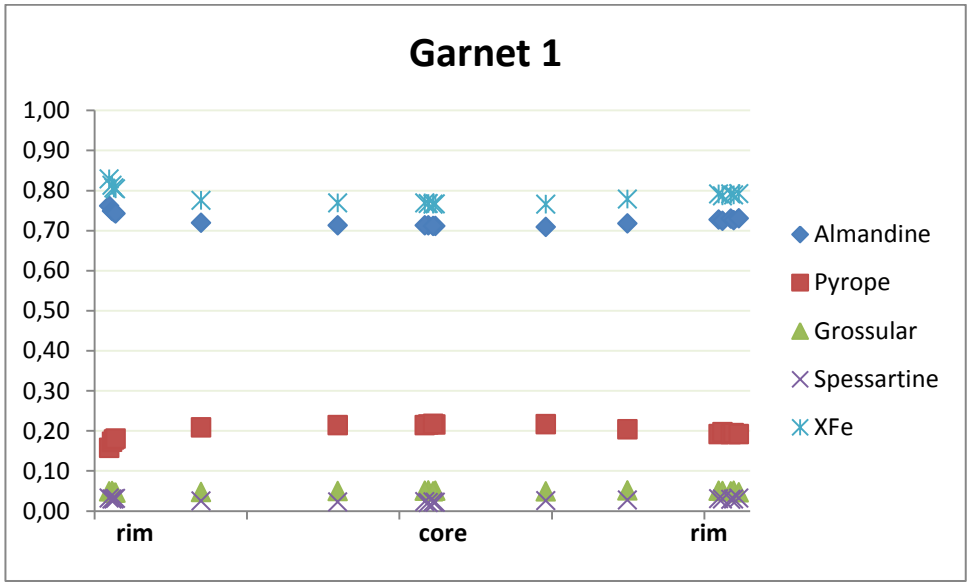

Figure 4.5 The diameter of garnet 1 is 4 mm

pronounced where garnet is in contact with biotite. The composition of the rim in contact with biotite is $Alm_{0.76}Pyp_{0.16}Grs_{0.05}Sps_{0.03}$, whereas the composition of garnet in contact with quartz is $Alm_{0.73}Pyp_{0.19}Grs_{0.05}Sps_{0.03}$.

Grossular and Spessartine, in low amounts, do not show any variation throughout the crystal.

The second type of garnet shows a modest zoning towards the rim as well. The zoning is more evident where garnet is in contact with biotite ($Alm_{0.82}Pyp_{0.18}Grs_{0.05}Sps_{0.02}$). Grossular and Spessartine values are the same of garnet 1. X_{Fe} increases towards the rim.

BIOTITE

We have carried out the analyses considering two microstructurally-defined types of biotite; coarse-grained biotite, which appears in the form of large flakes and fine-grained biotite, which wraps up the leucocratic lenses.

Fromthe results of Table 4.3 and appwndix 1. It is not possible to appreciate any compositional difference between these two types of crystals, which are characterized by constant X_{Mg} values (X_{Mg}=0.49-0.51) and a Ti content higher than in sample LY4f (Ti = 0.40-0.45 a.p.f.u.).

K-FELDSPAR

K-feldspar porphyroblasts are characterized by the presence of perthitic exolutions. K-feldspar is a solid solution between orthoclase and albite (X_{Or} = 0.86, X_{Ab} = 0.14). Anorthite is absent.

The perthitic exsolutions inside K-feldspar are albite rich (X_{Or} = 0.17, X_{Ab} = 0.83).

WHITE MICA

As in sample LY4f, white mica is muscovite-rich term, characterized by a modest phengitic component. The phengite component shows lower values compared with the previous sample. Paragonite content is very low (Na = 0.06-0.07 a.p.f.u.). Al^{VI} is 1.76-1.77 a.p.f.u. and Fe is 0.08 a.p.f.u.. Si ranges between 3.07 and 3.08 a.p.f.u..

Coarse-grained white mica and fine grained white mica are characterized by a different Ti content. Ti content of coarse-grained white mica ranges between 0.08 and 0.11 a.p.f.u. and Ti content of fine grained white mica ranges between 0.01 and 0.3.

4.3 DISCUSSION ON PHASE CHEMISTRY RESULTS

Garnet shows a homogeneous core. This is not uncommon for garnet crystals which have equilibrated in the granulite facies. The chemical diffusion, favored by the high temperature conditions, usually erases the zoning and smooths the bell-shaped growth patterns of almandine, pyrope, grossular and spessartine. In this sample, even the biggest garnet crystals do not show any chemical variation in the inner part.

In general, garnet crystals that have undergone high temperature diffusion in the granulite facies and later retrograde exchange of cations with biotite, do not show bell-shaped zoning profiles of Mn, Mg and Ca, typical of growth zoning (Tuccillo et al., 1990). Mg content, usually, has a flat trend in the internal part and decreases towards the rim; Mn content shows the opposite behavior.

In the studied samples, the zoning characterizes only the outermost part of the

crystals because of the retrograde exchange between garnet and biotite, during the retrograde path. This kind of zoning is not relevant in biotite, because some minerals better retain the chemical memory of their P-T history then others. In this particular case, diffusion is much more effective in biotite then in garnet.
During the retrograde path, continuous reactions such as:

Garnet + H_2O = biotite + Al-silicate + quartz (1)

involve the Fe-Mg exchange that causes a change in the Fe/(Fe+Mg) ratio of garnet and biotite. The value of the Fe/(Fe+Mg) ratio of garnet and biotite increases as the temperature decreases, therefore both garnet and biotite will be characterized by Fe-richer compositions.
The Ca zoning is produced by the reaction

Grossular + Al-silicate + quartz = Anorthite (2)

Grossular is on the high pressure side of the reaction, therefore an increase in Ca content in garnet is consistent with an increase in the pressure conditions.
The grossular profile of garnet 1 in sample LY131 is flat. This is probably due to the complete re-equibration of Ca in garnet during retrogression.
Considering the two types of crystals that we mentioned earlier, garnet does not show systematic variations in the chemical composition as a function of its microstructural occurrence. The assumption that we made earlier, namely that in the sample there were two generations of garnet crystals, is not confirmed by the chemical analyses. Furthermore, this is valid both for sample LY131 and sample LY4f.
The slight difference in almandine, pyrope, grossular and XMg contents of different garnets from the same thin section can be explained by a cut effect: i.e. that crystals of garnet are cut in different ways and orientations with respect to equatorial sections during the making of the thin section. If the garnet crystal is cut in the external part, the face shown in the thin section, of course, is smaller and is characterized by the chemical composition of the external part.
Figure 4.6 shows that the core of garnet crystals with sillimanite inclusions

(garnet 3) and garnet crystals without sillimanite inclusions (garnet 4) of sample LY4f have similar X_{Mg} values.

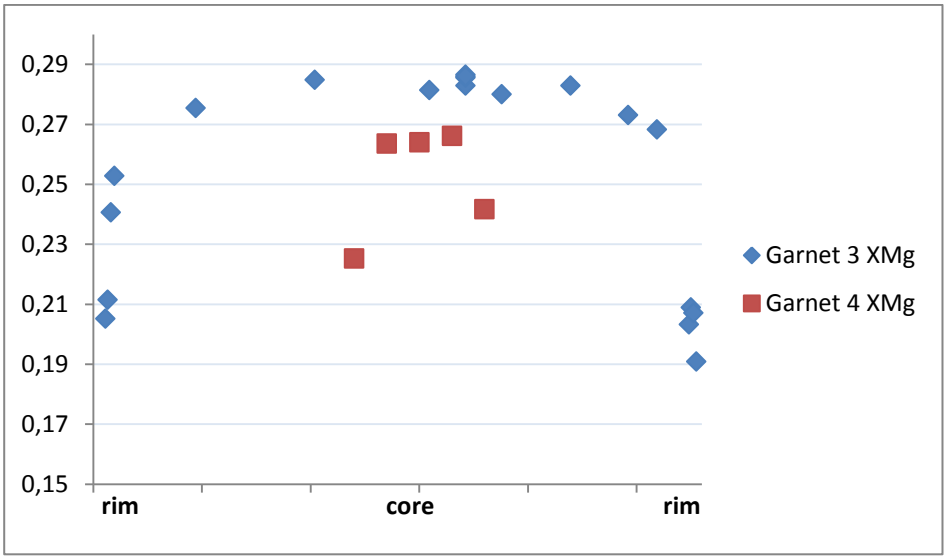

Figure 4.6 The diameter of garnet 3 is 3 mm (figure 4.4), whereas garnet 4 is 0.8 mm

In sample LY4f, coarse-grained biotite and fine-grained biotite show a different content in Si and in Al^{IV}. During the development of the foliation, while deformation was acting, solution transfer process probably took place. Large biotite flakes have partially dissolved and have recrystallized along the foliation planes as fine-grained crystals with different composition.

The diagram shown in figure 7 provides a useful classification of K-micas. The y axis corresponds to (Fe_{tot} + Mg + Ti - ^{VI}Al), whereas the x axis represents the quantity (Mg – Li). These operations are possible because the elements involved in the subtractions show a strong antithetical behavior in K-mica, therefore such elements can all be represented in a two-dimensional diagram (Tischendorf et al. 2004).

Muscovite crystals of sample LY4f are located in a slightly different position compared to muscovite crystals of sample LY131, because of the higher Fe content of muscovite in sample LY4f.

In the diagram of Figure 4.8, the composition of white mica crystals of sample LY131 overlaps the phengitic-white mica composition, whereas the white mica crystals of sample LY4f are located towards more Fe^{3+} rich-composition. This

result is ambiguous because sample LY4f is a graphite bearing-rock. This point should be treated more in detail but, however, this goes beyond the purposes of this work.

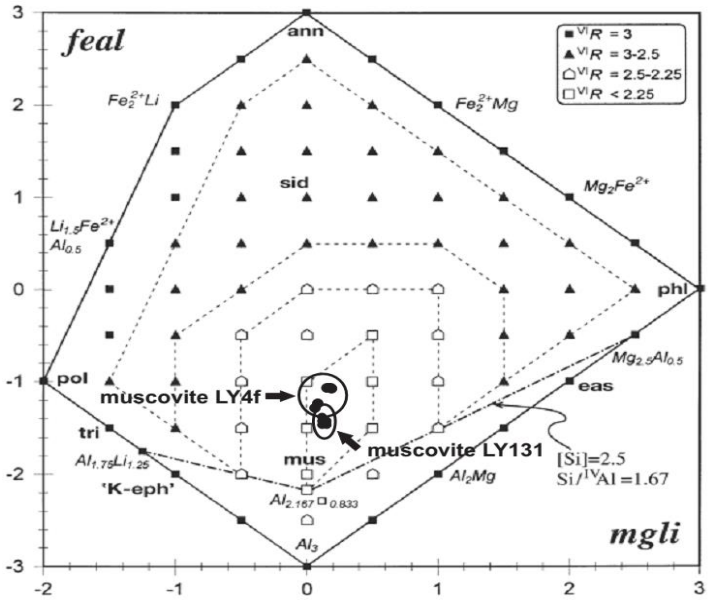

Figure 4.7: Feal vs mgli diagram, taken from Tischendorf et al. 2004, showing the composition an d classification of white mica crystals from samples LY4f and LY131

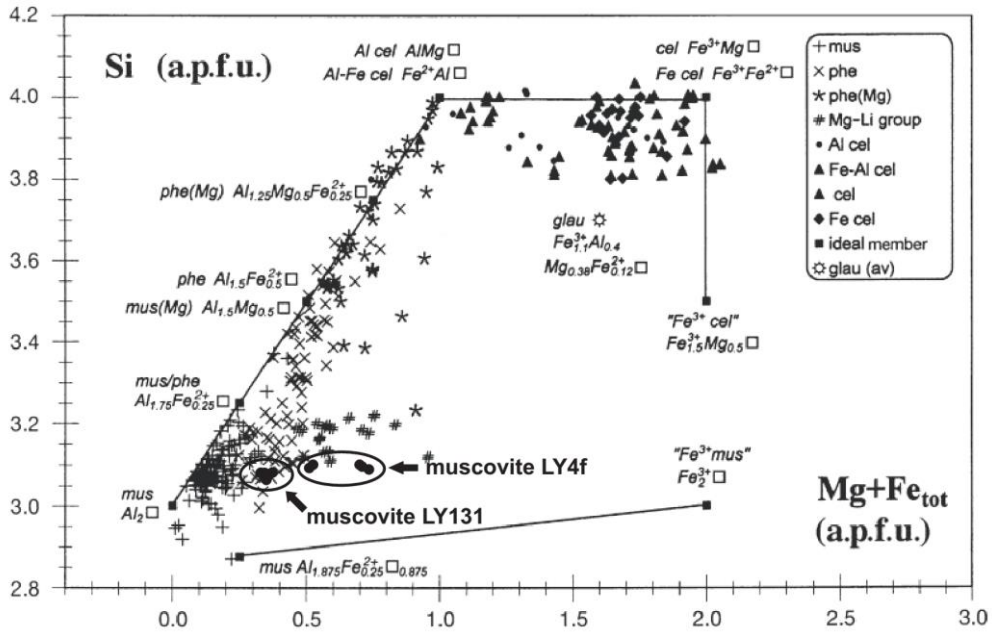

Figure 4.8: Diagram taken from Tischendorf et al. 2004 which correlates Si a.p.f.u. and Fe_{tot}+Mg a.p.f.u. in muscovites, phengite and celadonite

LY4f	Grt							Bt		Plg	Musc
	grt with sill inclusions			grt without sill inclusions			inclusion in grt	coarse grained	fine grained		
	rim-bt	core	rim-qtz	rim-bt	core	rim-qtz					
Na_2O	0,01	0,05		0,02		0,03	0,23	0,11	0,14	6,77	0,55
MgO	5,55	6,62	4,35	5,01	5,97	5,50	13,19	12,61	11,13	0,00	1,33
Al_2O_3	21,57	21,80	21,28	21,55	21,55	21,51	18,81	17,78	15,76	26,70	34,03
SiO_2	37,59	37,45	36,95	37,91	37,49	37,41	37,00	36,56	40,48	58,03	46,77
K_2O		0,03		0,02			9,43	9,63	9,37	0,13	11,24
CaO	3,58	2,36	4,60	3,41	2,47	2,68		0,03	0,01	8,27	
TiO_2	0,02	0,01	0,05	0,00	0,01		1,67	2,33	1,99		0,62
Cr_2O_3				0,02	0,03		0,02	0,06	0,01		
MnO	2,77	2,38	2,76	2,81	3,19	2,89		0,11	0,08		
FeO	28,95	30,03	30,15	30,71	29,67	30,76	15,00	16,02	15,29	0,10	4,07
Total	100,04	100,73	100,15	101,46	100,38	100,78	95,34	95,21	94,28	100,00	98,61
Si	2,97	2,94	2,94	2,97	2,96	2,95	5,49	5,48	6,59	2,60	3,05
Ti							0,19	0,26	0,24		0,03
Al	2,01	2,01	2,00	1,99	2,00	2,00	3,29	3,14	3,02	1,41	2,62
Al^{VI}							0,78	0,63	1,61		1,67
Al^{IV}				2,01	1,96	2,03	2,51	2,52	1,41		0,95
Cr								0,01			
Fe^{2+}	1,91	1,97	2,01	0,19	0,21	0,19	1,86	2,01	2,08		0,22
Mn	0,19	0,16	0,19					0,01	0,01		
Mg	0,65	0,77	0,52	0,59	0,70	0,65	2,92	2,82	2,70		0,13
Ca	0,30	0,20	0,39	0,29	0,21	0,23				0,40	
Na							0,07	0,03	0,04	0,59	0,07
K							1,79	1,84	1,95	0,01	0,94
Total	8,03	8,05	8,05	8,04	8,04	8,05	15,60	15,61	16,65	5,01	7,06
Alm	0,63	0,64	0,65	0,66	0,64	0,66					
Pyp	0,21	0,25	0,17	0,19	0,23	0,21					
Gros	0,10	0,06	0,13	0,09	0,07	0,07					
Spes	0,06	0,05	0,06	0,06	0,07	0,06					
X Fe	0,75	0,72	0,80	0,77	0,74	0,76	0,39	0,42	0,44		
X Mg	0,25	0,28	0,20	0,23	0,26	0,24	0,61	0,58	0,56		
X An										0,40	
X Ab										0,59	
X Or										0,01	

Table 4.2: microprobe and EDS analyses of the representative phases of sample LY4f

LY131	Grt						Bt		K-feld		Musc
	grt with sill inclusions			grt without sill inclusions			coarse-grained	Bt contact grt	K-feld	Perthite	
	rim-bt	core	rim-qtz	rim -qtz	core	rim-bt					
Na_2O	0,02	0,00	0,09	0,03	0,02	0,02	0,14	0,14	1,44	8,40	0,53
MgO	4,15	5,74	4,97	5,00	4,99	4,25	9,90	11,08			1,07
Al_2O_3	21,66	21,48	21,71	21,62	21,67	21,85	17,67	19,05	19,48	20,09	36,39
SiO_2	37,24	37,68	37,56	37,18	37,27	37,83	35,31	36,59	64,38	68,65	48,00
K_2O	0,04		0,25	0,00	0,00	0,02	9,61	9,57	14,13	2,66	11,33
CaO	1,79	1,86	1,67	1,96	1,91	1,77	0,04	0,00		0,20	
TiO_2	0,02	0,04	0,00	0,01	0,01	0,01	3,59	3,19			1,10
Cr_2O_3	0,02		0,02	0,06	0,03		0,02				0,06
MnO	1,48	1,08	1,45	1,06	1,01	0,87	0,01	0,06			
FeO	35,80	34,02	33,75	35,04	34,17	35,68	18,34	16,71			1,52
BaO									0,57		
Total	102,22	101,90	101,47	101,95	101,09	102,31	94,63	96,39	100,00	100	100,00
Si	2,94	2,95	2,96	2,93	2,95	2,96	5,90	5,42	2,96	3,00	3,05
Ti	0,00	0,00	0,00	0,00	0,00	0,00	0,45	0,36			0,05
Al	2,01	1,98	2,01	2,01	2,02	2,02	3,48	3,33	1,06	1,04	2,73
Al^{VI}							1,38	0,75			1,77
Al^{IV}							2,10	2,58			0,96
Cr											
Fe^{2+}	2,36	2,23	2,22	2,31	2,26	2,34	2,56	2,07			0,08
Mn	0,10	0,07	0,10	0,07	0,07	0,06	0,00	0,01			
Mg	0,49	0,67	0,58	0,59	0,59	0,50	2,46	2,45			0,10
Ca	0,15	0,16	0,14	0,17	0,16	0,15	0,01	0,00		0,01	
Na	0,00	0,00	0,01	0,00	0,00	0,00	0,05	0,04	0,13	0,71	0,06
K	0,00	0,00	0,03	0,00	0,00	0,00	2,05	1,81	0,83	0,15	0,92
Ba									0,01		
Total	8,06	8,06	8,05	8,07	8,05	8,03	16,96	15,48	4,99	4,91	7,00
Alm	0,76	0,71	0,73	0,74	0,73	0,77					
Pyp	0,16	0,21	0,19	0,19	0,19	0,16					
Gros	0,05	0,05	0,05	0,05	0,05	0,05					
Spes	0,03	0,02	0,03	0,02	0,02	0,02					
XFe	0,83	0,77	0,79	0,80	0,79	0,82	0,51	0,46			
XMg	0,17	0,23	0,21	0,20	0,21	0,18	0,49	0,54			
X An										0,01	
X Ab									0,14	0,82	
X Or									0,86	0,17	

Table 4.3: microprobe and EDS analyses of the representative phases of sample LY131

CHAPTER 5
THERMODYNAMIC MODELLING

5.1 INTRODUCTION

Thermodynamic modelling is a valuable tool to predict the behavior of a chemical system as a function of temperature, pressure or concentration of a component. The phase diagram sections calculated for a specific bulk composition are named pseudosections.

Pseudosections provide a straightforward representation of the stability fields of the stable mineral assemblages and they also show the reactions for a specific bulk composition (Holland and Powell, 1998).

Pseudosections differ from petrogenetic grids, because the latter are the representations of all possible relation of a compositional rock system. Therefore, they represent only discontinuous reactions and invariant points at the intersections of the discontinuous reactions. The pitfall of petrogenetic grids is that in any specific region several different mineral assemblages may be stable and, more importantly, only a few of the reactions depicted on the grid are relevant for the bulk composition of the rock of interest. Moreover, given that in the pelitic system most of the phases that govern the metamorphic reactions are solid solutions, continuous reactions may limit the stability field of the mineral assemblages of the rock-sample considered. In contrast to grid projections there is only one P-T-X state represented by any point in the pseudosection. It follows that at each point the composition and proportions of the phases and the thermodynamic properties are uniquely determined (Connolly and Petrini 2002).

Pseudosections are typically P-T, T-X and P-X diagrams. They show the stable mineral assemblages at any point, and the lines that define the stability fields may reflect both continuous and discontinuous reactions.

The most useful application of pseudosections is that they provide a relatively straightforward model for the behavior of a rock during metamorphim.

Pseudosections have also application in thermo-barometry, since they provide a

map of both mineral chemistry and mode as a function of P and T.

For both samples studied in this work the model chemical system used is MnNCaKFMASHT with the bulk composition provided by the X-Ray Fluorescence analyses.

Provided that both samples are graphite-bearing, the system is characterized by a graphite saturated C-O-H (COH) fluid. Therefore, the water activity in the fluid must be lowered because of the presence of diluting carbonic species such as CH_4 and CO_2. If the fluid phase in high temperature metapelites is essentially H_2O produced from the destabilization of phyllosilicates, the ratio between H_2 and O_2 components in the fluid is constrained at 2:1. In this case, the fluid composition is characterized by the maximum activity of water for a graphite saturated fluid.

However, redox processes might affect this assumption and make the fluid behavior more complex and less predictable. In any case, in the calculation of the pseudosections C is not considered, given the lack of information and thermodynamic data about the behavior of graphite-saturated fluids and melts at supra-solidus conditions, in particular about the partitioning of carbonic species between melt and fluid. With this omission, one should be aware that the fluid-bearing melting reactions which appear in the pseudosections, in nature are actually displaced towards higher temperatures of a few tens degrees, because of the presence of diluting carbonic species in the metamorphic fluid (see also chapter 1.5).

Bartoli et al. (2013) calculated a pseudosection for a graphitic migmatite including also O_2 and C in the calculation. They stated that the displacement of the solidus in graphite-bearing systems is 10-20 °C towards higher temperatures and the invariant melting point I_3 of Thompson and Algor (1977) is displaced of 0.5 kbar towards higher pressures. They affirm also that the topology of the calculated phase diagram in the supra-solidus region “does not differ significantly in graphite -bearing or graphite free systems”.

In this thesis, the calculations are performed with the Gibbs energy minimization (Connolly, 2009) with the thermodynamic database provided by Holland and Powell (1998) and revised in 2003.

The solution model of garnet from Ganguly et al. (1996) was used, biotite from Tajcmanova et al. (2009), white mica from Coggon and Holland (2002), K-feldspar from Thompson and Hovis (1979), plagioclase from Newton et al. (1981), ilmenite from White et al. (2000), orthopyroxene from Holland and Powell (1999), chlorite from Holland et al. (1998), staurolite from Holland and Powell (1998) and the melt phase from White et al. (2007).

The chemical system used to calculate the thermodynamic model should be the most complete possible, because the closer the chemical system to the modelled rock is, the fewer uncertainties in the calculation are involved. Even considering the largest chemical system that is possible to model, such as MnNCaKFMASHTOC, natural rocks may not be described completely, since some other components may be present in some phases and affect their stability field. For instance, zinc may be present in appreciable amount in staurolite and spinel, and fluorine or chlorine may be present in biotite (White et al. 2007).

Smaller and simplified chemical systems such as KFMASH or NCaKFMASH sometimes do not describe properly the behavior of natural rocks. Mn is important, because it influences the stability of garnet at low temperatures and low pressures (Spear, 1995). The presence of Ti is also significant because it affects the stability of biotite at high temperatures and it is a major constituent of ilmenite, a common mineral phase in metapelites.

5.2 PHASE EQUILIBRIA MODELLING FOR SAMPLE LY4f

5.2.1 T-X_{H2O} MODELLING

In order to calculate the P-T pseudosection of sample LY4f, I have considered the composition obtained from the X-ray fluorescence analyses for all the major oxides except for H_2O. The amount of water significantly affects the mineral equilibria and deserves further evaluation. The T-X_{H2O} pseudosection reported in figure 5.1 shows how the mineral equilibria vary with variable water content. The water content varies from 0 to the value that corresponds to the loss of ignition (2.46 wt%).

The stable mineral assemblage which characterizes the rock is garnet + biotite + plagioclase + sillimanite + quartz + melt, where K-feldspar is missing. In the presudosection, K-feldspar is not stable at high water values. Therefore I have chosen to calculate the pressure – temperature pseudosection at a value of water beyond the stability field of K-feldspar.

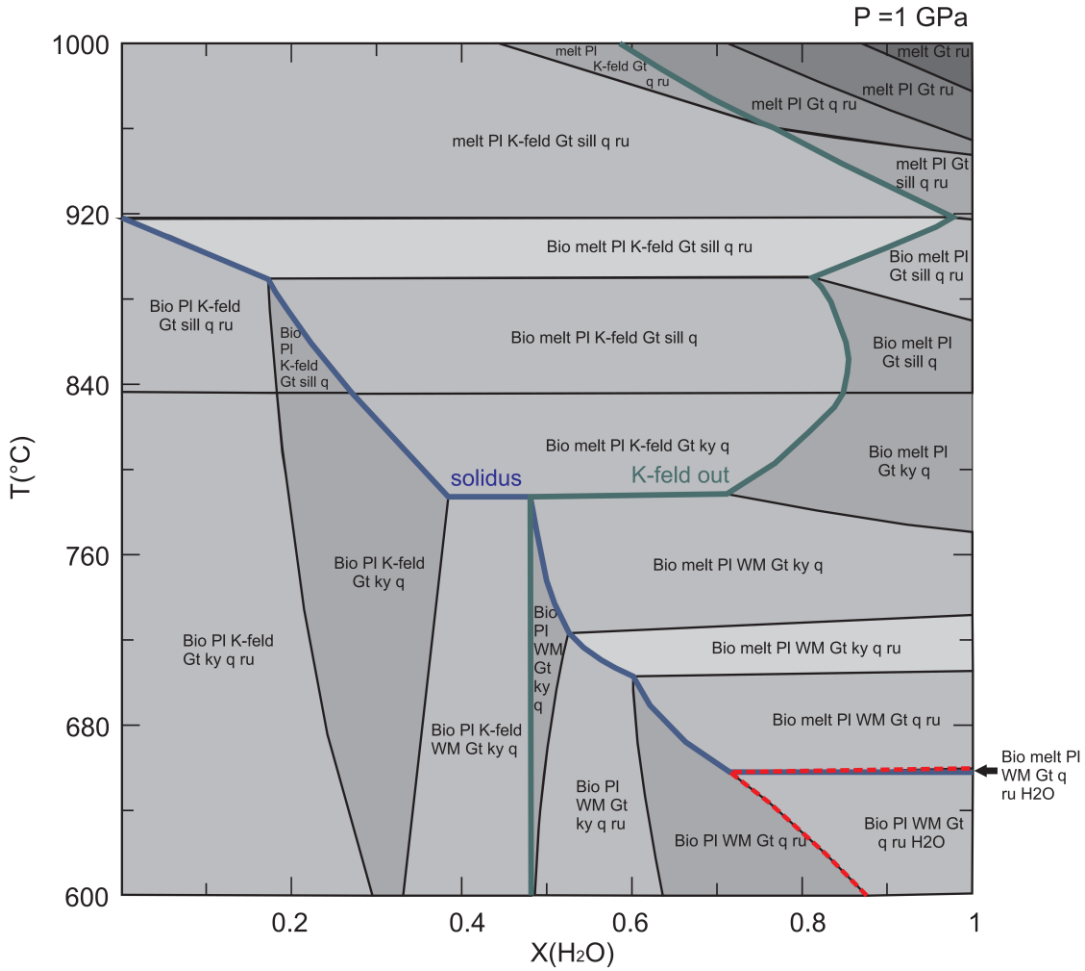

Figure 5.1 T-X_{H2O} pseudosection using the composition of sample LY4f: mol% Na_2O = 1.59 MgO = 6.37 Al_2O_3 = 11.62 SiO_2 = 59.23 K_2O = 2.43 CaO = 2.37 TiO_2 = 0.76 MnO = 0.16 FeO = 7.65. H_2O = 0 for X = 0, H_2O = 8.74 for X = 1. The water saturated region is delimited with the red dotted line. The solidus is highlighted with the blue line. The K-feldspar stability field is delimited with the dark green line.

I have chosen a H_2O content of 7.86 mol% equal to 2.26 wt%. At this condition the subsolidus mineral assemblage is water saturated, and, once the rock starts to melt, the water present in the system dissolves into the liquid without the formation of a vapor phase, since the amount of water is not enough to saturate

the liquid.

5.2.2 P-T MODELLING

Figure 5.2 shows the P-T pseudosection calculated in the MnNCaKFMASHT system. I have considered in the calculation all the minerals which potentially may be stable in a metapelitic composition.

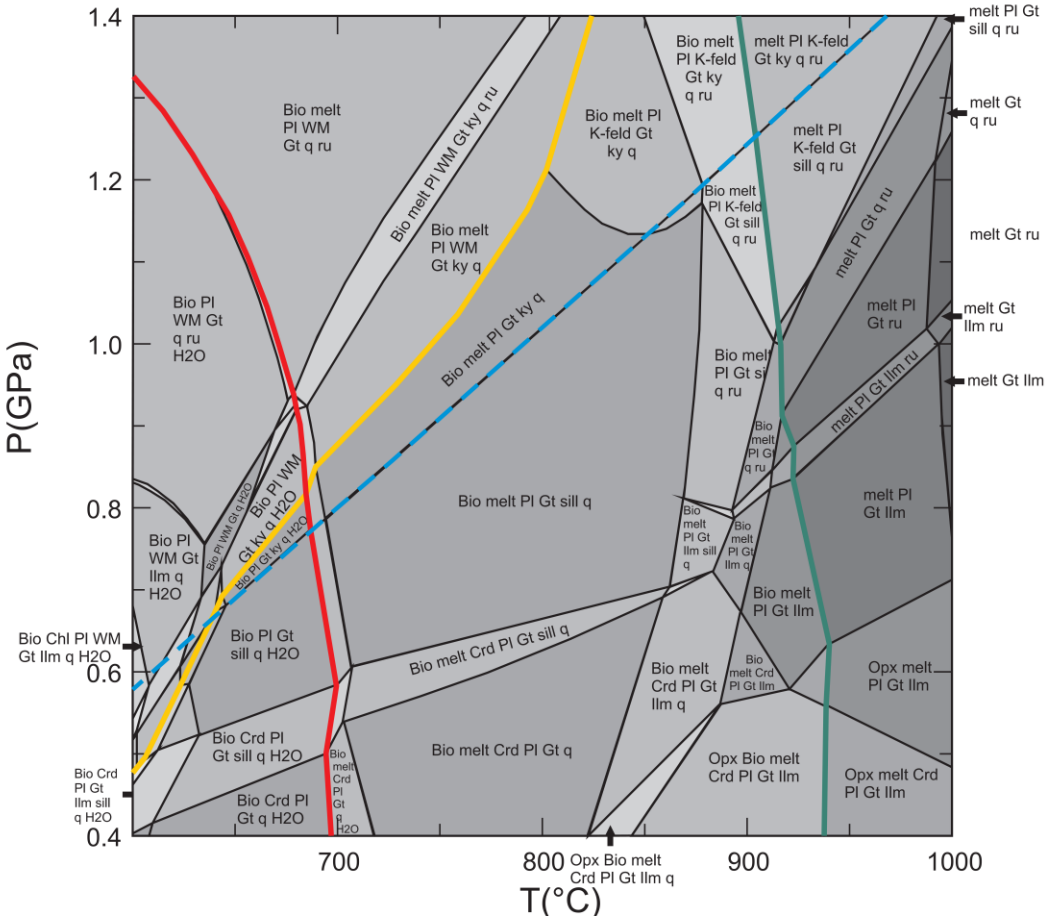

Figure 5.2 P-T pseudosection of sample LY4f calculated in mol% MnO = 0.16 Na_2O = 1.59 CaO = 2.37 K_2O = 2.43 FeO = 7.65 MgO = 6.37 Al_2O_3 = 11.39 SiO_2 = 59.26 TiO_2 = 0.76 H_2O = 7.86. The solidus is highlighed with the red line, white mica and biotite- out curves are highlighted respectively in yellow and green. The extension of the Ky-Sill polymorphic transition is outlined with the dashed blue line for clarity.

Therefore, I have added chlorite, staurolite, cordierite, orthopyroxene, K-feldspar, ilmenite and rutile to the phases present in the sample. Water is present in all the sub-solidus assemblages. As expected, the temperature of the solidus (red line) decreases as the pressure rises: at 0.6 GPa the rock. starts to melt at about 700°, whereas at 1.1 GPa the rocks starts to melt at about 650°. The intersection

between the white mica-out curve (yellow line) and the solidus is located at 0.8 GPa and 690°. The biotite-out curve occurs at about 920-930° and its location is not very pressure-sensitive. The biotite breakdown reaction

Biotite + sillimanite + plagioclase + quartz = garnet + liquid

is characterized by a continuous nature. It takes place over a large temperature interval, since biotite dehydration melting is shifted significantly towards higher temperature because of the presence of Ti in the system. At 0.8 GPa biotite starts to be consumed at about 700° and isn't completely exhausted until 920°.

Chlorite and staurolite appear in small quadrivariant or pentavariant field in the low temperature and low pressure part of the diagram. K-feldspar is present only at high pressures and high temperatures, because of the high water amount considered in the calculation (2.26%).

The stable mineral assemblage at the peak conditions observed in the sample is biotite + garnet + sillimanite + plagioclase + quartz + melt. It represents a large esavariant field (F = 10 – 6 + 2 = 6) in the middle of the P-T pseudosection (see discussion below).

5.2.3 REMOVING KYANITE FROM THE BULK COMPOSITION

Considering the microstructural observations performed on sample LY4f, it stands out that the rock that we observed is equilibrated in the sillimanite stability field. Kyanite, although abundant represents a relict phase from a previous metamorphic stage that is not testified by other phases in the rock.

In order to model the composition of the rock that actually was involved in the metamorphic reactions during attainment of peak conditions in the sillimanite stability field, I have removed the amount of kyanite present in the rock from the bulk composition. This procedure is often followed when refractory phases such as garnet, are observed in the rock (Stüwe, 1997). I have estimated on the basis of visual observation of the thin section that kyanite constitutes about the 20% of the rock.

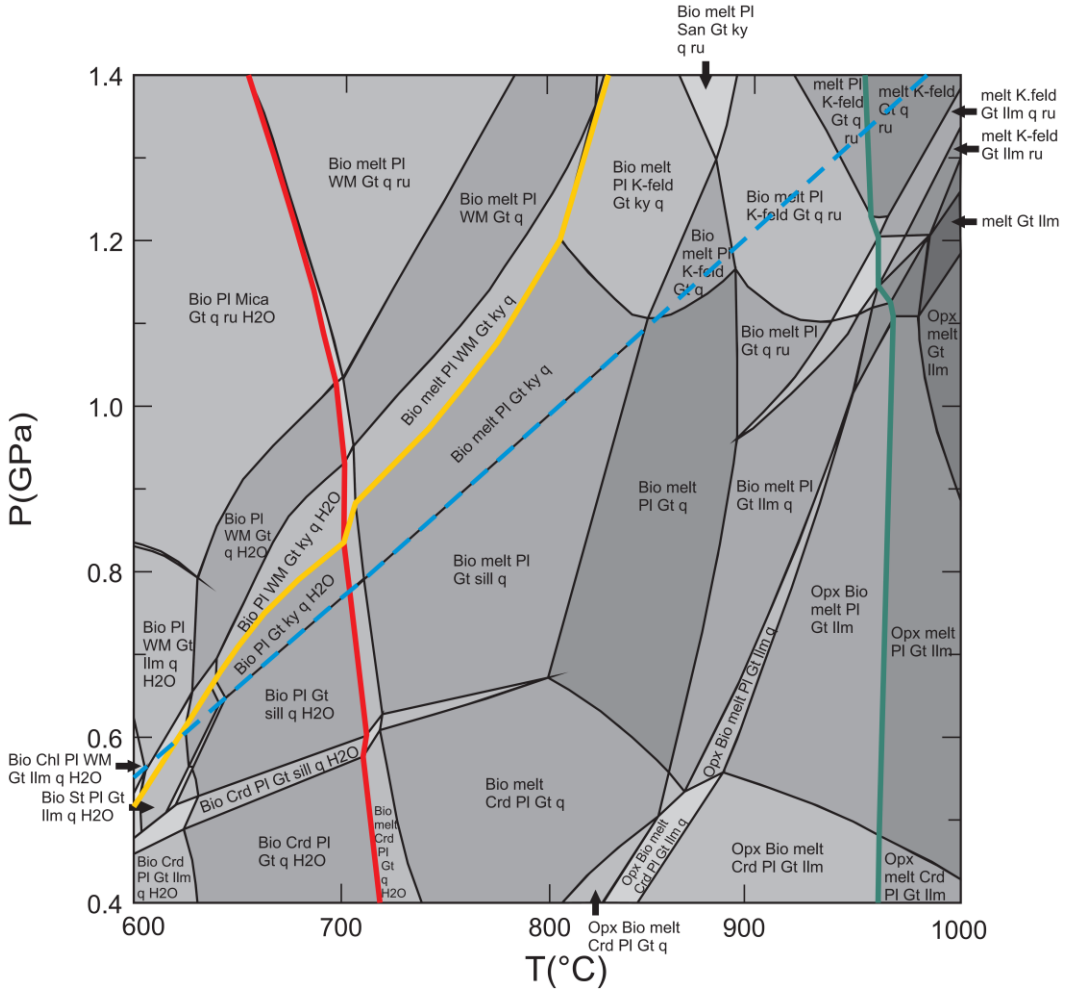

Figure 5.3 P-T pseudosection calculated removing kyanite from the bulk composition, so that the new composition is in mol% MnO = 0.16 Na_2O = 1.69 CaO = 2.51 K_2O = 2.58 FeO = 7.40 MgO = 6.78 Al_2O_3 = 10.59 SiO_2 = 58.41 TiO_2 = 0.80 H_2O = 7.86. The solidus is highlighed with the red line, white mica and biotite- out curves are highlighted respectively in yellow and green. The extension of the Ky-Sill polymorphic transition is outlined with the dashed blue line for clarity as in figure 5.2.

The pseudosection calculated removing 20% kyanite from the bulk composition is reported in figure 5.3. The first predictable effect of this operation is that the stability field of the Al_2SiO_5 polymorphs is restricted with respect to the bulk composition model (figure 5.4).

The solidus moves towards slightly higher temperatures (20°); the biotite-out curve has the same behavior. The peak mineral assemblage field is more restricted with respect to the previous model, since sillimanite melts out at lower temperature. It ranges between about 700° and 850° in temperature and about 0.6

and 1.1 GPa in pressure.

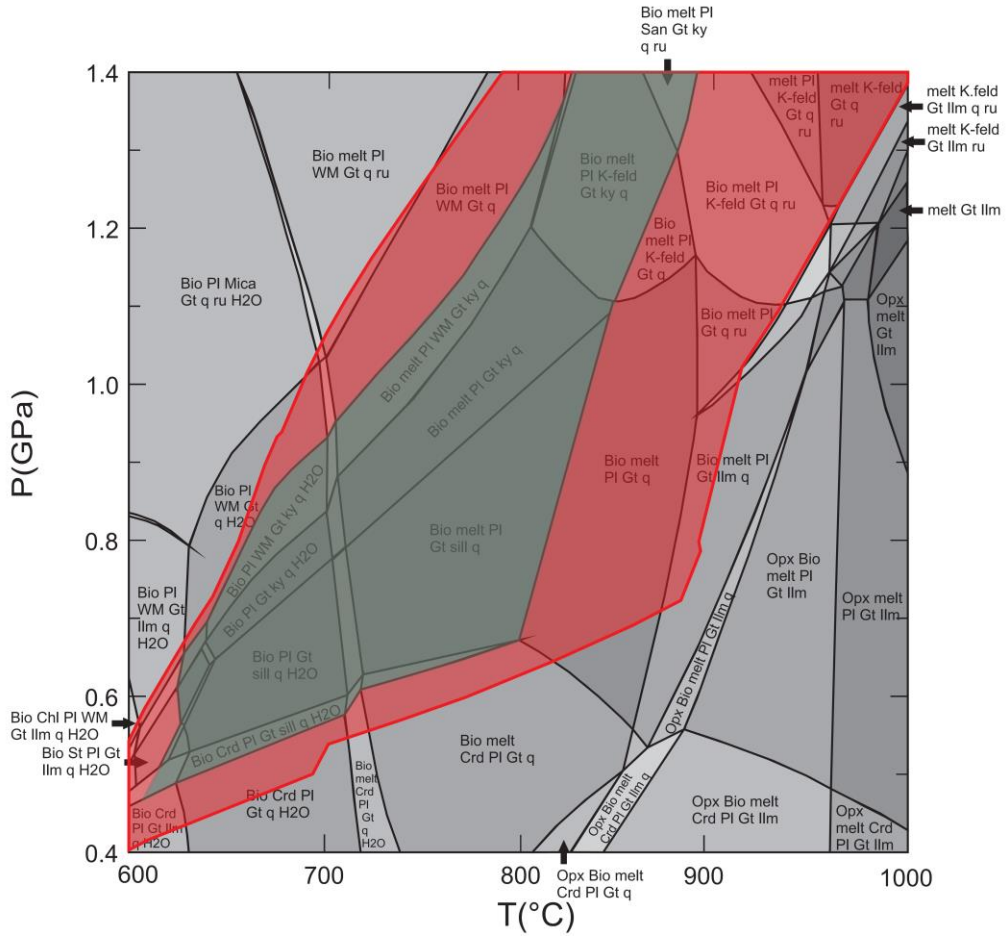

Figure 5.4 Comparison of modelled Al_2SiO_5 stability in the two pseudosections of figure 5.2 and figure 5.3. The red transparent field represents the Al_2SiO_5 bearing conditions for the bulk composition, whereas the green field represents the Al_2SiO_5-bearing stability field removing kyanite from the bulk composition as in figure 5.3.

5.2.4 P-T CONSTRAINTS OF THE METAMORPHIC EVENTS

As noted in the previous sections, the peak mineral assemblage biotite + garnet + sillimanite + plagioclase + quartz + melt is stable over a quite large P-T field.

In order to constrain more precisely the P-T field of equilibration recorded by sample LY4f, thermodynamic calculations allow to monitor the composition of solid solution phases by plotting curves of equal composition (isopleths) onto the pseudosection fields. The modelled compositions can thus be compared, also graphically, with the actual compositions of solutions measured by EMP and SEM. In this phase, I have considered the chemical composition of the solid

solutions phases such as biotite, garnet and plagioclase.

In order to constrain temperature, I have considered the X_{Mg} -value of biotite and garnet and the Ti content (a.p.f.u.) in biotite, since such parameters are more sensitive to temperature. X_{Mg} of biotite and garnet vary as a function of the continuous Fe-Mg exchange.

Biotite + sillimanite + plagioclase + quartz = garnet + liquid

As temperature rises, this reaction involves a continuous change of biotite and garnet composition, since the X_{Mg} value of both minerals increases (see also paragraph 1.3). As temperature lowers the reaction proceeds towards the opposite direction, so that the X_{Mg} value of garnet and biotite decreases (see also paragraph 4.3).

In order to constrain pressure, I have considered the grossular and anorthite content in garnet and plagioclase. Grossular and anorthite changes occurs because of the reaction

Anorthite = grossular + Al_2SiO_5 + quartz

which is a very common barometer in high grade metapelites, also called GASP (Winter, 2014).

The main metamorphic event is recorded by the core of large and inclusions-rich garnet porphyroblasts, by biotite and fibrolite inclusions inside garnet porphyroblasts. Garnet core is characterized by an XMg equal to 0.28-0.30 and grossular content of 0.06-0.07. Biotite inclusions inside garnet are characterized by XMg of 0.60. The calculated isopleths showing such values identify a region in the diagram, conciding with the phase field biotite + garnet + plagioclase + sillimanite + quartz + melt, which can be interpreted as the equilibration conditions for the peak mineral assemblage observed in the sample. The temperature and the pressure obtained are respectively 800$\pm$30° and 8.5$\pm$0.07GPa (figure 5.5 (a)). Also Plagioclase should be considered but the isopleth An = 40 plots outside the stability field of sillimanite. This suggests that plagioclase underwent a complete re-equilibration during the retrograde path. The

Ti content in biotite is not considered as well because such parameter is not compatible with the P-T conditions estimated above. The Ti measured in biotite inclusions is 0.10 a.p.f.u., whereas the value expected should be 0.21. Thermodynamic modelling also allows to constrain a last metamorphic stage occurring during the retrograde path, by using compositions of the rim of garnet porphyroblasts, of biotite flakes inside the matrix and of plagioclase crystals, which appear to have completely re-equilibrated their composition to the retrograde pressure and temperature conditions. The rim of garnet porphyroblasts is characterized by an X_{Mg} value of 0.20 and the grossular content is 0.11-0.13.

The X_{Mg} value of biotite flakes is 0.54-0-56 and the Ti content is 0.15 a.p.f.u. The anorthite of plagioclase is 0.39-0-41. The intersection of isopleths defines a relatively narrow P-T area which overlaps several small phase fields, including

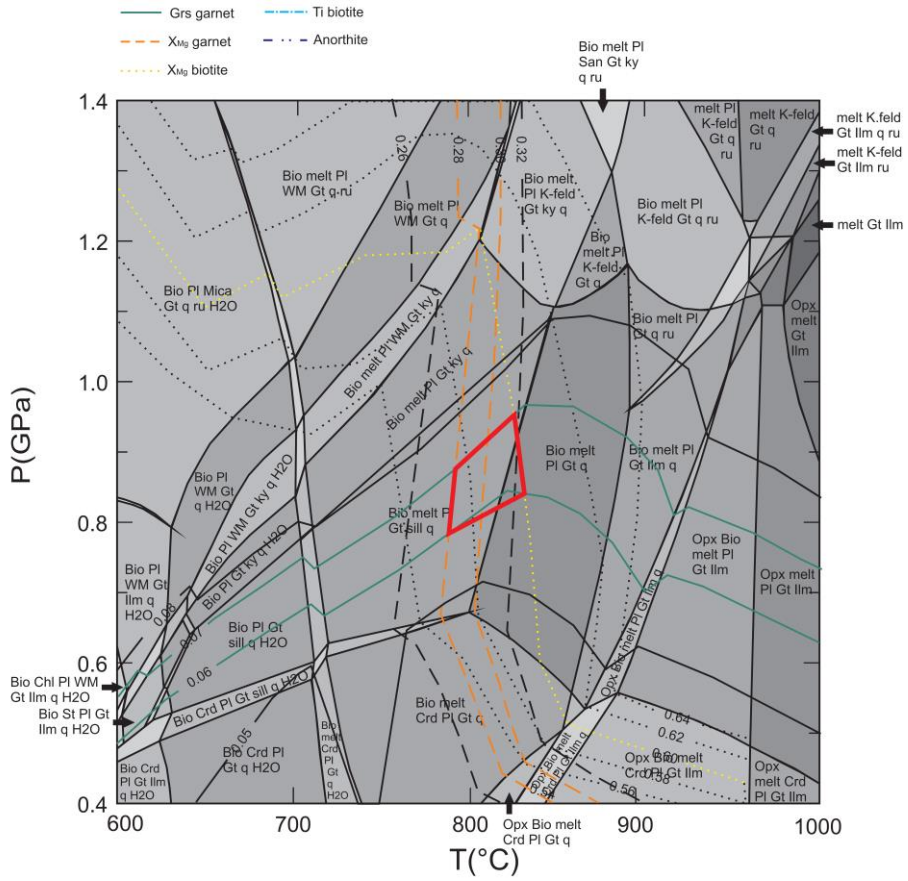

Figure 5.5 a) Contours for grossular, X_{Mg} value of garnet and X_{Mg} value of biotite. The inferred temperature and pressure conditions of the peak metamorphic event are highlighted with the red polygon. The mineral assemblage identified by the isopleths is biotite + garnet + plagioclase + sillimanite + quartz + melt.

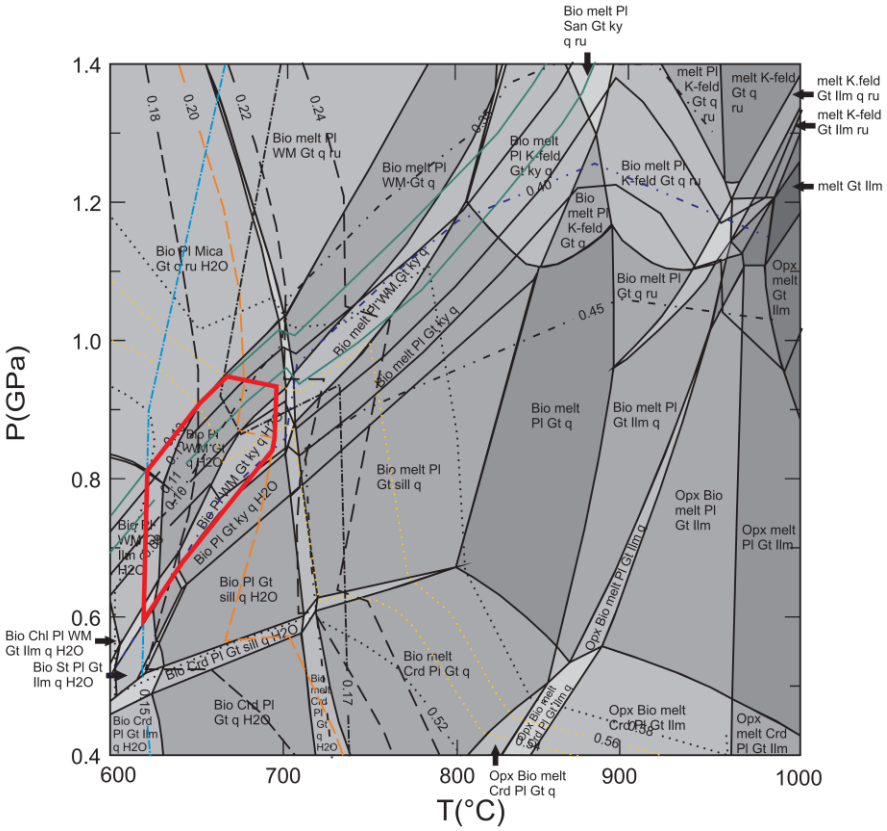

Figure 5.5 b) Contours for grossular, X_{Mg} value of garnet, X_{Mg} value of biotite, Ti in biotite and anorthite in plagioclase, The inferred temperature and pressure conditions of the retrograde metamorphism are highlighted with the red polygon. The mineral assemblage identified by the isopleths is biotite + garnet + plagioclase + white mica + quartz + H_2O.

also the field biotite + white mica + garnet + plagioclase + quartz + H_2O. Also this result is consistent with the observation of the natural sample. The temperature and the pressure obtained are respectively 650±30° and 0.77±1.8 GPa. Note, here and below, that P-T estimates are provided with uncertainties that represent the range of values determined graphically. These uncertainties are accompanied by the error intrinsic in the calculation that is generally considered to be at least ±50° and ±0.1 GPa.

5.2.5 P-T PATH OF SAMPLE LY4f

On the basis of the P-T constraints provided by comparing measured and modelled compositions of the solid solution phases, it is possible to infer the P-T

path that sample LY4f experienced. Figure 5.6 shows the three main metamorphic

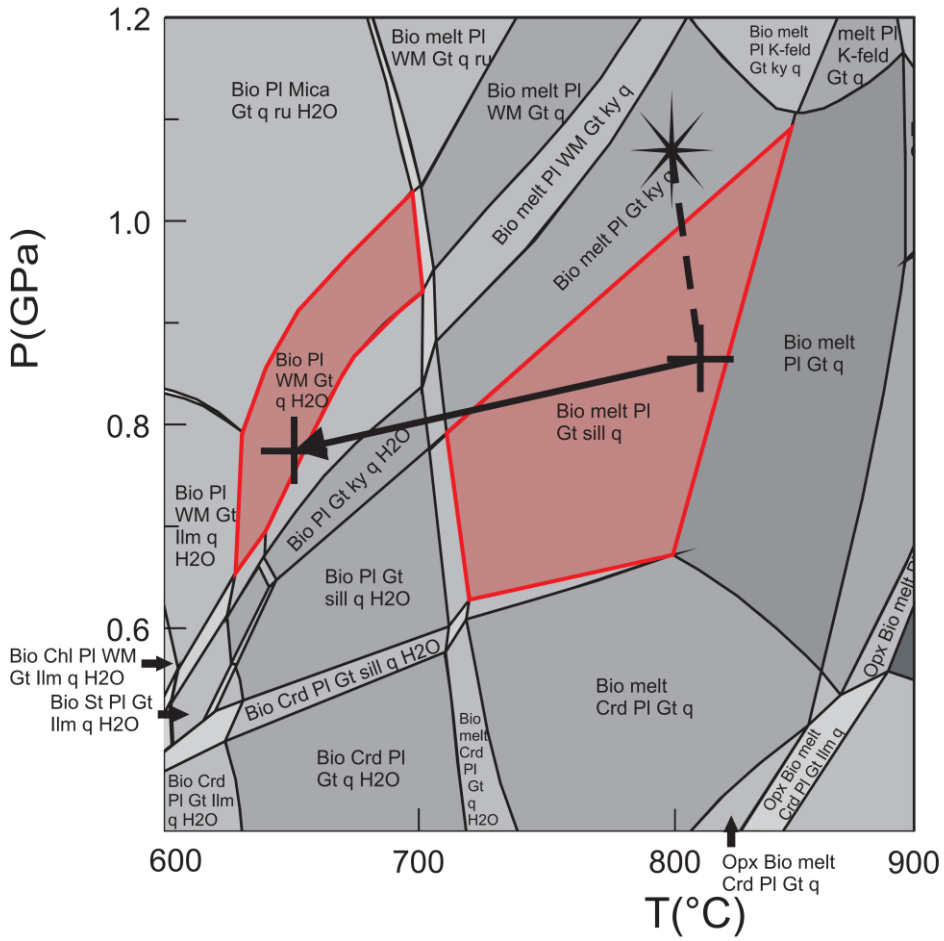

Figure 5.6 P-T section illustrating the inferred P-T path that sample LY4f experienced during the Caledonian orogeny. The fields of the peak mineral assemblage and of the mineral assemblage after the retrogression are highlighted in red.

stages recorded by the rock. The first event is marked by the asterisk and the trajectory to reach the following metamorphic stage is marked by the dashed line. The temperature and pressure conditions of the peak mineral assemblage and of the retrograde assemblage are marked with the black crosses, whereas the trajectory of the retrograde path is marked by the black bold arrow. I have decided to mark the first metamorphic event and the follwing trajectory with different annotations, since the location of these latter cannot be constrained with the studied samples nor is available from the literature. It should therefore be considered as hypothetical.

However, it is possible to affirm that the rock initially experienced an high

pressure and high temperature melt bearing event in the stability field of kyanite, followed by another high temperature melt-bearing event in the stability field of sillimanite, constrained at 800±30° and 8.5±0.07 GPa. Afterwards, the rock followed a retrograde trajectory and the temperature deacreased down to 650°. Along the retrograde path, the pressure variaton was not relevant, since the pressure decrease was less than 0.1 GPa.

5.2.6 T-Vol% DIAGRAM FOR THE RETROGRADE PATH

In order to figure out the reactions which characterize the retrograde path, a diagram that models the variation of the volume percantage of the phase involved has been calculated (figure 5.7). The diagram is calculated removing kyanite from the bulk composition, that is the same approch used for the models considered above.

The trend of the modal proportions of the phases (vol%) is significative, because it helps to figure out what reactions are taking place along the retrograde path. Such reactions are discussed in detail in the next paragraph.

The diagram in figure 5.7 shows that the amount of liquid gradually decreases as temperature lowers. Once it is completely crystallizzed, at about 700°, it releases the water that has not been consumed by the crystallization of biotite.

5.2.7 METAMORPHIC/ANATECTIC REACTIONS OF SAMPLE LY4f

As suggested by the presence of kyanite in the leucosome, partial melting took place also in the stability field of kyanite. Therefore the reaction

Kyanite = sillimanite (1)

occurred during a decompressive stage of the P-T path, that is represented by the dashed line in figure 5.6.

The reaction responsible for the microstructures which represent the peak metamorphic event is probably

Biotite + sillimanite + plagioclase + quartz = garnet + liquid (2)

This is probably a continuous reaction, as attested by the large multivariant field

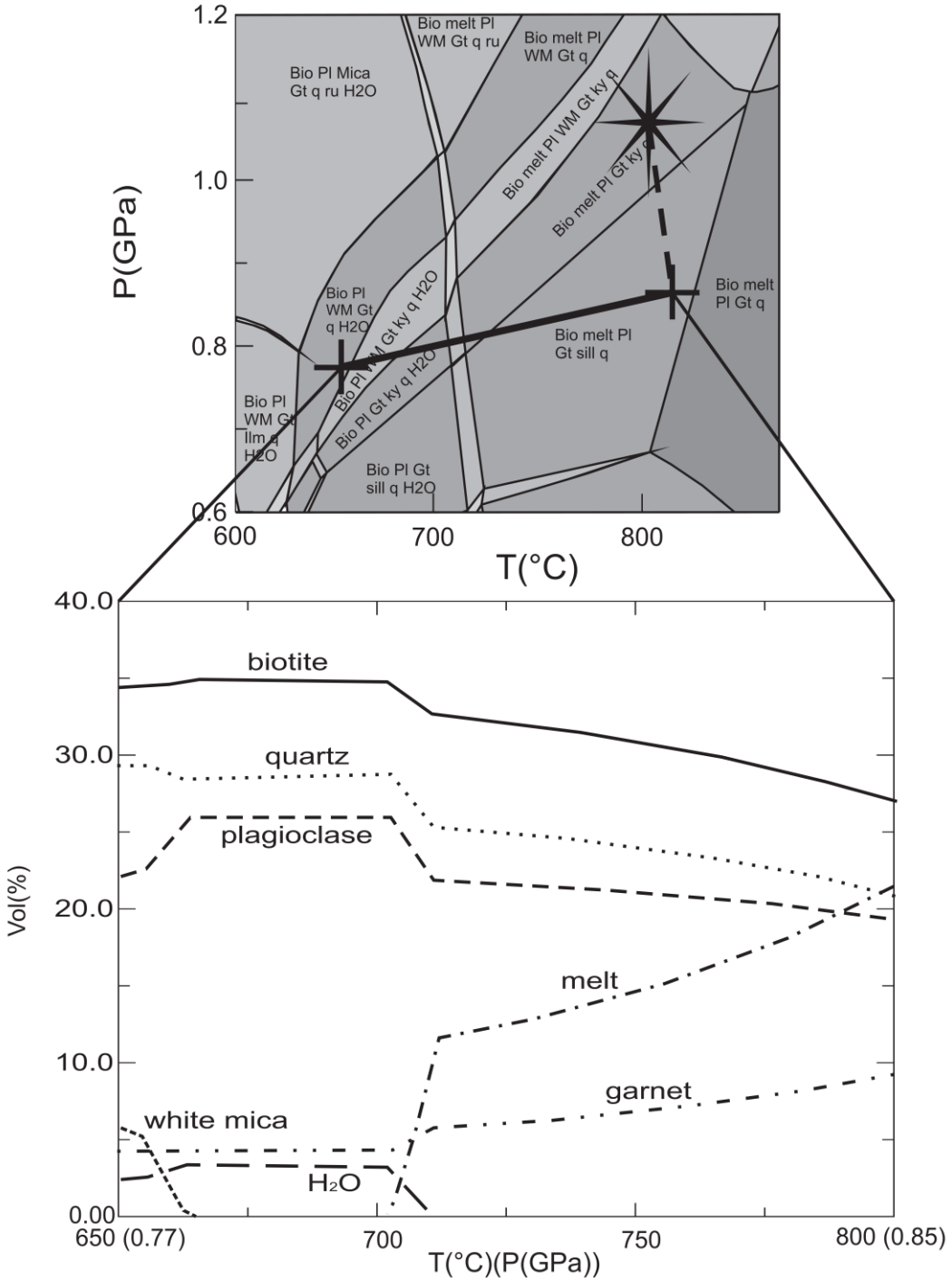

Figure 5.7 T-Vol% diagram considering the composition of LY4f removing removing kyanite from the bulk composition calculated in mol% MnO = 0.16 Na_2O = 1.69 CaO = 2.51 K_2O = 2.58 FeO = 7.40 MgO = 6.78 Al_2O_3 = 10.59 SiO_2 = 58.41 TiO_2 = 0.80 H_2O = 7.86. The pressure varies from 0.85 GPa to 0.77 GPa as a linear function of the temperature.

of the assemblage in P-T space. As reaction (2) proceeds the stable mineral assemblage becomes biotite + sillimanite + plagioclase + quartz + garnet + liquid. The newly-formed garnet is characterized by euhedral faces and it grows at the expense of biotite and sillimanite. During the growth stage, garnet entraps biotite, fibrolite and quartz crystals. The result of this process is the formation of euhedral-shape garnet porphyroblasts, characterized by biotite, sillimanite and quartz inclusions (figure 5.8).

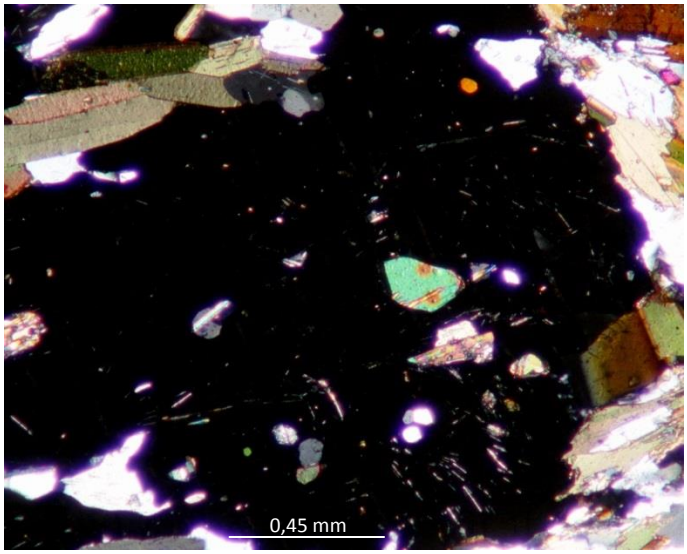

Figure 5.8 Garnet porphyroblasts produced by reaction (1). It is possible to notice that garnet is characterized by biotite, fibrolite and quartz inclusions. The fibrolite inclusions are dispersed throughout the whole crystal.

The garnet produced by this reaction is expected to be characterized also by increasing X_{Mg} towards the rim. However, the rock probably remained at high temperature conditions for enough time, for diffusion to erase the preexisting chemical profile, and to homogenize the original crystals zoning.

The water released by the dehydration of biotite dissolves into the liquid. At the peak metamorphic conditions, the volume of melt generated is roughly 22%.

On the cooling path, the melt begins to crystallize and it releases water, which becomes available for the crystallization of the hydrous minearals. The first mineral to crystallize from the melt is plagioclase and it is characterized by

euhedral grains, surrounded by growth faces, whereas quartz crystallizes later (figure 5.9).

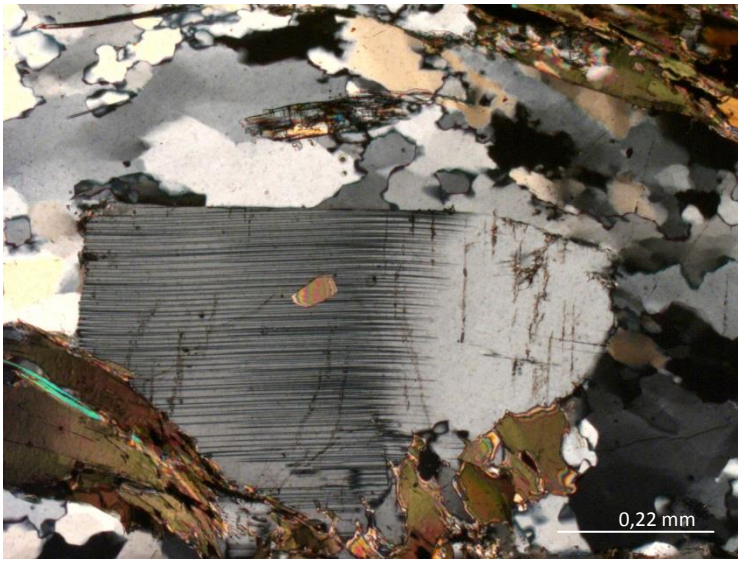

Figure 5.9 Leucosome in sample LY4f. Plagioclase grain, characterized by euhedral faces and surrounded by quartz and biotite, indicate crystallization from melt.

As temperature decreases, reaction (2) proceeds towards the opposite direction. The crystallized melt provides an internal source of water and reaction (3) on the retrograde path becomes

Garnet + liquid = biotite + sillimanite + plagioclase + quartz (3)

Garnet is progressively consumed, while biotite and sillimanite are produced. Part of the sillimanite crystallizes also in the leucosome. Biotite grows along the foliation planes and it forms large flakes (see also paragraph 3.1). When biotite is in contact with garnet, it forms the typical microstructure produced by reaction (3), where biotite partially replaces garnet (figure 5.10). The diagram in figure 5.7 shows that as the temperature lowers, garnet modal proportion decreases, whereas the modal proportions of biotite, plagioclase and quartz increase.

Biotite and garnet become Fe-richer and garnet in particular is characterized by decreasing X_{Mg} values towards the rim.

At about 700° the melt is completely crystallized and it releases the water that has

not been exhausted by the formation of the hydrate phases. As temperature further decreases retrograde white mica is also produced as a result of the reaction

Biotite + plagioclase + sillimanite + H2O = muscovite + quartz (4)

White mica is dispersed inside the matrix and it is typically associated with biotite. Note in figure 5.7 that white mica starts to form at about 670° and while it is produced, quartz volume % increases, whereas biotite and plagioclase volume % decreases.

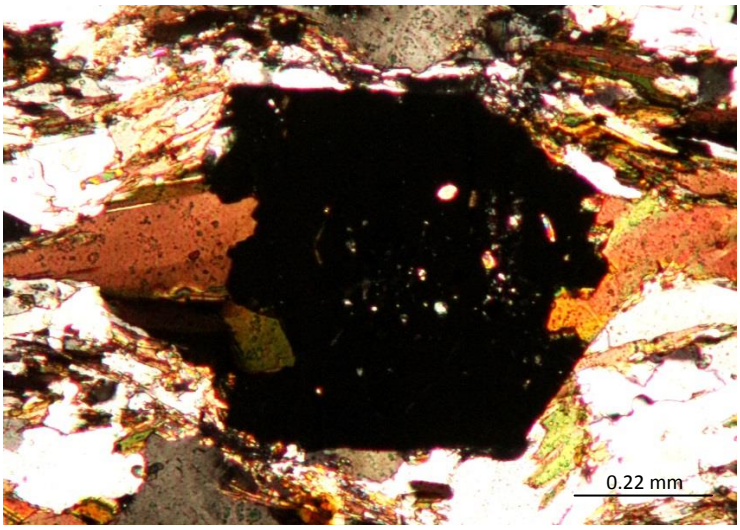

Figure 5.10 Biotite overgrowth on garnet. The garnet grain grown during the prograde melting reactions is later consumed during retrograde metamorphism.

The final product is a rock characterized by abundant biotite, plagioclase and quartz, retrograde white mica, partially resorbed garnet, sillimanite, crystallized melt and relict of kyanite porphyroblasts.

5.3 PHASE EQUILIBRIA MODELLING FOR SAMPLE LY131

5.3.1 T-X_{H2O} MODELLING

In order to model sample LY131, I have used the same approach, taken for sample LY4f. I have considered the composition obtained from the X-ray fluorescence

analyses for all the major oxides except for H_2O, given the dependence of the mineral assemblages on the amount water present in the system. As for sample LY4f the T-H_2O isobaric pseudosection is calculated for a water content varies from 0 to the value that corresponds to the loss of ignition (1.64 wt%). I have set the amount of water at 2.5 mol% (0,90 wt%), in order for the mineral assemblage observed in the rock (biotite + garnet + sillimanite + K-feldspar + plagioclase + melt) to be stable. At this condition the sub-solidus assemblage is water undersaturated, indicating that the melting reactions are fluid-absent. The only source of water are the hydrate phases, such as biotite and white mica; the water produced from biotite and white mica breakdown dissolves into the liquid without the formation of a vapor phase (Vielzeuf and Holloway, 1988).

5.3.2 P-T MODELLING

The P-T pseudosection for sample LY131, calculated in the MnNCaKFMASHT system, is reported in figure 5.11. I have considered all the phases which potentially may crystallize for the quartzo-felspathic composition at the temperature and pressure of interest, such as biotite, garnet, white mica, plagioclase, quartz, sillimanite, kyanite, K-feldspar, chlorite, staurolite, cordierite, orthopyroxene, ilmenite, rutile and the melt phase. Water is absent in all the sub-solidus assemblages except in three fields located in the low pressure and low temperature part of the diagram. The solidus (red line) has the opposite behavior with respect to previous sample, since the temperature of the solidus increases as the pressure rises. This is due to the fluid absent nature of the solidus, which has a positive slope.

The intersection between the white mica-out curve (yellow line) and the solidus occurs at about 0.8 GPa and 650°. The temperature of biotite-out curve decreases as pressure drops, so that at high pressure biotite is completely consumed at about 920°, whereas at 0.4 GPa biotite is exhausted at 850°.

Biotite breakdown reaction is continuous and it takes place over a large temperature interval, because of the presence of Ti in the system. Biotite is initially consumed as a result of the reaction

Biotite + sillimanite + plagioclase + quartz = garnet + liquid

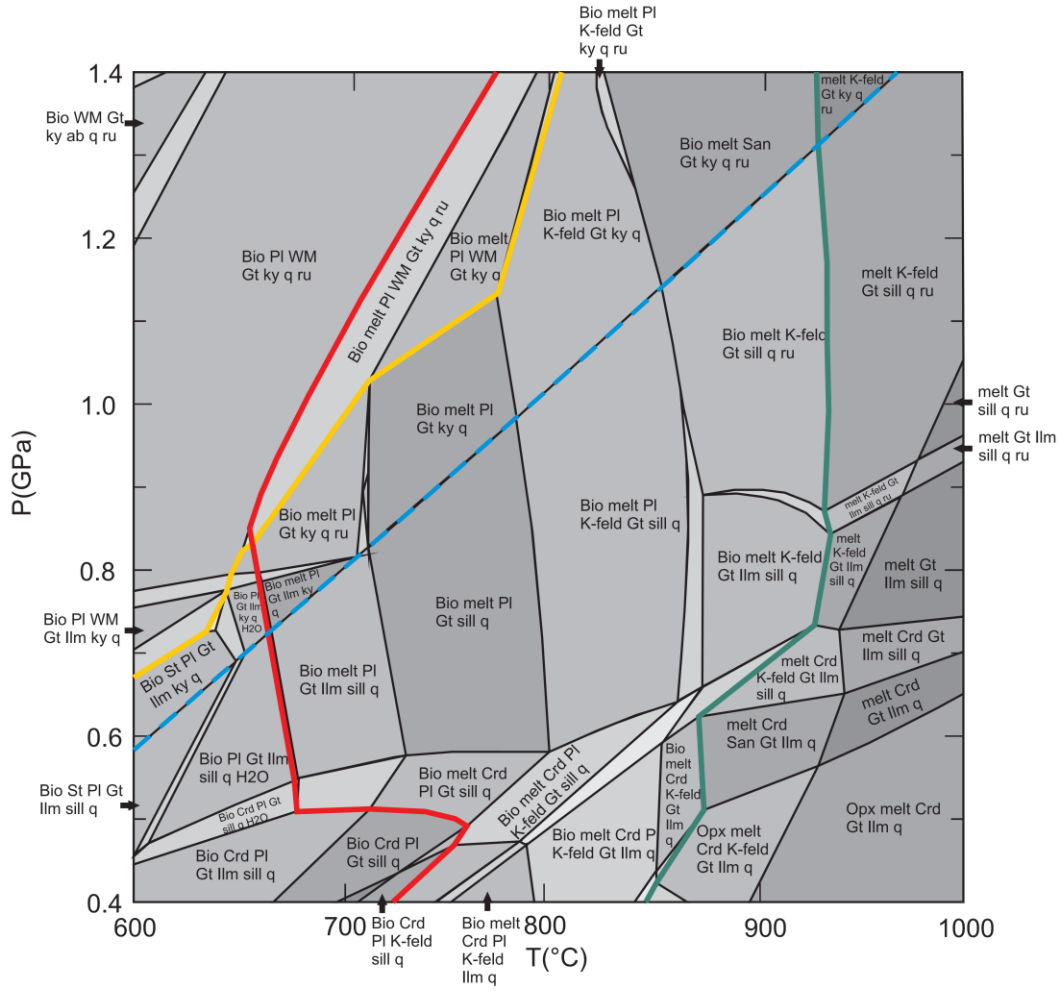

Figure 5.11 P-T pseudosection of sample LY131 calculated in mol% MnO = 0.06 Na_2O = 0.37 CaO = 0.23 K_2O = 1.42 FeO = 4.19 MgO = 3.24 Al_2O_3 = 6.70 SiO_2 = 77.60 TiO_2 = 0.61 H_2O = 2.50. The solidus is highlighed with the red line, white mica and biotite- out curves are highlighted respectively in yellow and green. The extension of the Al_2SiO_5 polymorphs reaction is extended with the dashed blue line for clarity.

nevertheless, at 800° K-feldspar starts to form, so that biotite breakdown reaction becomes

Biotite + sillimanite + plagioclase + quartz = garnet + K-feldspar + liquid

Staurolite appears in the low temperature and low pressure part of the diagram, whereas chlorite is not present at all. K-feldspar, differently from sample LY4f is

present throughout the whole pressure range.

The stable mineral assemblage at the peak conditions observed in the sample is biotite + garnet + sillimanite + plagioclase + K-feldspar + quartz + melt. It represents a large pentavariant field (F = 10 – 7 + 2 = 5) in the middle of the figure.

5.3.3 P-T CONSTRAINTS FOR THE METAMORPHIC EVENTS

In order to constrain the different metamorphic events recorded by sample LY131, I have considered the chemical composition of the solid solution phases such as biotite and garnet. The approach is the same as that used for sample LY4f.

The parameters used to constrain the temperature are X_{Mg} of garnet and biotite and Ti content in biotite, that are the same used for sample LY4f with the only exception that the reaction that relates the compositional variations of these minerals changes slightly because of the presence of K-feldspar:

Biotite + sillimanite + plagioclase + quartz = garnet + K-feldspar + liquid

In order to constrain pressure, I have considered the grossular content of garnet. Three main metamorphic events are detectable in the rock. The first one is represented by kyanite crystals wrapped up and partially replaced by fibrolite. This first event cannot be constrained since it is not testified by solid solution phases.

The peak metamorphic event is represented by the core of garnet porphyroblasts, by biotite flakes and fibrolite inclusions inside garnet porphyroblasts. Garnet core is characterized by an X_{Mg} equal to 0.23. Biotite flakes are characterize by X_{Mg} equal to 0.50 and a Ti content of 0.22 a.p.f.u.. The isopleths characterized by these values identify a region in the pseudosection that overlaps two mineral assemblages, such as biotite + garnet + plagioclase + sillimanite + quartz + melt and biotite + garnet + plagioclase + K-feldspar + sillimanite + quartz + melt. The second mineral assemblage corresponds to the peak assemblage observed in the sample, which contains also K-feldspar.

The temperature obtained is 790$\pm$10° (figure 5.12). The pressure of the peak

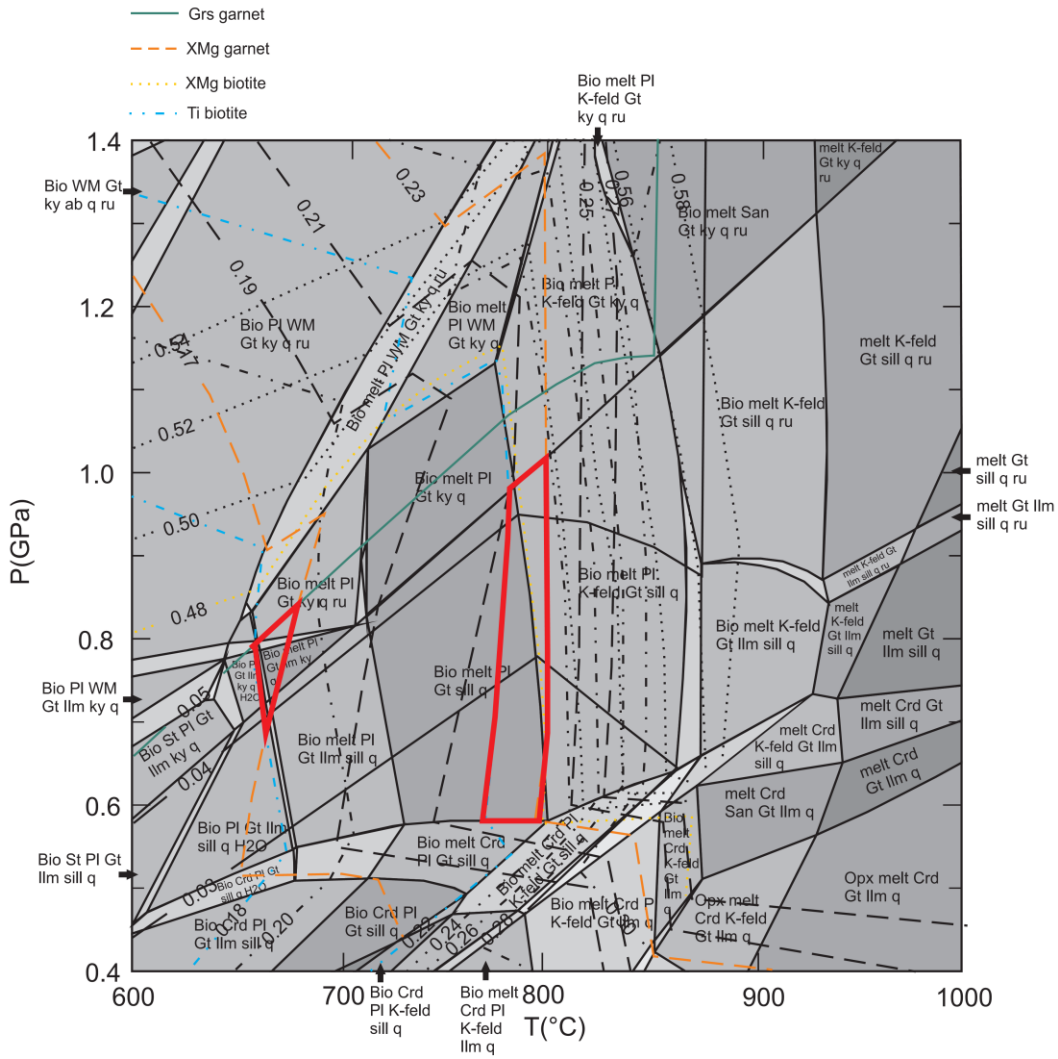

Figure 5.12 Contours for grossular, X_{Mg} value of garnet, X_{Mg} value of biotite and Ti content in biotite. The inferred temperature and pressure conditions of the peak and the retrograde metamorphic event are highlighted with the red polygons.

metamorphic event cannot be constrained, since grossular content of garnet appears to be completely riequilibrated to the retrograde conditions, even in the core of the largest crystals.

The last metamorphic stage is the result of the retrograde process. It is represented by the composition of the rim of garnet porphyroblasts, and by biotite in contact with garnet. The rim of garnet porphyroblasts is characterized by an X_{Mg} value of 0.17 and the grossular content is 0.05. The Ti content in biotite is 0.15 a.p.f.u. The X_{Mg} value of biotite is not considered, since it does not match which the other parameters (X_{Mg} = 0.54).

The isopleths form a polygon that overlaps several small assemblage fields. The low pressure tip of the red polygon overlaps a field characterized by the assemblage biotite + white mica + garnet + plagioclase + quartz + ilmenite. This is consistent with the retrograde mineral assemblage observed in the sample, except for ilmenite. However, the calculated modal proportion of ilmenite is 0.14%, therefore it can be neglected. The temperature and the pressure obtained are respectively 670±10° and 0.75±0.07 GPa.

5.3.4 P-T PATH OF SAMPLE LY131

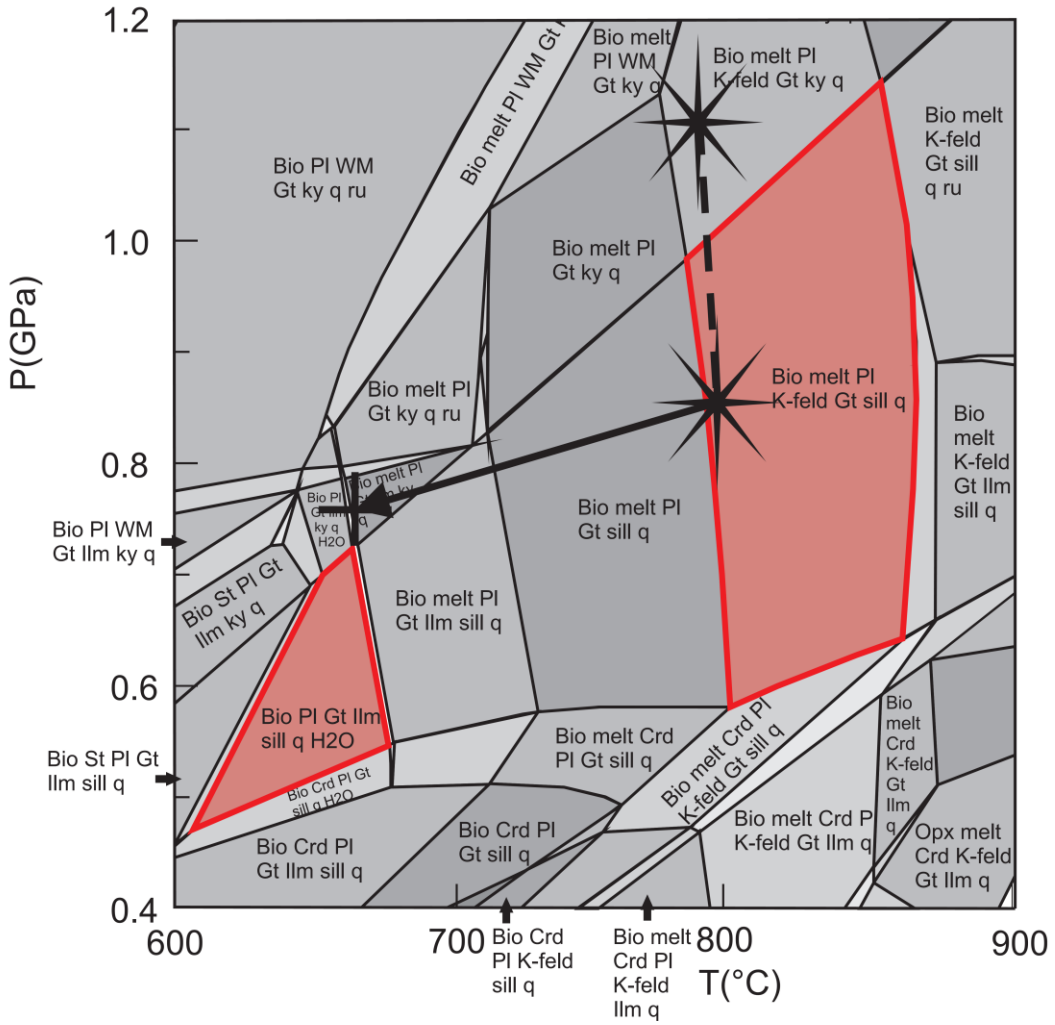

Figure 5.13 P-T section illustrating the inferred P-T path that sample LY131 experienced during the Caledonian orogeny. The fields of the peak mineral assemblage and of the mineral assemblage after the retrogression are highlighted in red.

Figure 5.13 reports the P-T path of sample LY131, inferred by means of the calculated contours of the composition of the solid solution phases.

The first and the second metamorphic events are marked by the asterisks and the trajectory that connects these latter is marked by the dashed line. The temperature and pressure conditions of the retrograde assemblage is marked with the black cross, whereas the trajectory of the retrograde path is marked by the black bold line. I have decided to mark the second metamorphic event like the first one, because it is not completely constrained since the pressure is uncertain.

Also sample LY131 initially experienced an high pressure and high temperature melt bearing event in the stability field of kyanite, followed by another high temperature melt-bearing event in the stability field of sillimanite, constrained at 790±10° and between 0.6 and 1 GPa. Afterwards, the rock followed a retrograde trajectory and the retrograde assemblage equilibrated at 670±10°C and 0.75±0.07 GPa.

5.3.5 METAMORPHIC/ANATECTIC REACTIONS OF SAMPLE LY131

The reaction responsible for the microstructures which represent the peak metamorphic event is the continuous reaction

Biotite + sillimanite + plagioclase + quartz = garnet + K-feldspar + liquid (5)

Once this reaction is crossed the stable mineral assemblage becomes biotite + sillimanite + plagioclase + quartz + garnet + K-feldspar + liquid. Reaction (5) involves the crystallization of K-feldspar porphyroblasts and euhedral garnet porphyroblasts characterized by biotite, quartz and sillimanite inclusions. The prograde garnet is likely to be characterized by increasing X_{Mg} values towards the rim, however, the permanence at high temperature conditions will cause the compositional zoning to be flattened. Very little liquid is produced, since at the peak metamorphic conditions it constitutes the 3% of the rock.

On the cooling path, the liquid begins to crystallize and it releases water. Reaction (5) is crossed towards the opposite direction and becomes

Garnet + K-feldspar + liquid = biotite + sillimanite + plagioclase + quartz (6)

Garnet is continuously replaced by biotite and sillimanite and it is characterized by decreasing X_{Mg} values towards the rim (figure 5.14).

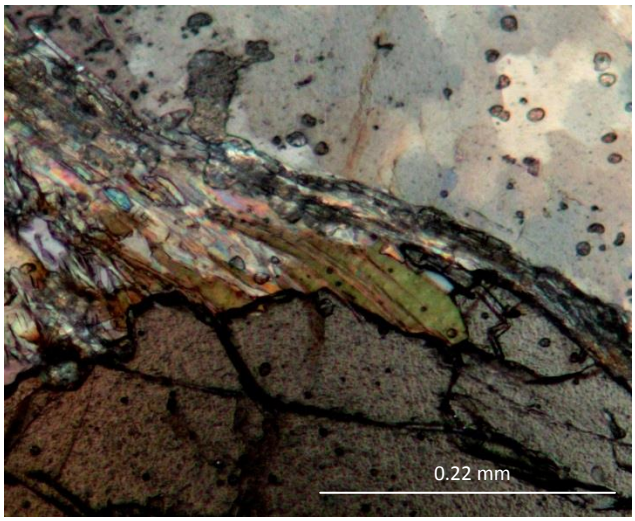

Figure 5.14 Garnet partially resorbed by biotite and fibrolite.

An abundant amount of sillimanite is produced along the foliation during this phase, since it constitutes roughly the 6-7% of the rock.
As cooling continues, K-feldspar is consumed in the production of late muscovite as a result of the reaction

K-feldspar + sillimanite + H_2O = muscovite + quartz (7)

The final product is a rock formed for the major part by recrystallized quartz, biotite, very little plagioclase, retrograde white mica, partially resorbed garnet and K-feldspar porphyroblasts, relatively abundant sillimanite, films of crystallized melt and partially replaced kyanite crystals.

CHAPTER 6

CONCLUSIONS

The characterization of the metamorphic events which the Nordmannwick nappe experienced during the Caledonian Orogeny was possible by means of the petrological study of two samples of migmatites (LY4f and LY131).

According to the microstructural observations, kyanite represents a relict phase, which crystallized before the sillimanite included in garnet porphyroblasts. Kyanite has never been observed as inclusions in garnet. A second generation of sillimanite crystallized during retrogression and it is located along the foliation.

The chemical analyses performed with the EMP and SEM pointed out that there is no chemical difference between the two types of garnet distinguished by the microstructural observation, therefore the garnets have similar zoning patterns and absolute values of element concentrations, and these features are compatible with a single episode of garnet growth.

The thermodynamic modelling applied to both samples allowed us to constrain quite satisfactorily the P-T conditions of equilibration of the peak anatectic assemblage in the sillimanite field, and the subsequent retrograde evolution during cooling and melt crystallization. In addition, we could figure out the metamorphic reactions and a sequence of three main metamorphic events (figure 6.1). Sample LY4f experienced a high temperature and high pressure metamorphic event, testified by the presence of kyanite porphyroblasts inside the matrix and inside the leucosome. This stage cannot be constrained thermobarometrically in the studied samples. The rock then followed a decompressive stage that led to the peak metamorphic event characterized by a stable mineral assemblage constituted by biotite + garnet + plagioclase + quartz + sillimanite + melt. The pressure and the temperature obtained are 0.85 ± 0.7 GPa and $800 \pm 30°$. Afterwards the rock followed a retrograde trajectory along which temperature and pressure decreased down to $650° \pm 30°$ and 0.77 ± 1.8 GPa The stable mineral assemblage after the

retrogression became biotite + garnet + plagioclase + quartz + sillimanite + white mica.

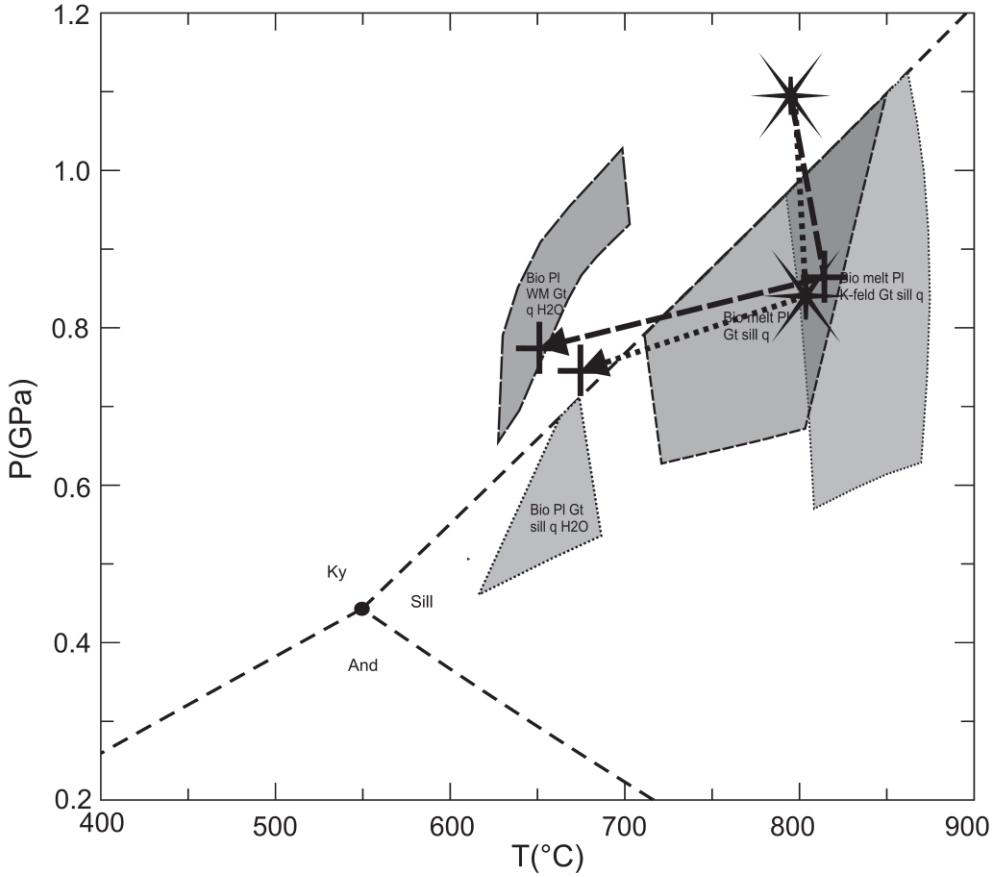

Figure 6.1 Schematic P-T section illustrating the P-T path inferred for sample LY4f and LY131. The trajectory and the mineral assemblage fields for sample LY4f are contoured with the dashed line, whereas the trajectory and the mineral assemblage fields for sample LY131 are contoured with the dotted line. The Al_2SiO_5 phase diagram calculated with Perple_X is added for clarity. The position of the high-pressure event is speculative, since its temperature and pressure are not constrained. Also the position of the peak metamorphic event of sample LY131 is not completely fixed since the pressure has not been constrained.

Also Sample LY131, collected not far from LY4f, experienced a similar evolution with a high pressure metamorphic phase, followed by a high temperature melt-bearing event. During this phase, the rock developed a stable mineral assemblage composed by biotite + garnet + plagioclase + K-feldspar + quartz + sillimanite +

leucocratic segregations. The estimated temperature is 790±10°, whereas the pressure has not been constrained because of the complete re-equilibration of garnet during retrogression. Along the retrograde path the rock equilibrated at 670°±10° and 0.75±0.07 GPa. The retrograde mineral assemblage is biotite + garnet + plagioclase + quartz + sillimanite + white mica.

Both of the studied samples underwent a peak metamorphic event and a retrograde path characterized by fairly the same temperature and pressure. The peak and the retrograde mineral assemblages are constituted by different phases because of the different bulk rock composition. The difference in melt production (22 vol% sample LY4f vs 3 vol% LY131) between the two samples is probably due to the compositional differences and the different amount of water present in the system.

The interpretations given by Nardini (2013) and Hibelot (2013) are not confirmed in this work. The fibrolite inclusions inside garnet porphyroblasts do not appear to represent a previous pre-Caledonian metamorphic event, but are here interpreted as post-dating kyanite along a clockwise P-T path (Fig. 6.1). This evolution could result single metamorphic cicle that took place during the emplacement of the Caledonian Orogen. However, it's useful to point out that if chronologically separate a high-temperature metamorphic event actually took place before the Caledonian orogeny, it could be difficult to constrain since the following high temperature melt-bearing event might have deleted its chemical and microstructural signature.

I conclude writing that I went through a lot of "problems" modelling these rocks. The major challenges were to make the models the more likely possible to the natural samples and to use the variations of the chemical composition of the minerals to reconstruct the P-T path. The diffusion that took place in the granulite facies and the retrograde process involved a significant variation in the composition of the solid solution phases. The chemical signature was certainly modified and it is likely that part of it was completely erased, making the reconstruction of the metamorphic history more uncertain. That is why dealing with high temperature metamorphic rocks represents a challenging task.

REFERENCES

Andréasson, P. 1994, "The Baltoscandian margin in Neoproterozoic-early Palaeozoic times. Some constraints on terrane derivation and accretion in the Arctic Scandinavian Caledonides", *Tectonophysics,* vol. 231, no. 1, pp. 1-32.

Andresen, A. 1988, "Caledonian terrains of Northern Norway and their characteristics", *trabahos de geologia,* vol. 17, pp. 103-117.

Andresen, A. & Steltenpohl, M.G. 1994, "Evidence for ophiolite obduction, terrane accretion and polyorogenic evolution of the north Scandinavian Caledonides", *Tectonophysics,* vol. 231, no. 1, pp. 59-70.

Bartoli, O., Tajčmanová, L., Cesare, B. & Acosta-Vigil, A. 2013, "Phase equilibria constraints on melting of stromatic migmatites from Ronda (S. Spain): insights on the formation of peritectic garnet", *Journal of Metamorphic Geology,* vol. 31, no. 7, pp. 775-789.

Cesare, B. 1995, "Graphite precipitation in C—O—H fluid inclusions: closed system compositional and density changes, and thermobarometric implications", *Contributions to Mineralogy and Petrology,* vol. 122, no. 1-2, pp. 25-33.

Coggon, R. & Holland, T. 2002, "Mixing properties of phengitic micas and revised garnet-phengite thermobarometers", *Journal of Metamorphic Geology,* vol. 20, no. 7, pp. 683-696.

Connolly, J. 2009, "The geodynamic equation of state: what and how", *Geochemistry, Geophysics, Geosystems,* vol. 10, no. 10.

Connolly, J. 1995, "Phase diagram methods for graphitic rocks and application to the system C− O− H− FeO− TiO2− SiO2", *Contributions to Mineralogy and Petrology,* vol. 119, no. 1, pp. 94-116.

Connolly, J. & Petrini, K. 2002, "An automated strategy for calculation of phase diagram sections and retrieval of rock properties as a function of physical conditions", *Journal of Metamorphic Geology,* vol. 20, no. 7, pp. 697-708.

Ganguly, J., Cheng, W. & Tirone, M. 1996, "Thermodynamics of aluminosilicate garnet solid solution: new experimental data, an optimized model, and thermometric applications", *Contributions to Mineralogy and Petrology,* vol. 126, no. 1-2, pp. 137-151.

Gromet, L.P., Haskin, L.A., Korotev, R.L. & Dymek, R.F. 1984, "The "North American shale composite": its compilation, major and trace element characteristics", *Geochimica et Cosmochimica Acta,* vol. 48, no. 12, pp. 2469-2482.

Hacker, B.R., Kelemen, P.B. & Behn, M.D. 2011, "Differentiation of the continental crust by relamination", *Earth and Planetary Science Letters,* vol. 307, no. 3, pp. 501-516.

Hibelot, T. 2013, "Relationships between deformation and metamorphism in the Normannwick nappe, south of Lyngseidet: a focus on high grade relicts", *Msc Thesis.*

Holness, M.B., Cesare, B. & Sawyer, E.W. 2011, "Melted rocks under the microscope: microstructures and their interpretation", *Elements,* vol. 7, no. 4, pp. 247-252.

Le Breton, N. & Thompson, A.B. 1988, "Fluid-absent (dehydration) melting of biotite in metapelites in the early stages of crustal 110nataxis", *Contributions to Mineralogy and Petrology,* vol. 99, no. 2, pp. 226-237.

Nardini, L. 2013, "Metamorphic evolution and relationships between deformation and 110nataxis110ism in the Nordmannwick nappe in Lyngenfjord area, north of Lyngseidet", *MsC Thesis*.

Passchier, C.W. & Trouw, R.A. 1996, *Microtectonics,* Springer.

Powell, R. & Holland, T. 1999, "Relating formulations of the thermodynamics of mineral solid solutions: activity modeling of pyroxenes, amphiboles, and micas", *American Mineralogist,* vol. 84, pp. 1-14.

Powell, R., Holland, T. & Worley, B. 1998, "Calculating phase diagrams involving solid solutions via non-linear equations, with examples using THERMOCALC", *Journal of Metamorphic Geology,* vol. 16, no. 4, pp. 577-588.

Roberts, D. 2003, "The Scandinavian Caledonides: event chronology, palaeogeographic settings and likely modern analogues", *Tectonophysics,* vol. 365, no. 1, pp. 283-299.

Rosenberg, C. & Handy, M. 2005, "Experimental deformation of partially melted granite revisited: implications for the continental crust", *Journal of Metamorphic Geology,* vol. 23, no. 1, pp. 19-28.

Sawyer, E.W., Cesare, B. & Brown, M. 2011, "When the continental crust melts", *Elements,* vol. 7, no. 4, pp. 229-234.

Spear, F.S. 1995, *Metamorphic phase equilibria and pressure-temperature-time paths*, Mineralogical Society of America Washington.

Spear, F.S., Kohn, M.J. & Cheney, J.T. 1999, "P-T paths from anatectic pelites", *Contributions to Mineralogy and Petrology,* vol. 134, no. 1, pp. 17-32.

Stüwe, K. 1997, "Effective bulk composition changes due to cooling: a model predicting complexities in retrograde reaction textures", *Contributions to Mineralogy and Petrology,* vol. 129, no. 1, pp. 43-52.

Tajčmanová, L., Connolly, J. & Cesare, B. 2009, "A thermodynamic model for titanium and ferric iron solution in biotite", *Journal of Metamorphic Geology,* vol. 27, no. 2, pp. 153-165.

Thompson, A.B. & Algor, J.R. 1977, "Model systems for 111nataxis of pelitic rocks", *Contributions to Mineralogy and Petrology,* vol. 63, no. 3, pp. 247-269.

Thompson, J. & Hovis, G.L. 1979, "Entropy of mixing in sanidine", .

Tischendorf, G., Rieder, M., Förster, H., Gottesmann, B. & Guidotti, C.V. 2004, "A new graphical presentation and subdivision of potassium micas", *Mineralogical Magazine,* vol. 68, no. 4, pp. 649-667.

Tuccillo, M., Essene, E. & Van Der Pluijm, B. 1990, "Growth and retrograde zoning in garnets from high-grade, metapelites: Implications for pressure-temperature paths", *Geology,* vol. 18, no. 9, pp. 839-842.

Vielzeuf, D. & Holloway, J.R. 1988, "Experimental determination of the fluid-absent melting relations in the pelitic system", *Contributions to Mineralogy and Petrology,* vol. 98, no. 3, pp. 257-276.

White, R.W., Stevens, G. & Johnson, T.E. 2011, "Is the crucible reproducible? Reconciling melting experiments with thermodynamic calculations", *Elements,* vol. 7, no. 4, pp. 241-246.

White, R., Powell, R. & Holland, T. 2007, "Progress relating to calculation of partial melting equilibria for metapelites", *Journal of Metamorphic Geology,* vol. 25, no. 5, pp. 511-527.

White, R., Powell, R. & Holland, T. 2001, "Calculation of partial melting equilibria in the system Na_2O–CaO–K_2O–FeO–MgO–$Al2O_3$–SiO_2–H_2O (NCKFMASH)", *Journal of Metamorphic Geology,* vol. 19, no. 2, pp. 139-153.

White, R., Powell, R., Holland, T. & Worley, B. 2000, "The effect of TiO_2 and Fe_2O_3 on metapelitic assemblages at greenschist and amphibolite facies conditions: mineral equilibria calculations in the system K_2O-FeO-MgO-Al_2O_3-

SiO_2-H_2O-TiO_2-Fe_2O_3", *Journal of Metamorphic Geology,* vol. 18, no. 5, pp. 497-512.

Winter, J.D. 2014, *Principles of igneous and metamorphic petrology,* Pearson.

APPENDIX

MICROCHEMICAL DATA

LY4f chemical composition of the mineral phases (garnet, biotite, plagioclase)

GARNET 1

	rim											core	
Na_2O	0.01	0.03	0.03	0.00	0.00	0.00	0.00	0.00	0.00	0.00	0.01	0.00	0.05
MgO	5.55	5.73	5.89	5.91	6.98	7.10	6.66	6.65	6.59	6.29	6.47	6.25	6.62
Al_2O_3	21.57	21.54	21.49	21.36	21.88	21.36	21.47	21.69	21.57	21.45	21.64	21.63	21.80
SiO_2	37.59	37.57	37.59	37.44	38.02	37.44	37.43	37.91	37.38	37.27	37.66	37.67	37.45
K2O	0.00	0.00	0.00	0.00	0.04	0.00	0.01	0.00	0.04	0.00	0.00	0.01	0.03
CaO	3.58	3.41	3.05	2.89	2.25	2.22	2.46	2.35	2.71	2.42	2.47	2.61	2.36
TiO_2	0.02	0.00	0.01	0.03	0.00	0.02	0.02	0.00	0.00	0.03	0.04	0.00	0.01
Cr_2O_3	0.00	0.05	0.01	0.01	0.00	0.00	0.00	0.02	0.01	0.03	0.00	0.04	0.00
MnO	2.77	2.86	2.70	2.83	2.16	1.97	2.41	2.40	2.37	2.77	2.54	2.58	2.38
FeO	28.95	28.73	29.75	29.79	30.29	29.64	29.98	30.20	29.63	30.03	30.27	30.41	30.03
Total	100.04	99.92	100.52	100.27	101.62	99.74	100.44	101.22	100.31	100.30	101.11	101.20	100.73
Si	2.97	2.97	2.96	2.96	2.95	2.95	2.94	2.96	2.94	2.94	2.95	2.95	2.94
Ti	0.00	0.00	0.00	0.00	0.00	0.00	0.00	0.00	0.00	0.00	0.00	0.00	0.00
Al	2.01	2.00	1.99	1.99	2.00	1.99	1.99	1.99	2.00	2.00	1.99	1.99	2.01
Cr	0.00	0.00	0.00	0.00	0.00	0.00	0.00	0.00	0.00	0.00	0.00	0.00	0.00
Fe^{2+}	1.91	1.90	1.96	1.97	1.96	1.96	1.97	1.97	1.95	1.98	1.98	1.99	1.97
Mn^{2+}	0.19	0.19	0.18	0.19	0.14	0.13	0.16	0.16	0.16	0.19	0.17	0.17	0.16
Mg	0.65	0.67	0.69	0.70	0.81	0.83	0.78	0.77	0.77	0.74	0.75	0.73	0.77
Ca	0.30	0.29	0.26	0.24	0.19	0.19	0.21	0.20	0.23	0.21	0.21	0.22	0.20
Na	0.00	0.00	0.01	0.00	0.00	0.00	0.00	0.00	0.00	0.00	0.00	0.00	0.01
K	0.00	0.00	0.00	0.00	0.00	0.00	0.00	0.00	0.00	0.00	0.00	0.00	0.00
Tot	8.03	8.03	8.05	8.05	8.05	8.05	8.06	8.05	8.06	8.06	8.05	8.05	8.06
Alm	0.63	0.62	0.63	0.64	0.63	0.63	0.63	0.64	0.63	0.64	0.64	0.64	0.64
Pyp	0.21	0.22	0.22	0.22	0.26	0.27	0.25	0.25	0.25	0.24	0.24	0.23	0.25
Gros	0.10	0.09	0.08	0.08	0.06	0.06	0.07	0.06	0.07	0.07	0.07	0.07	0.06
Spes	0.06	0.06	0.06	0.06	0.05	0.04	0.05	0.05	0.05	0.06	0.05	0.05	0.05
X_{Fe}	0.75	0.74	0.74	0.74	0.71	0.70	0.72	0.72	0.72	0.73	0.72	0.73	0.72
X_{Mg}	0.25	0.26	0.26	0.26	0.29	0.30	0.28	0.28	0.28	0.27	0.28	0.27	0.28

	core										rim	
Na_2O	0.00	0.02	0.00	0.00	0.04	0.00	0.03	0.00	0.00	0.00	0.00	0.00
MgO	6.54	6.67	6.60	6.56	6.79	6.21	5.79	5.48	5.06	5.20	4.79	4.35
Al_2O_3	21.90	21.87	21.76	21.85	21.73	21.66	21.79	21.75	21.60	21.38	21.51	21.28
SiO_2	37.79	37.75	37.76	37.89	37.83	37.68	37.85	37.90	37.70	37.51	37.43	36.95
K2O	0.01	0.00	0.00	0.00	0.02	0.00	0.00	0.00	0.00	0.00	0.01	0.00
CaO	2.33	2.36	2.49	2.42	2.19	2.20	2.82	3.61	3.78	3.65	4.00	4.60
TiO_2	0.02	0.00	0.01	0.03	0.00	0.00	0.01	0.00	0.00	0.01	0.01	0.05
Cr_2O_3	0.00	0.02	0.03	0.00	0.03	0.00	0.05	0.02	0.01	0.03	0.03	0.00
MnO	2.56	2.41	2.49	2.42	2.45	2.76	2.96	2.91	2.88	2.83	2.82	2.76
FeO	30.33	30.44	29.89	30.11	30.71	30.15	30.37	30.18	30.25	29.85	30.16	30.15
Total	101.47	101.54	101.02	101.27	101.80	100.67	101.68	101.84	101.30	100.47	100.75	100.15
Si	2.94	2.94	2.95	2.95	2.94	2.96	2.95	2.95	2.96	2.96	2.69	2.94
Ti	0.00	0.00	0.00	0.00	0.00	0.00	0.00	0.00	0.00	0.00	0.00	0.00
Al	2.01	2.01	2.00	2.01	1.99	2.00	2.00	2.00	2.00	1.99	1.82	2.00
Cr	0.00	0.00	0.00	0.00	0.00	0.00	0.00	0.00	0.00	0.00	0.00	0.00
Fe^{2+}	1.98	1.98	1.95	1.96	2.00	1.98	1.98	1.97	1.99	1.97	1.81	2.01
Mn^{2+}	0.17	0.16	0.16	0.16	0.16	0.18	0.20	0.19	0.19	0.19	0.17	0.19
Mg	0.76	0.77	0.77	0.76	0.79	0.73	0.67	0.64	0.59	0.61	0.51	0.52
Ca	0.19	0.20	0.21	0.20	0.18	0.19	0.24	0.30	0.32	0.31	0.31	0.39
Na	0.00	0.00	0.00	0.00	0.01	0.00	0.00	0.00	0.00	0.00	0.00	0.00
K	0.00	0.00	0.00	0.00	0.00	0.00	0.00	0.00	0.00	0.00	0.00	0.00
Tot	8.05	8.06	8.05	8.04	8.07	8.04	8.05	8.05	8.04	8.04	7.32	8.05
Alm	0.64	0.64	0.63	0.64	0.64	0.64	0.64	0.64	0.64	0.64	0.65	0.65
Pyp	0.24	0.25	0.25	0.25	0.25	0.24	0.22	0.21	0.19	0.20	0.18	0.17
Gros	0.06	0.06	0.07	0.07	0.06	0.06	0.08	0.10	0.10	0.10	0.11	0.13
Spes	0.05	0.05	0.05	0.05	0.05	0.06	0.06	0.06	0.06	0.06	0.06	0.06
X_{Fe}	0.72	0.72	0.72	0.72	0.72	0.73	0.75	0.76	0.77	0.76	0.78	0.80
X_{Mg}	0.28	0.28	0.28	0.28	0.28	0.27	0.25	0.24	0.23	0.24	0.22	0.20

GARNET 2

	rim												core
Na_2O	0.00	0.02	0.03	0.03	0.03	0.00	0.01	0.00	0.03	0.01	0.00	0.02	0.00
MgO	5.00	5.32	5.56	5.86	6.17	5.42	6.41	6.46	6.41	6.31	5.79	6.55	6.66
Al_2O_3	21.59	21.33	21.37	21.48	21.64	21.35	21.69	21.59	21.44	21.62	25.57	21.65	21.55
SiO_2	37.45	37.48	37.17	37.24	37.63	37.14	37.70	37.71	37.45	37.95	37.55	37.70	37.78
K2O	0.05	0.00	0.02	0.00	0.01	0.02	0.00	0.00	0.03	0.01	0.00	0.00	0.00
CaO	3.99	3.69	3.19	2.66	2.51	2.99	2.69	2.73	2.66	2.73	2.67	2.71	2.28
TiO_2	0.00	0.00	0.02	0.00	0.02	0.01	0.01	0.00	0.01	0.00	0.01	0.00	0.00
Cr_2O_3	0.01	0.04	0.00	0.00	0.05	0.03	0.01	0.03	0.06	0.00	0.00	0.01	0.00
MnO	2.40	2.57	2.65	2.71	2.65	2.62	2.61	2.46	2.38	2.43	2.31	2.43	2.50
FeO	30.49	29.95	30.59	30.50	30.60	30.77	30.25	30.58	30.04	29.63	28.11	30.26	30.73
Total	101.00	100.42	100.60	100.49	101.30	100.36	101.39	101.56	100.50	100.69	102.00	101.33	101.51
Si	2.95	2.96	2.94	2.94	2.94	2.95	2.94	2.94	2.95	2.97	2.87	2.94	2.69
Ti	0.00	0.00	0.00	0.00	0.00	0.00	0.00	0.00	0.00	0.00	0.00	0.00	0.00
Al	2.00	1.99	1.99	2.00	2.00	2.00	2.00	1.99	1.99	1.99	2.30	1.99	1.81
Cr	0.00	0.00	0.00	0.00	0.00	0.00	0.00	0.00	0.00	0.00	0.00	0.00	0.00
Fe^{2+}	2.01	1.98	2.02	2.01	2.00	2.04	1.97	2.00	1.98	1.94	1.79	1.98	1.83
Mn^{2+}	0.16	0.17	0.18	0.18	0.18	0.18	0.17	0.16	0.16	0.16	0.15	0.16	0.15
Mg	0.59	0.63	0.66	0.69	0.72	0.64	0.75	0.75	0.75	0.74	0.66	0.76	0.71
Ca	0.34	0.31	0.27	0.23	0.21	0.25	0.22	0.23	0.22	0.23	0.22	0.23	0.17
Na	0.00	0.00	0.00	0.00	0.01	0.00	0.00	0.00	0.00	0.00	0.00	0.00	0.00
K	0.00	0.00	0.00	0.00	0.00	0.00	0.00	0.00	0.00	0.00	0.00	0.00	0.00
Tot	8.05	8.05	8.07	8.06	8.06	8.06	8.06	8.07	8.06	8.03	7.98	8.06	7.35
Alm	0.65	0.64	0.65	0.65	0.64	0.66	0.63	0.64	0.64	0.63	0.64	0.63	0.64
Pyp	0.19	0.20	0.21	0.22	0.23	0.21	0.24	0.24	0.24	0.24	0.23	0.24	0.25
Gros	0.11	0.10	0.09	0.07	0.07	0.08	0.07	0.07	0.07	0.07	0.08	0.07	0.06
Spes	0.05	0.06	0.06	0.06	0.06	0.06	0.06	0.05	0.05	0.05	0.05	0.05	0.05
X_{Fe}	0.77	0.76	0.76	0.74	0.74	0.76	0.73	0.73	0.72	0.72	0.73	0.72	0.72
X_{Mg}	0.23	0.24	0.24	0.26	0.26	0.24	0.27	0.27	0.28	0.28	0.27	0.28	0.28

					rim
Na_2O	0.01	0.03	0.00	0.00	0.05
MgO	6.22	5.11	5.07	4.96	4.61
Al_2O_3	21.71	21.34	21.25	21.23	21.23
SiO_2	37.58	37.23	37.24	36.97	37.00
K2O	0.00	0.01	0.02	0.04	0.01
CaO	2.24	4.16	4.13	4.33	4.63
TiO_2	0.01	0.00	0.01	0.04	0.05
Cr_2O_3	0.03	0.02	0.00	0.00	0.03
MnO	2.74	2.44	2.56	2.42	2.25
FeO	31.02	30.33	30.43	30.66	30.96
Total	101.56	100.68	100.71	100.66	100.81
Si	2.94	2.94	2.95	2.93	2.93
Ti	0.00	0.00	0.00	0.00	0.00
Al	2.00	1.99	1.98	1.98	1.98
Cr	0.00	0.00	0.00	0.00	0.00
Fe^{2+}	2.03	2.01	2.01	2.03	2.05
Mn^{2+}	0.18	0.16	0.17	0.16	0.15
Mg	0.72	0.60	0.60	0.59	0.54
Ca	0.19	0.35	0.35	0.37	0.39
Na	0.00	0.01	0.00	0.00	0.01
K	0.00	0.00	0.00	0.00	0.00
Tot	8.06	8.06	8.06	8.07	8.07
Alm	0.65	0.64	0.64	0.65	0.65
Pyp	0.23	0.19	0.19	0.19	0.17
Gros	0.06	0.11	0.11	0.12	0.13
Spes	0.06	0.05	0.05	0.05	0.05
X_{Fe}	0.74	0.77	0.77	0.78	0.79
X_{Mg}	0.26	0.23	0.23	0.22	0.21

GARNET 3

	rim								core				
Na_2O	0.03	0.01	0.00	0.05	0.00	0.02	0.02	0.00	0.00	0.00	0.02	0.00	0.00
MgO	4.62	4.82	5.52	5.81	6.39	6.60	6.60	6.58	6.63	6.71	6.78	5.61	6.66
Al_2O_3	21.24	21.42	21.52	21.51	21.63	21.64	21.31	21.52	21.62	21.71	21.54	21.39	21.69
SiO_2	37.34	37.20	37.32	37.58	37.63	37.73	37.50	37.50	37.43	37.50	37.56	37.04	37.62
K2O	0.03	0.02	0.04	0.00	0.00	0.00	0.02	0.00	0.02	0.02	0.00	0.00	0.01
CaO	2.64	2.56	2.57	2.59	2.28	2.56	2.66	2.50	2.36	2.35	2.35	2.32	2.23
TiO_2	0.02	0.01	0.00	0.00	0.02	0.02	0.05	0.03	0.03	0.00	0.02	0.02	0.03
Cr_2O_3	0.00	0.02	0.01	0.02	0.02	0.04	0.05	0.03	0.00	0.03	0.02	0.04	0.05
MnO	3.24	3.31	3.09	3.05	3.01	2.58	2.62	2.71	2.61	2.59	2.54	2.66	2.51
FeO	31.89	32.03	31.05	30.60	29.97	29.54	30.05	29.18	29.95	29.93	30.17	31.81	30.09
Total	101.05	101.39	101.12	101.21	100.94	100.73	100.90	100.04	100.64	100.84	100.99	100.90	100.88
Si	2.96	2.94	2.94	2.95	2.95	2.95	2.94	2.69	2.94	2.94	2.94	2.93	2.94
Ti	0.00	0.00	0.00	0.00	0.00	0.00	0.00	0.00	0.00	0.00	0.00	0.00	0.00
Al	1.98	2.00	2.00	1.99	2.00	2.00	1.97	1.82	2.00	2.00	1.99	1.99	2.00
Cr	0.00	0.00	0.00	0.00	0.00	0.00	0.00	0.00	0.00	0.00	0.00	0.00	0.00
Fe^{2+}	2.11	2.12	2.05	2.01	1.96	1.93	1.97	1.75	1.97	1.96	1.98	2.10	1.97
Mn^{2+}	0.22	0.22	0.21	0.20	0.20	0.17	0.17	0.16	0.17	0.17	0.17	0.18	0.17
Mg	0.55	0.57	0.65	0.68	0.75	0.77	0.77	0.70	0.78	0.78	0.79	0.66	0.78
Ca	0.22	0.22	0.22	0.22	0.19	0.21	0.22	0.19	0.20	0.20	0.20	0.20	0.19
Na	0.01	0.00	0.00	0.01	0.00	0.00	0.00	0.00	0.00	0.00	0.00	0.00	0.00
K	0.00	0.00	0.00	0.00	0.00	0.00	0.00	0.00	0.00	0.00	0.00	0.00	0.00
Tot	8.05	8.06	8.06	8.06	8.05	8.05	8.07	7.33	8.06	8.06	8.07	8.07	8.05
Alm	0.68	0.68	0.66	0.65	0.63	0.63	0.63	0.62	0.63	0.63	0.63	0.67	0.64
Pyp	0.18	0.18	0.21	0.22	0.24	0.25	0.25	0.25	0.25	0.25	0.25	0.21	0.25
Gros	0.07	0.07	0.07	0.07	0.06	0.07	0.07	0.07	0.06	0.06	0.06	0.06	0.06
Spes	0.07	0.07	0.07	0.07	0.06	0.06	0.06	0.06	0.06	0.06	0.05	0.06	0.05
X_{Fe}	0.79	0.79	0.76	0.75	0.72	0.72	0.72	0.71	0.72	0.71	0.71	0.76	0.72
X_{Mg}	0.21	0.21	0.24	0.25	0.28	0.28	0.28	0.29	0.28	0.29	0.29	0.24	0.28

					rim	
Na_2O	0.00	0.02	0.06	0.00	0.03	0.01
MgO	6.47	6.26	4.31	4.41	4.43	4.11
Al_2O_3	21.78	21.40	21.32	21.45	21.55	21.39
SiO_2	37.56	37.66	37.50	37.97	37.49	37.39
K2O	0.03	0.02	0.02	0.00	0.02	0.01
CaO	2.30	2.33	4.84	4.74	4.85	4.32
TiO_2	0.00	0.00	0.00	0.01	0.02	0.02
Cr_2O_3	0.00	0.00	0.02	0.00	0.04	0.00
MnO	2.71	2.92	3.03	2.77	2.89	3.14
FeO	30.70	30.45	30.13	29.73	30.23	31.07
Total	101.56	101.05	101.25	101.07	101.55	101.47
Si	2.93	2.95	2.96	2.98	2.95	2.95
Ti	0.00	0.00	0.00	0.00	0.00	0.00
Al	2.00	1.98	1.98	1.99	2.00	1.99
Cr	0.00	0.00	0.00	0.00	0.00	0.00
Fe^{2+}	2.00	2.00	1.99	1.95	1.99	2.05
Mn^{2+}	0.18	0.19	0.20	0.18	0.19	0.21
Mg	0.75	0.73	0.51	0.52	0.52	0.48
Ca	0.19	0.20	0.41	0.40	0.41	0.37
Na	0.00	0.00	0.01	0.00	0.00	0.00
K	0.00	0.00	0.00	0.00	0.00	0.00
Tot	8.07	8.06	8.06	8.02	8.06	8.05
Alm	0.64	0.64	0.64	0.64	0.64	0.66
Pyp	0.24	0.23	0.16	0.17	0.17	0.16
Gros	0.06	0.06	0.13	0.13	0.13	0.12
Spes	0.06	0.06	0.07	0.06	0.06	0.07
X_{Fe}	0.73	0.73	0.80	0.79	0.79	0.81
X_{Mg}	0.27	0.27	0.20	0.21	0.21	0.19

GARNET 4

	rim		core		rim
Na_2O	0.02	0	0	0.02	0.03
MgO	5.01	6.06	5.97	6.06	5.5
Al_2O_3	21.55	21.54	21.55	21.42	21.51
SiO_2	37.91	37.61	37.49	37.19	37.41
K2O	0.02	0	0	0.01	0
CaO	3.41	2.56	2.47	2.34	2.68
TiO_2	0.00	0	0.01	0.01	0
Cr_2O_3	0.02	0.02	0.03	0	0
MnO	2.81	3.02	3.19	3.14	2.89
FeO	30.71	30.17	29.67	29.79	30.76
Total	101.46	100.98	100.38	99.98	100.78
Si	2.97	2.95	2.96	2.95	2.95
Ti	0.00	0.00	0.00	0.00	0.00
Al	1.99	1.99	2.00	2.00	2.00
Cr	0.00	0.00	0.00	0.00	0.00
Fe^{2+}	2.01	1.98	1.96	1.97	2.03
Mn^{2+}	0.19	0.20	0.21	0.21	0.19
Mg	0.59	0.71	0.70	0.72	0.65
Ca	0.29	0.22	0.21	0.20	0.23
Na	0.00	0.00	0.00	0.00	0.00
K	0.00	0.00	0.00	0.00	0.00
Tot	8.04	8.05	8.04	8.05	8.05
Alm	0.66	0.64	0.64	0.64	0.66
Pyp	0.19	0.23	0.23	0.23	0.21
Gros	0.09	0.07	0.07	0.06	0.07
Spes	0.06	0.06	0.07	0.07	0.06
X_{Fe}	0.77	0.74	0.74	0.73	0.76
X_{Mg}	0.23	0.26	0.26	0.27	0.24

BIOTITE

	bt inclusion grt	bt inclusion grt	bt contact grt	bt contact grt	bt inclusion grt	bt inclusion grt
Na_2O	0.17	0.14	0.16	0.17	0.22	0.23
MgO	11.90	12.93	12.10	11.80	13.32	13.19
Al_2O_3	18.33	19.27	18.10	18.02	19.92	18.81
SiO_2	36.09	36.95	36.05	35.89	37.58	37.00
K2O	9.57	9.45	9.70	9.59	9.48	9.43
CaO	0.00	0.04	0.03	0.02	0.00	0.00
TiO_2	2.22	1.62	2.21	2.57	1.15	1.67
Cr_2O_3	0.01	0.00	0.02	0.05	0.05	0.02
MnO	0.00	0.04	0.10	0.07	0.00	0.00
FeO	16.00	14.71	16.51	17.13	13.99	15.00
Total	94.29	95.15	94.98	95.30	95.70	95.34
Si	5.46	5.98	5.44	5.41	5.51	5.49
Ti	0.25	0.20	0.25	0.29	0.13	0.19
Al	3.27	3.68	3.22	3.20	3.44	3.29
Al^{VI}	0.73	1.66	0.66	0.62	0.96	0.78
Al^{IV}	2.54	2.02	2.56	2.59	2.49	2.51
Cr	0.00	0.00	0.00	0.01	0.01	0.00
Fe^{2+}	2.03	1.99	2.08	2.16	1.72	1.86
Mn^{2+}	0.00	0.01	0.01	0.01	0.00	0.00
Mg	2.69	3.12	2.72	2.65	2.91	2.92
Ca	0.00	0.01	0.00	0.00	0.00	0.00
Na	0.05	0.04	0.05	0.05	0.06	0.07
K	1.85	1.95	1.87	1.85	1.77	1.79
Tot	15.60	16.98	15.65	15.64	15.55	15.60
X_{Fe}	0.43	0.39	0.43	0.45	0.37	0.39
X_{Mg}	0.57	0.61	0.57	0.55	0.63	0.61

	bt contact grt		biotite matrix		Bt fine grained	
Na_2O	0.14	0.11	0.14	0.08	0.14	
MgO	11.86	12.61	12.07	9.91	11.13	
Al_2O_3	18.17	17.78	17.80	14.06	15.76	
SiO_2	36.02	36.56	35.87	52.45	40.48	
K2O	9.80	9.63	9.62	8.95	9.37	
CaO	0.02	0.03	0.00	0.00	0.01	
TiO_2	2.41	2.33	2.52	1.99	1.99	
Cr_2O_3	0.06	0.06	0.06	0.00	0.01	
MnO	0.09	0.11	0.07	0.08	0.08	
FeO	17.19	16.02	16.53	13.96	15.29	
Total	95.76	95.21	94.68	101.48	94.28	
Si	5.41	5.48	5.93	6.99	6.59	
Ti	0.27	0.26	0.31	0.20	0.24	
Al	3.22	3.14	3.47	2.21	3.02	
Al^{VI}	0.63	0.63	1.39	1.20	1.61	
Al^{IV}	2.59	2.52	2.07	1.01	1.41	
Cr	0.01	0.01	0.01	0.00	0.00	
Fe^{2+}	2.16	2.01	2.28	1.56	2.08	
Mn^{2+}	0.01	0.01	0.01	0.01	0.01	
Mg	2.66	2.82	2.97	1.97	2.70	
Ca	0.00	0.00	0.00	0.00	0.00	
Na	0.04	0.03	0.05	0.02	0.04	
K	1.88	1.84	2.03	1.52	1.95	
Tot	15.66	15.62	17.06	14.48	16.65	
X_{Fe}	0.45	0.42	0.43	0.44	0.44	
X_{Mg}	0.55	0.58	0.57	0.56	0.56	

LY131 chemical composition of the mineral phases (garnet, biotite and K-feldspar)

GARNET 1

	rim							core					
Na_2O	0.02	0.01	0.01	0.04	0.00	0.04	0.00	0.01	0.00	0.00	0.01	0.02	0.00
MgO	4.15	4.57	4.69	4.77	5.53	5.69	5.78	5.74	5.74	5.81	5.73	5.39	5.00
Al_2O_3	21.66	21.60	21.85	21.79	21.69	21.79	21.45	21.47	21.48	21.48	21.55	21.85	21.71
SiO_2	37.24	37.56	37.57	37.57	37.61	37.41	37.75	37.53	37.68	37.58	37.63	37.80	37.50
K2O	0.04	0.01	0.01	0.00	0.02	0.02	0.00	0.00	0.00	0.02	0.01	0.01	0.00
CaO	1.79	1.82	1.67	1.69	1.75	1.83	1.89	1.89	1.86	1.82	1.79	1.88	1.82
TiO_2	0.02	0.04	0.03	0.03	0.02	0.07	0.02	0.03	0.04	0.00	0.01	0.04	0.00
Cr_2O_3	0.02	0.01	0.03	0.02	0.02	0.00	0.00	0.00	0.00	0.00	0.02	0.01	0.01
MnO	1.48	1.37	1.36	1.44	1.16	1.06	1.02	0.97	1.08	1.06	1.19	1.28	1.40
FeO	35.80	35.34	34.87	34.88	34.07	33.72	33.87	33.78	34.02	33.84	33.43	33.82	33.78
Total	102.22	102.33	102.10	102.23	101.86	101.62	101.76	101.41	101.90	101.61	101.37	102.11	101.21
Si	2.94	2.95	2.95	2.95	2.95	2.93	2.96	2.69	2.95	2.95	2.95	2.95	2.96
Ti	0.00	0.00	0.00	0.00	0.00	0.00	0.00	0.00	0.00	0.00	0.00	0.00	0.00
Al	2.01	2.00	2.02	2.01	2.00	2.01	1.98	1.81	1.98	1.99	1.99	2.01	2.02
Cr	0.00	0.00	0.00	0.00	0.00	0.00	0.00	0.00	0.00	0.00	0.00	0.00	0.00
Fe^{2+}	2.36	2.32	2.29	2.29	2.23	2.21	2.22	2.02	2.23	2.22	2.20	2.21	2.23
Mn^{2+}	0.10	0.09	0.09	0.10	0.08	0.07	0.07	0.06	0.07	0.07	0.08	0.08	0.09
Mg	0.49	0.53	0.55	0.56	0.65	0.66	0.67	0.61	0.67	0.68	0.67	0.63	0.59
Ca	0.15	0.15	0.14	0.14	0.15	0.15	0.16	0.14	0.16	0.15	0.15	0.16	0.15
Na	0.00	0.00	0.00	0.01	0.00	0.01	0.00	0.00	0.00	0.00	0.00	0.00	0.00
K	0.00	0.00	0.00	0.00	0.00	0.00	0.00	0.00	0.00	0.00	0.00	0.00	0.00
Tot	8.06	8.05	8.04	8.05	8.05	8.06	8.05	7.34	8.06	8.06	8.05	8.04	8.03
Alm	0.76	0.75	0.75	0.74	0.72	0.71	0.71	0.71	0.71	0.71	0.71	0.72	0.73
Pyp	0.16	0.17	0.18	0.18	0.21	0.21	0.22	0.22	0.21	0.22	0.22	0.20	0.19
Gros	0.05	0.05	0.05	0.05	0.05	0.05	0.05	0.05	0.05	0.05	0.05	0.05	0.05
Spes	0.03	0.03	0.03	0.03	0.02	0.02	0.02	0.02	0.02	0.02	0.03	0.03	0.03
X_{Fe}	0.83	0.81	0.81	0.80	0.78	0.77	0.77	0.77	0.77	0.77	0.77	0.78	0.79
X_{Mg}	0.17	0.19	0.19	0.20	0.22	0.23	0.23	0.23	0.23	0.23	0.23	0.22	0.21

			rim	
Na_2O	0.00	0.04	0.01	0.09
MgO	5.21	5.03	5.11	4.97
Al_2O_3	21.62	22.04	21.75	21.71
SiO_2	37.63	37.68	37.46	37.56
K2O	0.03	0.05	0.13	0.25
CaO	1.82	1.79	1.84	1.67
TiO_2	0.00	0.02	0.01	0.00
Cr_2O_3	0.00	0.02	0.02	0.02
MnO	1.36	1.33	1.39	1.45
FeO	34.16	34.07	34.07	33.75
Total	101.84	102.08	101.78	101.47
Si	2.95	2.95	2.94	2.96
Ti	0.00	0.00	0.00	0.00
Al	2.00	2.03	2.01	2.01
Cr	0.00	0.00	0.00	0.00
Fe^{2+}	2.24	2.23	2.24	2.22
Mn^{2+}	0.09	0.09	0.09	0.10
Mg	0.61	0.59	0.60	0.58
Ca	0.15	0.15	0.15	0.14
Na	0.00	0.01	0.00	0.01
K	0.00	0.01	0.01	0.03
Tot	8.05	8.04	8.06	8.05
Alm	0.72	0.73	0.73	0.73
Pyp	0.20	0.19	0.19	0.19
Gros	0.05	0.05	0.05	0.05
Spes	0.03	0.03	0.03	0.03
X_{Fe}	0.79	0.79	0.79	0.79
X_{Mg}	0.21	0.21	0.21	0.21

GARNET 2

	rim		core	rim
Na_2O	0.03	0.00	0.02	0.02
MgO	5.00	5.14	4.99	4.25
Al_2O_3	21.62	21.70	21.67	21.85
SiO_2	37.18	37.53	37.27	37.83
K2O	0.00	0.00	0.00	0.02
CaO	1.96	1.87	1.91	1.77
TiO_2	0.01	0.00	0.01	0.01
Cr_2O_3	0.06	0.00	0.03	0.00
MnO	1.06	0.87	1.01	0.87
FeO	35.04	34.43	34.17	35.68
Total	101.95	101.55	101.09	102.31
Si	2.93	2.95	2.95	2.96
Ti	0.00	0.00	0.00	0.00
Al	2.01	2.01	2.02	2.02
Cr	0.00	0.00	0.00	0.00
Fe^{2+}	2.31	2.26	2.26	2.34
Mn^{2+}	0.07	0.06	0.07	0.06
Mg	0.59	0.60	0.59	0.50
Ca	0.17	0.16	0.16	0.15
Na	0.00	0.00	0.00	0.00
K	0.00	0.00	0.00	0.00
Tot	8.07	8.04	8.05	8.03
Alm	0.74	0.73	0.73	0.77
Pyp	0.19	0.20	0.19	0.16
Gros	0.05	0.05	0.05	0.05
Spes	0.02	0.02	0.02	0.02
X_{Fe}	0.80	0.79	0.79	0.82
X_{Mg}	0.20	0.21	0.21	0.18

K-FELDSPAR			BIOTITE				
				biotite matrix	biotite matrix	Bt contact grt	bt contact grt
Na_2O	1.16	2.04	Na_2O	0.07	0.14	0.13	0.14
MgO	0	0.01	MgO	10.18	9.9	10.71	11.08
Al_2O_3	18.35	17.98	Al_2O_3	17.85	17.67	18.53	19.05
SiO_2	62.85	63.25	SiO_2	35.52	35.31	35.53	36.59
K2O	14.56	13.39	K2O	9.67	9.61	9.41	9.57
CaO	0.1	0.08	CaO	0	0.04	0.00	0.00
TiO_2	0.02	0	TiO_2	3.47	3.59	3.24	3.19
Cr_2O_3	0.03	0.01	Cr_2O_3	0	0.02	0.08	0.00
MnO	0	0	MnO	0.06	0.01	0.01	0.06
FeO	0	0.01	FeO	17.96	18.34	18.26	16.71
Total	97.07	96.77	Total	94.78	94.63	95.91	96.39
Si	2.98	3.00	Si	5.42	5.90	5.35	5.42
Al	1.03	1.00	Ti	0.40	0.45	0.37	0.36
Ti	0.00	0.00	Al	3.21	3.48	3.29	3.33
Cr	0.00	0.00	Al^{VI}	0.62	1.38	0.64	0.75
Fe^{2+}	0.00	0.00	Al^{IV}	2.58	2.10	2.65	2.58
Mn^{2+}	0.00	0.00	Cr	0.00	0.00	0.01	0.00
Mg	0.00	0.00	Fe^{2+}	2.29	2.56	2.30	2.07
Ca	0.01	0.00	Mn^{2+}	0.01	0.00	0.00	0.01
Na	0.11	0.19	Mg	2.31	2.46	2.40	2.45
K	0.88	0.81	Ca	0.00	0.01	0.00	0.00
Ba	0.00	0.00	Na	0.02	0.05	0.04	0.04
Tot	5.00	5.00	K	1.88	2.05	1.81	1.81
X_{An}	0.01	0.00	Tot	15.53	16.96	15.56	15.48
X^{Ab}	0.11	0.19	X_{Fe}	0.50	0.51	0.49	0.46
X_{Or}	0.89	0.81	X_{Mg}	0.50	0.49	0.51	0.54